UNIVERSITY OF THE
FREE STATE
UNIVERSITEIT VAN DIE
VRYSTAAT
YUNIVESITHI YA
FREISTATA

UFS
UV

# AN INVESTIGATION OF THE TRACE ELEMENT COMPOSITIONS OF GOLD FROM ZIMBABWE AND SOUTH AFRICA: IMPLICATIONS FOR TRACING THE SOURCE OF ARCHEOLOGICAL GOLD ARTEFACTS

## BY

### Robert Netshitungulwana

**SUPERVISOR: Prof. Marian Tredoux**

**CO-SUPERVISOR: Dr Leon Jacobson**

Dissertation submitted in fulfillment of the requirement of the degree of Masters of Science at the University of the Free State
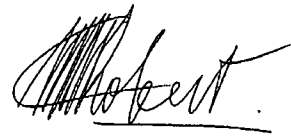
**University of the Free State**

**Department of Geology**

**March 2011**

# DECLARATION

The content of this work is my own and has not previously been submitted for a degree at this or any other university. The work of other people is acknowledged by references.

Robert Netshitungulwana
Department of Geology
University of the Free State
March 2011

# DEDICATION

*This thesis is dedicated to the following people: my wife, Tendani Shumani Netshitungulwana; my children, Ndiene Mukundi and Mulanga Vhuthuhawe; my parents Marubini Mercy and Tshamaano Philemon; my brothers, Aaron Mpfariseni, Azwinndini Sariel, Ntakuseni, Mmbavhalelo, Mmbulungeni Elijah, Makwarela Moses and Rofhiwa; my sisters, Rechael, Rendani, Matodzi, Lydia, Lufuno and all members of our extended family I omitted. I assume this would be our document, which will be read by generations to come, linking our grandchildren to us.*

# ACKNOWLEDGEMENTS

# ABSTRACT

The early black farmers who settled in southern Africa were involved in trading and metal technology. The history of mining for metals like iron, copper, tin and gold in southern Africa spans at least the past 2000 years. The main aim of the research was to test the viability of using gold chemistry to compare the composition of gold ores in South Africa and Zimbabwe with those of the archaeological gold artefacts from Thulamela, Mapungubwe and Great Zimbabwe. Samples from the Archaean greenstone belts in South Africa and Zimbabwe, as well as samples from ores associated with the Witwatersrand Supergroup, were used in the study. Trace element signatures were determined by laser ablation inductively coupled plasma mass spectrometry (LA-ICP-MS), a technique whereby low concentrations (down to low ppb levels) can be detected. In addition, Ag concentrations (wt %) were determined using a scanning electron microprobe, so that Ag could be used as an internal standard during the LA-ICP-MS runs to give semi-quantitative data. The most commonly occurring isotopes in gold, namely, $^{56}$Fe, $^{59}$Co, $^{60}$Ni $^{63}$Cu, $^{66}$Zn, $^{75}$As, $^{188}$Os, $^{105}$Pd, $^{195}$Pt, $^{202}$Hg, $^{107,109}$Ag, and $^{204,\ 206,207,208}$Pb and $^{209}$Bi, were used to construct the signatures, using their intensities in the mass spectra in counts per second (cps). Isotopic ratios were used to compare the gold ores with each other. The results show some variations in the signatures of gold from the greenstone belts and the Witwatersrand Basin. The $^{107}$Ag and $^{202}$Hg concentrations in gold from the Witwatersrand Basin are high compared to the greenstone belts. These differences have implications for the various models of gold deposition in these environments, pointing to different geochemical histories. Multivariate correspondence analysis plots for the major gold deposits show the wide group of the Barberton samples with little or no distinctive characteristics, compared to the Zimbabwean gold samples. The Witwatersrand gold plotted differently to the Barberton Greenstone Belt but closely related to the Zimbabwean greenstone belts. The ratio plot of $^{56}$Fe/$^{107}$Ag versus $^{202}$Hg/$^{107}$Ag shows that archaelogical gold artefacts differ completely from the natural gold, indicating that the gold could not merely have been cold-worked, as has been suggested. This suggests that gold from any one archaeological site could not be related to any particular or even regional source. This could be associated with the possibility of mixing of gold from multiple sources, recycling, contamination in melting and trade in items.

# LIST OF TABLES

# LIST OF FIGURES

# TABLE OF CONTENTS

# 1 INTRODUCTION

The early black farmers who settled in southern Africa were involved in trading and metal technology (Summers, 1969; Phimister, 1976; Oddy, 1983, 1984). The archaeological evidence shows that trading and metal technology were practised before colonizers from Europe arrived in southern Africa. Great Zimbabwe was acknowledged to have housed about 18,000 inhibitants and flourished between about AD 1290 and AD 1450 (Miller, 2001; Huffman, 2007, 2009). It was an empire that included the present day Zimbabwe, western parts of Botswana, northern parts of South Africa and parts of Mozambique, where most of the trading activities occurred (Jacobson *et al.,* 2002). The empire was thought to have ceased because of the over-utilization of natural resources, and internal conflicts. The chiefs migrated to the north and south in search of new sources of ivory and metals for their trading activities (Jacobson *et al.,* 2002 and the references therein).

The locations of early gold mines that were prospected, the mining techniques used, the recovery of gold from the ore, and trade were intensively discussed by Miller *et al.* (2000) and references therein. Maritime trade increased from small beginnings late in the first millennium AD, was well established by the 10$^{th}$ century AD and reached a peak in the 15$^{th}$ century AD. The internal conflicts (internecine strife) paved a way for the modern European colonizers. The Voortrekkers in the 18$^{th}$ century AD used old trade routes which were established from Delgoabaai and Inhaunbaue by early settlers (de Vaal, 1984; 1985).

## 1.1 Research Background

In 1936 Letcher had already asked very important questions (Letcher, 1936). Who were the first people to discover gold in Africa? How and where did they find gold and what uses did they have for the precious metal? What became of all this gold? Where and by whom was it absorbed? Indeed many scientists have tried to answer some of the questions he asked. To address these questions it is important to look back on the introduction of metals in southern Africa.

The history of mining for metals in southern Africa spans at least the past 2000 years (Oddy, 1984; Miller, 1995). That there was exploitation of metals like iron, copper, tin and gold, is supported by archaeological evidence. The earliest evidence for iron production in southern Africa was slags from the $2^{nd}$ to $6^{th}$ century AD sites in southern Mocambique. Also, evidence was found at Broederstroom (South Africa) dating to between the $4^{th}$ and $7^{th}$ centuries AD, and at Divuyu in Botswana from the mid $6^{th}$ century AD (Miller, 1995).

The early copper mining in southern Africa spans AD 770 and 1750 for mines at Loolekop, Sealene and Kgopolwe in the Phalaborwa district. The Messina district also has evidence of early copper mining, but it has not been dated yet. The Phalaborwa and Messina district areas became major copper producers in the $20^{th}$ century. Olifantspoort and the Dwarsberg in the western Transvaal and near Rooiberg were also early copper mining areas (Miller, 1995).

The ancient tin sources were restricted to the mines of Rooiberg in the central Transvaal. Tin mining has been dated back to the $15^{th}$ to $17^{th}$ centuries AD (Miller, 1995). Tin was alloyed with copper for bronze (Cowey, 1994).

2

Humans have known about gold since pre-historic times. The earliest gold objects of all ancient civilizations were fashioned directly from native gold (Boyle, 1979), without any metallurgical treatment. In Africa, the tombs of the Pharaohs contained various gold artefacts that date back to 1350 BC (Boyle, 1979). In southern Africa, gold first appears during the Late Iron Age, after about AD 1000. Gold artefacts were found in elite burials sites such as Mapungubwe and Thulamela and also in the political centers such as Great Zimbabwe.
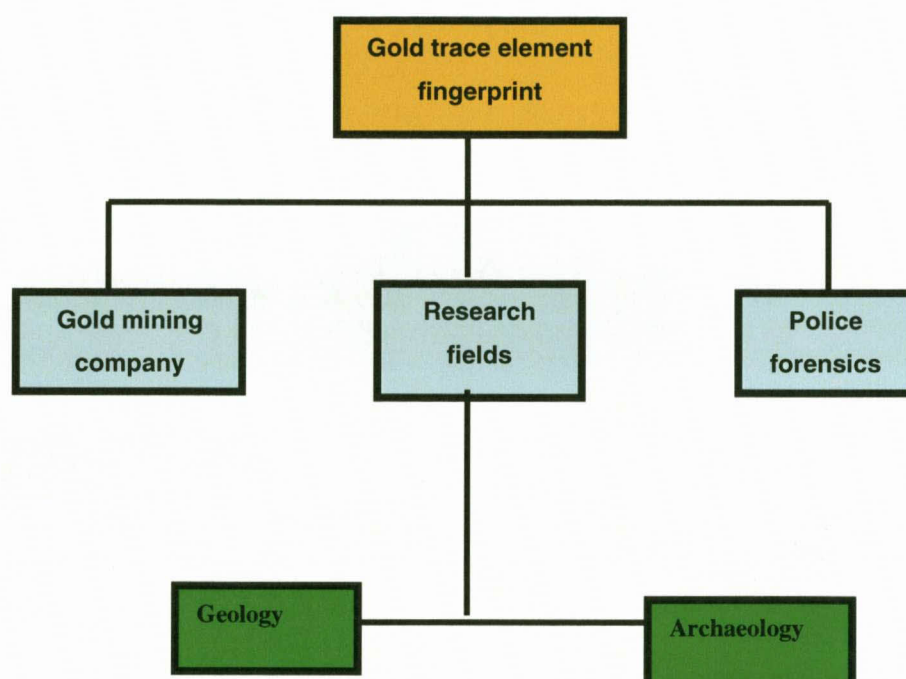


**Figure 1-1 A diagram showing various different geoscientific research areas that could benefit from a gold trace element database for reference or consultation purposes.**

Characterization of the trace and ultra-trace element signatures in native gold is generally known as gold fingerprinting and was developed about 25 years ago (Watling *et al.*, 1994). The technology used for gold trace element analysis by laser ablation inductively coupled mass spectrometry (LA-ICP-MS), which greatly improved the accuracy of gold fingerprinting, was started in the 1990s. The earliest

3

fingerprinting of native gold by this method was done in Australia by Watling *et al.* (1994), and was aimed at sourcing stolen gold for return to mining companies. The gold fingerprint database has been admitted as evidence in courts of law in the case of bullion theft (Watling *et al.,* 1994). Figure 1-1 shows various geoscientific research areas that could benefit from a gold trace element database for reference purposes.

## 1.2 Previous Studies

An archaeological study done by Oddy (1984) shows that the history of mining and quarrying for metal ores in southern Africa dates as far back as 2 000 years. However, the history of indigenous metal technology remains largely unknown. This is due to some extent to uncertainty about the source of gold used to produce various artefacts, such as beads, bangles, statues and sheets, which have been recovered from the graves at archaeological sites such as Mapungubwe, Thulamela and Great Zimbabwe (Figure 1-2). Current research followed previous studies done on the archaeological gold artefacts at Mapungubwe and Thulamela (Oddy, 1984; Grigorova *et al.,* 1998; Desai, 2001). These studies were based on the presence or absence of elements only and there was no actual data which could have been used in subsequent comparison.

Table 1-1 from the previous studies indicates two different chemical signatures in the Mapungubwe gold artefacts. The first group was marked by the presence of strontium, mercury, rare earth elements, platinum group elements and barium. The second group has platinum group elements only and no other contaminants (Desai, 2001; Grigarova *et al.,* 1998; Miller *et al.,* 2000, 2001).

4

Table 1-1 Summary of the trace elements signatures for the Thulamela and Mapungubwe archaelogical samples (after Desai, 2001).

| Elements | Thulamela | Mapungubwe | |
|---|---|---|---|
| | | A | B |
| Strotium | ✓ | | |
| Mercury | ✓ | | ✓ |
| Rare Earth Elements | ✓ | ✓ | |
| Platinum Group Elements | ✓ | ✓ | ✓ |
| Bismuth | ✓ | | |
| Barium | ✓ | | |
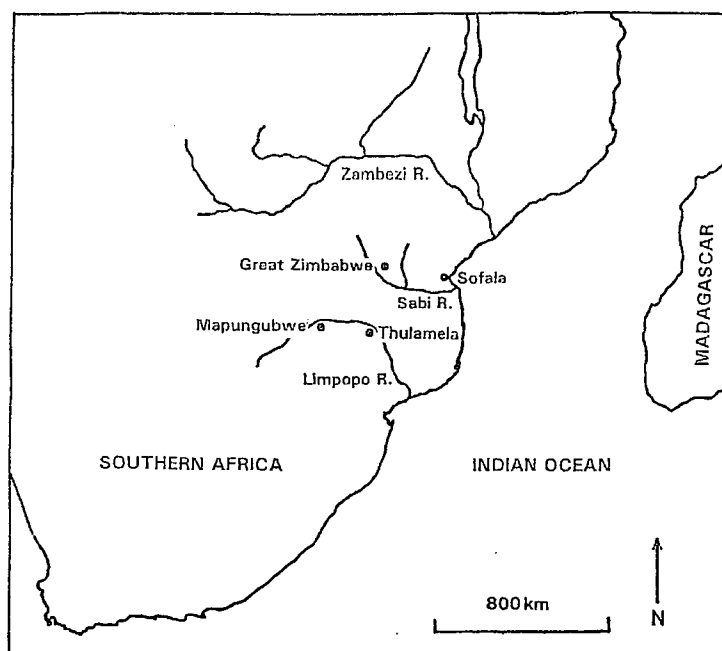


Figure 1-2 A map of important archaeological sites in southern Africa, with important waterways regarding trade shown (Swan, 1994; Miller *et al.*, 2000).

Gold artefacts from Thulamela have chemical signatures marked by the presence of strontium, mercury, rare earth elements, platinum group elements and barium, similar to the Mapungubwe artefacts. It was concluded by Miller *et al.* (2001) that the gold used to make certain artefacts from Mapungubwe come from one gold source, whereas gold used to make the other artefacts come from a different source. The gold source common to the metal goldsmiths of the Thulamela gold artefacts suggests that the two societies (Thulamela and Mapungubwe) had access to the same source of gold. Gold artefacts from Bosutswe showed no link to gold originating from either Mapungubwe or Thulamela (Grigorova *et al.,* 1998).

Ginwala *et al.* (1986) have used proton induced techniques for the determination of some trace impurities in gold objects but analytical determinations were hindered by the gold background.

## 1.3 Project Objectives

The main aim of the research reported in this document was to test the viability of using gold chemistry to compare the composition of native gold ores in South Africa and Zimbabwe with those of the archaeological gold artefacts from Thulamela, Mapungubwe and Great Zimbabwe. Any similarities observed between the composition of the gold ores and artefacts, may help in the establishment of possible gold trade routes of archaeological importance. Gold ore samples from various localities in southern Africa, representing the most significant gold ore districts, namely, the Barberton, Murchison, Giyani and Pietersburg Greenstone Belts, the Witwatersrand Basin and the Zimbabwean craton, were procured for analysis.

In order to achieve the main aim of the research, as stated above, the following tasks

were undertaken:

(a) the development of a consistent analytical protocol for gold samples using a laser ablation inductively coupled plasma mass spectrometer (LA-ICP-MS);

(b) the comparison of gold ore composition with those of the archaeological gold artefacts recovered from the ancient sites of Mapungubwe, Thulamela and Great Zimbabwe. An attempt was made to determine:

- whether distinct regional sources of gold could be identified;

- whether the gold used in these artefacts was sourced from multiple gold ore deposits as a consequence of complex trading routes and systems at that time;

- whether gold trade between sites could be traced by identification of characteristic gold compositions; and

- what metallurgical techniques, if any, were employed in the processing of gold; for example, whether systematic alloying with silver or copper was practised.

## 1.4   General Geochemistry of Gold

This section summarizes the previous work on the general geochemistry of native gold. The trace elements present in native gold are related in some way to the processes associated with the original mineralization event. In order to understand the differences in composition of natural gold samples, it is important to review the geochemical behaviour of this metal during mineralization.

Gold is a soft, yellow metal and has high electrical and thermal conductivity, exceeded only by copper and silver (Boyle, 1979; Gasparrin, 1993). In its pure state

7

gold is the most malleable and ductile of all the transition metals. Gold is a member of the group 11 elements in the periodic table and when compared to the other elements in the periodic table, it shows similarities with those in group 10 (nickel, palladium and platinum) and of course the other elements in group 11 (copper and silver). Gold can also form amalgams with mercury and the other elements in group 12 (zinc and cadmium) (Boyle, 1979; Gasparrin, 1993; Seward, 1984).

Gold may be found in one of the following three oxidations states: the native (0), aurous (+1) and the auric (+3) states. Boyle (1979) and Seward (1984) discuss the general characteristics of gold cations, commenting that Au (I) forms a number of organometallic compounds, whereas Au (III) forms both inorganic and organometallic complexes. They comment that the solubility of gold in geochemical environments results from its general properties and that the only indisputable processes occur in gossans, where gold is either dissolved by mercury (thus forming amalgams), or reacts with $Cl_2$ released by NaCl reacting with $MnO_2$, to form chlorine complexes, which transport gold and other metals.

## 1.5  Composition of Native Gold

Native gold contains the following major elements: 80 to 99 % gold, 1 to 15 % silver and up to 5 % copper. Minor elements present include up to 1 % mercury and iron, with nickel, cobalt, zinc, palladium, platinum and lead all typically at parts per million (ppm) level (Chisholm, 1979; Sie *et al.,* 1996; Frimmel and Gartz, 1997; Allan and Woodcock, 2001 and references therein).'

In nature, native gold can be found alloyed or contaminated (especially under oxidizing conditions) with other major, trace and ultra-trace elements, which provide

useful information about the origin and the ore formation processes of gold (Erasmus *et al.,* 1987; Minter *et al.,* 1993; Watling *et al.,* 1999; Chapman *et al.,* 2002; Guerra, 2004; Guerra *et al.,* 2005; Raymond *et al.,* 2005). The contaminating elements can be classified into two main categories, namely, (1) the more volatile chalcophile elements, such as zinc, cadmium, lead, bismuth, mercury, silver, and copper; and (2) the less volatile siderophile elements, such as iridium, osmium, palladium, platinum, rhenium, rhodium and ruthenium (Boyle, 1979; Roeder, 1984; Erasmus *et al.,* 1987; Reisberg *et al.,* 2004). During ore formation (hydrothermal or placer) the inter-element signature should reflect the unique characteristics of the processes involved in the resultant ore deposits, as will be discussed in the following sections.

## 1.5.1 Hydrothermal Gold

In hydrothermal gold deposits, major and trace elements that can be identified in native gold may owe their presence to different types of ligands such as $CO^{-3}$, $Cl^-$, $Br^-$ and $HS^-$ that were responsible for transporting gold and other metals in solution (e.g. Seward, 1984), as different types of metal complexes (Boyle, 1984; Fyfe and Kerrich, 1984). According to Fyfe and Kerrich (1984), most elements that accompany gold during fluid transportation are also concentrated during deposition/precipitation, along with gold (Groves and Foster, 1991; Groves *et al.,* 1998). The elements that are deposited with gold include zinc, cadmium, lead, bismuth, mercury, silver, copper and platinum group elements (Reisberg *et al.,* 2004; Nakagawa *et al.,* 2005).

## 1.5.2 Placer Gold

In placer gold, the mechanical weathering which causes the relocation of dispersed grains in primary gold ore deposits, e.g. the physical transport in fluvial systems,

often leads to an enhancement of gold purity by leaching out silver (Mosier *et al.*, 1989; Nakagawa *et al.*, 2005). Previous work on the general characteristics of placer gold has shown that gold grains frequently have a rim of silver depletion caused by the probable dissolution of silver in an oxidizing environment or during transportation (Chisholm, 1979). Any other base metal present in placer gold will also be removed selectively by leaching and the rate of leaching will be in the following descending order of leachability: iron>nickel>copper>silver (Chisholm, 1979). The platinum-group elements are not leached from native gold (Antweiler and Campbell, 1977; Siebert *et al.*, 2005; Falconer *et al.*, 2005). The concentration of platinum-group elements is therefore expected to be high in native gold compared to silver and the base metals in relation to the original concentration.

Hypothetically, the different gold deposits selected will exhibit different chemical signatures because the deposits are from different environments of formation (hydrothermal for greenstones, modern placer for the Witwatersrand gold). The previous study (Chisholm, 1979; Antweiler and Campbell, 1977) shows that alluvial gold will be enriched in the platinum group elements and depleted in the base metal; the inverse is true for hydrothermal gold.

# 2  SAMPLE DESCRIPTIONS

## 2.1  South African Gold Ores

South African gold ore samples in this study were obtained from the Transvaal Museum in Pretoria, Iziko Museums in Cape Town and the natural resource company Anglogold Ashanti in Johannesburg. The sample descriptions are presented in Table 2-1. The sample identity numbers that were used are those assigned by the donors and are presented as follows: MGSs are those from the Transvaal Museum; Gs are those from the Iziko Museum and 2Bs are those from Anglogold Ashanti.

The samples originated from the following gold mines in South Africa: New Consort, Sheba, Alpine and Agnes mines from the Barberton Greenstone Belt; Gravellotte Mine from the Murchison Greenstone Belt; the Marabastadt Goldfield in the Pietersburg Greenstone Belt; Birthday Mine in the Giyani Greenstone Belt; City Deep Mine, Ventersdorp Contact Reef (VCR) (South Deep Mine), Carbon Leader Reef (Tautona Mine), Inner Basin Reef (West Rand Group), Contact Reef (Nolingwa Mine), B Reef (Welkom Goldfield) and the Leader Reef quartzite in the Witwatersrand Basin; the Sabie-Pilgrim's Rest Goldfield in the Transvaal Supergroup and "Knysna" gold ore from the Cape Supergroup (Figure 2-1).

The geological settings for the Barberton and Witwatersrand gold ore provinces from which most samples originated are discussed in the following sections and summarized in Table 2-1.
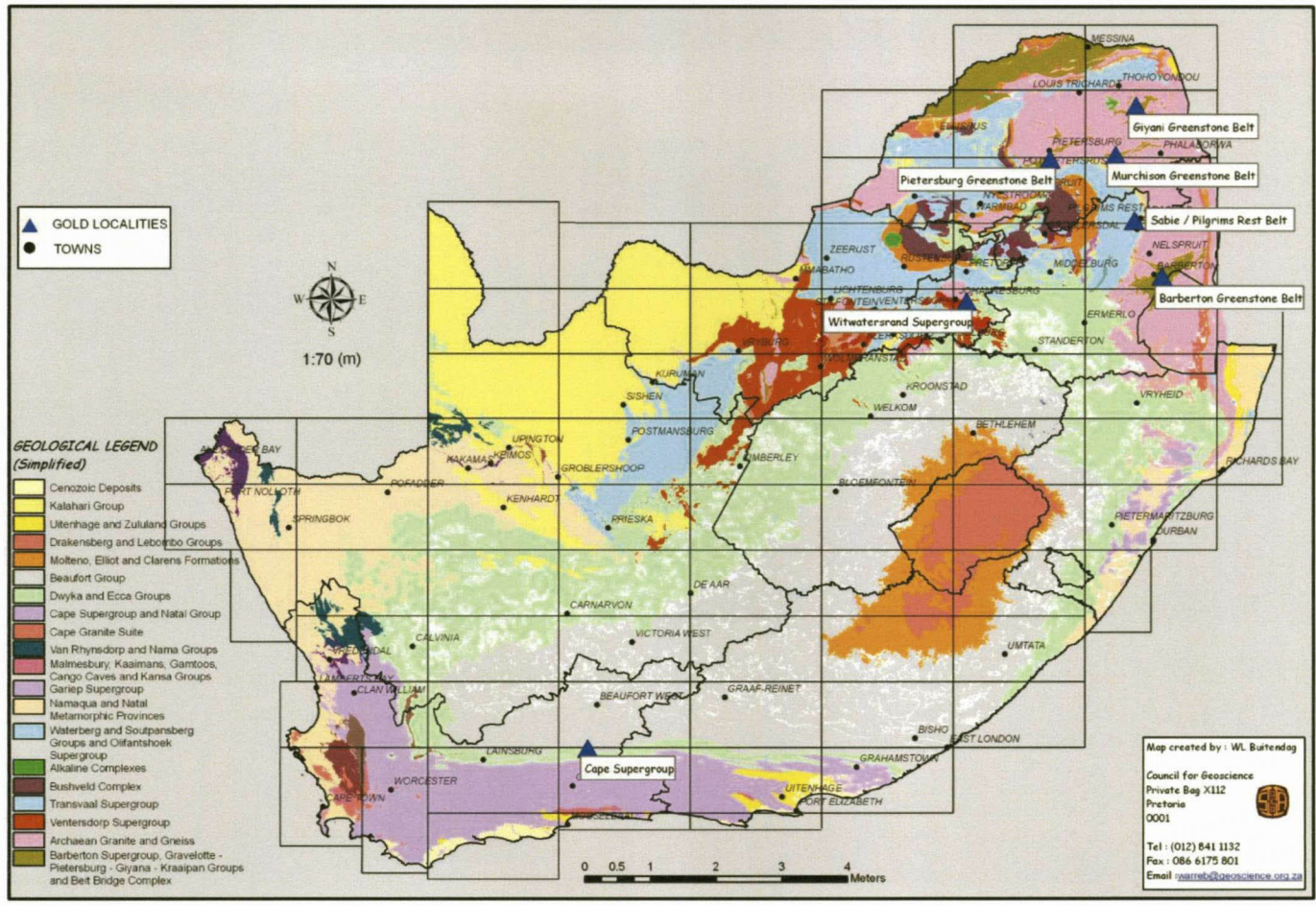
**Figure 2-1 Simplified geological map of South Africa, Lesotho and Swaziland showing the locality of gold in the Barberton, Murchison, Giyani and Pietersburg Greenstone Belts and the Transvaal (Sabie-Pilgrim's Rest Goldfield), Witwatersrand and Cape Supergroups (Buitendag, 2007).**

12

## 2.1.1 Barberton Greenstone Belt

The Archaean Barberton Greenstone Belt has been extensively studied (e.g. de Wit *et al.,* 1992; de Ronde *et al.,* 1991; de Ronde and de Wit, 1994; Williams, 1997). It is found in the Lowveld of the Mpumalanga Province (formally known as the Eastern Transvaal) and Swaziland (Figure 2-1). U-Pb and Pb-Pb dates of ca. 3.0 to 3.5 Ga were reported by de Ronde and de Wit (1994) and references therein. The ages of the rocks of the belt span approximately 500 Ma. The Barberton stratigraphy comprises the Onverwacht, Fig Tree and Moodies Groups (Viljoen and Viljoen, 1969; SACS, 1980). The three groups are surrounded by granitoid plutons (Figure 2-2; Yoshihara and Hamano, 2004; de Wit, 1998). Major rock types of the greenstone belt are komatiite, peridotite, magnesium-rich basalt, tholeiite, tuff, agglomerate, carbonaceous shaly chert, banded chert, banded iron formation and calc-silicate rocks with quartz-diopside-plagioclase-garnet assemblages (Cochran, 1982; Ward and Wilson, 1998).

The New Consort Mine is located in a contact zone between the Onverwacht Group and metapilites of the Fig Tree Group (Figure 2-2). Gold was discovered in the New Consort area in 1886 and mining was operating as an amalgamation of smaller companies (Voges, 1986). Mineralization in the New Consort Mine is generally associated with a quartz rich layer known as a New Consort Bar, which is 4m thick, with laminated, siliceous cherty rock inter-layered with sulphide-rich bands (Anhaeusser and Maske, 1986; de Ronde *et al.,* 1992). Mineralization is closely associated with the komatiite volcanics of the Onverwacht Group (Viljoen, 1984). The dominant sulphide is arsenopyrite, which occurs as disseminated needles in massive layers with other sulphides, such as pyrrhotite and chalcopyrite. Gold

13

mineralization is generally found adjacent to the Kaap Valley tonalite and other granitoid contacts, along major shear zones and along the Komati and Steynsdorp anticlines (Cochran, 1982).
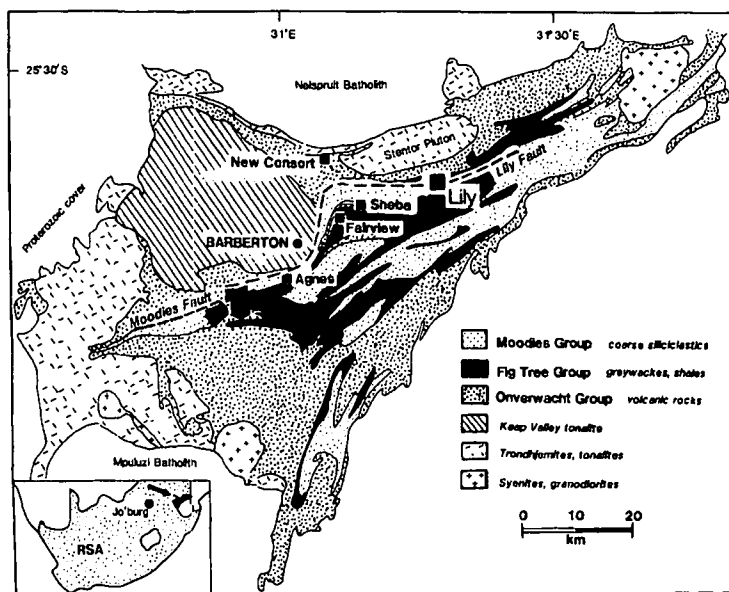
Figure 2-2 Generalized geological map of the Barberton Greenstone Belt, South Africa, showing the localities of some main gold mines (after de Ronde and de Wit, 1994).

The Sheba Mine is hosted within the rocks of the Moodies Group. Gold was discovered in the area in 1884 by Edwin Bray (Anhaeusser, 1974). In the 1980s mining was operated as an amalgamation of numerous small workings in the Sheba Valley (Wagener and Wiegand, 1986). The gold ores of both the Sheba and the Fairview mines are localized in two major synclines, which are the Eureka and Ulundi synclines. The Eureka syncline consists of the numerous fractures oriented parallel to the Sheba fault. Mineralization occurred by means of epigenetic hydrothermal solutions as the sulphide reefs include disseminated to massive pyrite and arsenopyrite (Wagener and Wiegand, 1986). The fractures may also be associated with breccia, quartz, calcite, arsenopyrite, pyrite and gold occurring in greywacke and shale (Schürmann et al., 2000).

14

The Agnes Mine gold was discovered in 1890 (Ward and Wilson, 1998). The Agnes Mine is located within the siltstones and the shales of the Clutha Formation of the Moodies Group (Houstoun, 1987). Gold mineralization is predominantly confined to two subparallel and subvertical fractures of the fault zone (Ward and Wilson, 1998). Mineralization occurs within dark brown grey mylonites, intrafolial smoky quartz-carbonate veins with occasional free gold and pyritic gold-quartz-carbonate veins, which are the most common ore types (Ward and Wilson, 1998).

## 2.1.2  Witwatersrand Supergroup

The Witwatersrand Supergroup is believed to have formed over a period of 360 Ma years between 3.07 and 2.71 Ga and its depositional history has been well documented (Robb and Meyer, 1995). The ultimate collision of the Kaapvaal and Zimbabwean cratons was associated with the tectonic evolution of a basin (Robb and Meyer, 1995).  The Witwatersrand Basin has an elongated structure stretching approximately 500 km from north-east to the south-west (du Plessis *et al.,* 1984). It consists of an approximately 7000m thick ancient sedimentary succession belonging to the Witwatersrand Supergroup and overlies Archaean greenstones and granites of the basement complex or the volcano-sedimentary Dominion Group (Erasmus *et al.,* 1987; Robb and Meyer, 1995).

The Witwatersrand Basin is divided into the West Rand of (2.97 to 2.91 Ga) and Central Rand (2.89 to 2.84 Ga) groups (Figure 2-3). The deposition of the Dominion Group took place between 3.09 and 3.07 Ga. Deposition at the West Rand Group commenced subsequently at 2.97 Ga, i.e. with a 100 Ma hiatus appearing between the West Rand and Dominion Groups.

15
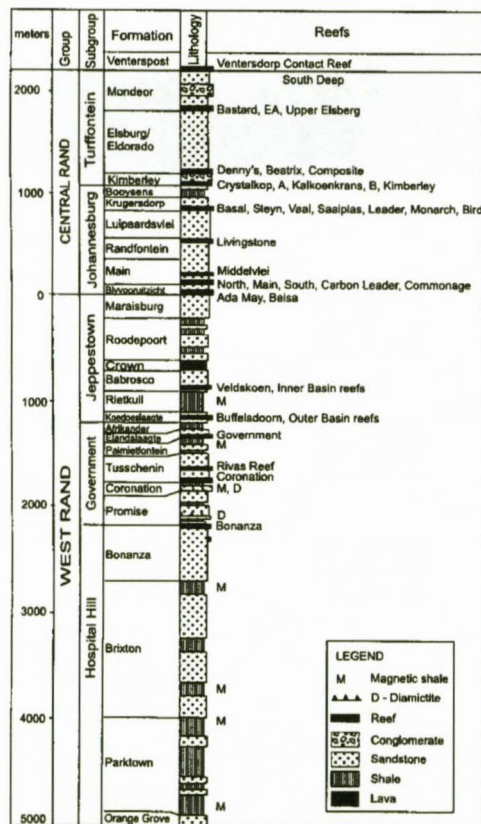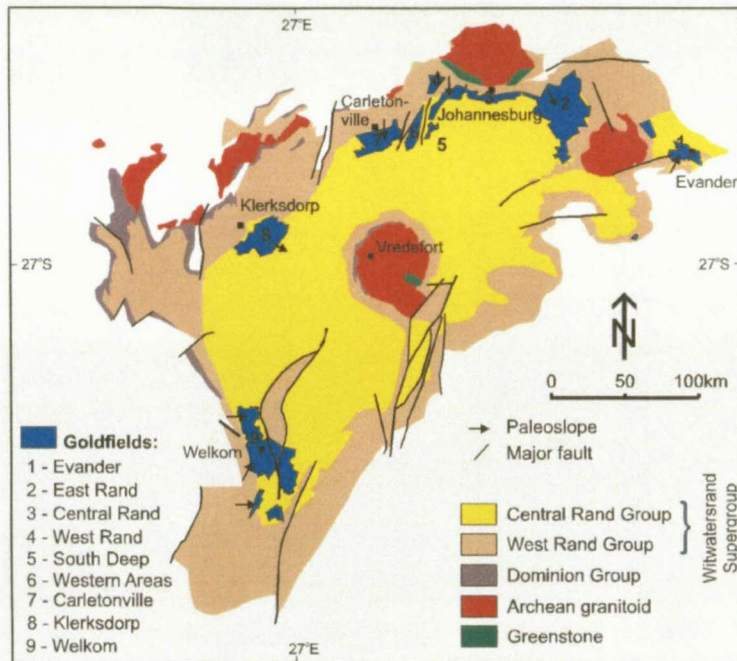
**Figure 2-3 Simplified geological map with the major goldfields and a generalized stratigraphic column of the Witwatersrand Supergroup (after Frimmel and Minter, 2002; Frimmel, 2005).**

The completion of deposition of the West Rand Group is marked by the Crown lavas which extruded at 2.91 Ga and which were followed by the deposition of the Central Rand Group. The Ventersdorp lavas extruded at 2.78 Ga to overlie the Central Rand Group (Robb and Meyer, 1995; Robb and Robb, 1998; Frimmel and Minter, 2002; Frimmel, 2005).

The West Rand Group is divided into Hospital Hill, Government and Jeppestown subgroups, whereas the Central Rand Group is divided into Johannesburg and Turffontein subgroups (Figure 2-3).

Most of the economically important Witwatersrand reefs are concentrated within the Central Rand Group and the locations of the different gold reefs are shown in Figure 2-3 (Robb and Meyer, 1995; Robb and Robb, 1998; Frimmel and Minter, 2002). The Central Rand Goldfield is located around Johannesburg and is the second most productive gold producer after the East Rand Goldfield. It is composed of the Main Reef, the Main Leader Reef and the South Reef, where most of the gold has been won. City Deep Mine is located at the lowest portion of the Main Reef (Robb and Robb, 1998).

The ore bodies within the Welkom Goldfield occur within the Central Rand Group, which sub-outcrops beneath the younger cover comprising the Karoo and the Ventersdorp sequence. They contain the Basal Reef and the Leader Reef, which both contain the A and B Reefs. The B Reef is mined sporadically mainly at the Lorraine and Free Gold North Mines (Robb and Robb, 1998).

The Carletonville Goldfield is located within the Central Rand Group at the base of the Ventersdorp lavas, and the most economic horizon includes the Carbon Leader

17

and the Middelvlei reefs.

The Klerksdorp Goldfield occurs within the Central Rand Group and has produced about 4900t of gold. It is composed of the Vaal Reef and the Ventersdorp Contact Reef (Robb and Robb, 1998).

The West Rand Goldfield consists of exposed rocks of both the Central Rand Group and the West Rand Group, covered by the younger Ventersdorp and Transvaal sequence. The other goldfields in the Central Rand Group include Evander and South Rand (Robb and Robb, 1998), which will not be discussed in this project as no samples from these areas were included in the research.

Table 2-1 Macroscopic descriptions of the visible gold samples collected in South Africa. The sample numbers are those assigned by the donors. Where applicable, samples are referred to figures.

| Sample no. | Gold deposits (Locality) | Geological setting and the environment of formation | Sample description |
|---|---|---|---|
| G84 (a) | City Deep Mine | City Deep gold deposit is located in the rocks of the Central Rand Group of the Witwatersrand Basin. The modified placer gold deposit was later modified by hydrothermal fluids. | The gold ore sample consists of rounded milky quartz pebbles. The gold has mineralized within the quartz pebbles along with sulphide minerals like sphalerite and galena. The gold ore also consists of a metamorphic mineral chlorite. The grains are >1.8 mm (Figure 2-5). |
| G84 (b) | City Deep Mine | Same as above. | The gold ore sample consists of milky quartz. The grains are <2 mm. The gold has mineralized within the quartz grains with pyrite and galena. The reddish colour on the surface of the ore is due to the presence of hematite. |
| 2B602 | Inner Basin Reef | The gold deposit is a modified placer. | The ore consists of a poorly sorted quartz pebble conglomerate. The pebble size ranges from 1 to 3 cm in diameter. The gold is finely (<2 mm grain size) disseminated within the host rock. |
| 2B603 | Carbon Leader Reef | The gold deposit is located in the Witwatersrand Basin, within the rocks of the Central Rand Group of the Welkom Gold fields. The gold deposit is a modified placer (Robb and Meyer, 1995; Robb and Robb, 1998; Frimmel and Minter, 2002; Frimmel, 2005). | The ore consists of well-sorted sandstone. There is a carbon layer with cleavage perpendicular to the bedding plane. The gold mineralization is associated with the cleavage direction. The gold is fine grained (>2.5 mm) and disseminated within the host rock. |
| 2B604 | Leader Reef | Same as in Carbon Leader Reef. | The gold ore consists of well-rounded and angular grains of quartz. The quartz grains are >1 cm and poorly sorted. The mineral chlorine is present in the ore. Gold grains are > 2 mm. |
| 2B605 | C Reef | Same as in Carbon Leader Reef. | A conglomerate ore consists of poorly sorted well-rounded pebbles. The ore contains of a distinctive layer of carbon approximately 2 mm thick. The gold has mineralized within this layer in between the quartz grains. The pebble grain size ranges from 0.5 to 1 cm. The gold grains are <2 mm. |
| 2B607 | B Reef | Same as in Carbon Leader Reef. | The gold is hosted in fine-grained and well sorted sandstone. The sandstone contains of a distinctive layer of carbon where gold has mineralized. The gold grains are <2 mm. The gold is associated with other sulphide minerals like |

| Sample no. | Gold deposits (Locality) | Geological setting and the environment of formation | Sample description |
|---|---|---|---|
| | | | pyrite. |
| 2B608 | South Deep Mine | Same as in Carbon Leader Reef. | The gold is associated with the mineralized quartz vein confined by pyritic ore. The gold grains are <2 mm and disseminated within the quartz vein. |
| 2B609 | Birimiam Reef | The information of this Reef was not provided by the donor. | The ore consists of milky white quartz veins and occasionally clear quartz crystals. The gold grains are <2 mm. Mineralization occurred within inter-locked grains of quartz parallel to the bedding. |
| MGS10591 | New Consort Mine | The gold deposit is located in the Barberton Greenstone Belt. The gold deposit is located between the contact zone of the Onverwacht Group and Fig Tree Group rocks. The mineralization is hydrothermal and associated with komatiite volcanics (Cochran, 1982; Viljoen, 1984; Anhaeusser and Maske, 1986). | The gold ore is dark greenish in colour due to the ferro-magnesium rock forming minerals. The gold grains are >2 mm. The other sulphide minerals (pyrite, arsenopyrite) are present (Figure 2-6). |
| MGS (?) | Sheba Mine | The gold deposit is located in the Barberton Greenstone Belt, within the metasedimentary rocks of the Moodies Group within the Main Reef Complex and the Zwartkoppie ore shoot (Anhaeusser, 1974; Wagner and Wiegand, 1986; Schürmann et al., 2000). | The gold ore consists of quartz. The gold grains are <2 mm and disseminated within the host rocks. |
| MGS 101 (a,b) | Agnes Mine | The gold deposit is located in the Barberton Greenstone Belt, within the metasedimentary rocks of the Moodies Group. The mineralization is hydrothermal (Houstoun, 1987). | **MGS 101(a):** The gold ore consists of smoky quartz, with fractures in two directions. The surface is reddish in colour, due to the presence of hematite. Occasionally yellowish in colour because of goethite present. Gold grains are >3 mm and occur as massive throughout the host rock (Figure 2-7).<br><br>**MGS 101(b):** The gold ore consists of smoky quartz, with fractures in two directions. The surface is reddish in colour, due to the presence of hematite. Occasionally yellowish in colour because of the goethite present. Gold occurs as massive throughout the host rock, with grains >3 mm. |
| MGS (?) | Birthday Mine | The gold deposit is located in the Giyani Greenstone Belt, within the rocks of BIF, quartzite, tremolite-actinolite schist, amphibolites and minor dolomites. Mineralization occurred in | The gold ore consists of smoky quartz. The reddish brown colour is due to the presence of hematite. The gold is disseminated within the host rock. Mineralization occurred within the quartz vein (Figure 2-8). |

| Sample no. | Gold deposits (Locality) | Geological setting and the environment of formation | Sample description |
|---|---|---|---|
| | | quartz and is associated with sulphide replacement (de Wit et al., 1992; Brandl and de Wit, 1997; Gan and van Reenen, 1997; Ward and Wilson, 1998). | |
| MGS102, 112 (a,b) | Marabastadt Goldfield | The gold deposit is located in the Pietersburg Greenstone Belt, within felsic, mafic and ultramafic and volcano-sedimentary rocks of the Uitkyk Formation. | **MGS 102:** The gold ore is reddish brown on the surface due to the presence of iron rich minerals. The gold has mineralized within the highly weathered zone. The gold grains are (<1.5 to 2 mm) disseminated throughout the host rock.<br><br>**MGS 112a:** The gold ore is reddish and consists of milky quartz. The gold ore was highly weathered on the surface. Gold grains are <1.5 to 2 mm and disseminated throughout the host rock (Figure 2-9).<br><br>**MGS 112b:** The gold ore consists of clear rounded grains of quartz. The grains are cemented together by calcrete and iron cement. There is a presence of hematite and goethite giving rise to yellowish and reddish spots. The gold is visible and finely (<1.5 to 2 mm) disseminated throughout the host rock (Figure 2-9). |
| G80 | Gravellotte Mine, Murchison Greenstone Belt | The gold deposit is hosted at the rocks of the Murchison Greenstone Belt. Mineralization has occurred within the antimony mine. | The host mineral is antimony. The gold is visible and massive with grains <2 mm (Figure 2-10). |
| G85 (three samples) | Sabie Pilgrims Rest Goldfield | The gold deposit occurs within the rocks of the Proterozoic Transvaal Supergroup in the Malmani Subgroup of the Chuniespoort Group. The gold is hosted in sheet-like gold-quartz-carbonatite-sulphide veins (Tyler and Tyler, 1996; Harley and Charlesworth, 1996; Killick and Scheepers, 2005). | **Lydenburg (A):** Gold nuggets, five pieces. The gold grains are >2mm. The gold is associated with the heavy minerals like galena and sphalerite with some hematite (Figure 2-11).<br><br>**Goedeverwacht (B):** The gold ore is reddish to yellowish in colour due to the presence of iron rich minerals (hematite and goethite). Gold grains are >2 mm (Figure 2-11).<br><br>**New Chum Pilgrims Rest (C):** The ore is reddish brown due to the presence of hematite. The gold is finely disseminated with grains <2 mm (Figure 2-11). |
| G30 | De Kaap Goldfield, Transvaal | The information of this gold deposit was not | The gold ore consists of clear quartz. The surface of the |

| Sample no. | Gold deposits (Locality) | Geological setting and the environment of formation | Sample description |
|---|---|---|---|
| | | found in literature. | quartz is occasionally reddish due to the presence of hematite. Gold is finely disseminated with grains <2 mm. The gold mineralization has occurred along the available fractures in quartz. |
| MGS111 (a,b) | Knysna Mine | Situated about 17 km north west of Knysna. The gold is hosted within the rocks Table Mountain Group of the Cape Supergroup. Mineralization has occurred in quartz at the Millwood Gully, a tributary of Hominy River discovered by Thomas Bain in 1886. | **MGS111a:** The ore consists of milky quartz. The gold ore is light greenish in colour with a prominent cleavage in one direction. There is a presence of galena mineral. Gold was visible and localized throughout the host rock with grains >2 mm.<br><br>**MGS 111b:** The ore consists of milky quartz. The gold is localized throughout the host rock with grains >2 mm (Figure 2-12). |

## 2.2 Zimbabwe Gold Ores

The Zimbabwean gold ore samples were obtained from the Museum of Human Sciences (formerly Queen Victoria Museum) in Zimbabwe and Iziko Museums in Cape Town. Gold ore samples were originally from the following gold mines (Figure 2-4): Reef of Gaika, Don Selukwe, Yankee Doodle and Lower Gwelo mines from the Midland Greenstone Belt; Mberengwa (Belingwe) Mine from the Belingwe Greenstone Belt; Hope Reef from the Harare Greenstone Belt; Gadzema from the Buchwa Greenstone Belt; Victoria Reef from the Masvingo Greenstone Belt; and Zambezi gold ore. Geographical coordinates information of the gold ores was not provided by the donor. Bartholomew (1990) has the list of mines with geographic coordinates, and this information was useful. Samples received with names similar to gold mines were located on a geological map (Figure 2-4). The general descriptions of the Zimbabwean gold ore samples are presented in Table 2-2.

Gold ore deposits in Zimbabwe are associated with Archaean granitoid rocks (Figure 2-4) or greenstone xenoliths within the granitoids (Campbell and Pitfield, 1994; Kalbskopf and Nutt, 2003). They are classified into stratabound and non-stratabound deposits and they are distributed within the rocks of the Sebakwian Group (3.5 Ga), Bulawayan Group (2.9 Ga to 2.7 Ga) and Shamvaian Group (2.7 Ga) (Foster and Wilson, 1984; Dirks and van der Merwe, 1997; Dirks *et al.,* 1999). The stratabound deposits comprise BIF that are intercalated with volcanics and sedimentary lithologies; whereas approximately 60 % of the non-stratabound gold deposits were derived from the mafic rocks, 17 % from ultramafic rocks, 13 % from the granitoid rocks and relatively small quantities from the felsic volcanics and sedimentary lithologies (Foster and Wilson, 1984).

23

The Zimbabwean gold mineralization is thought to have occurred in three phases. The hydrothermal phase associated with the mineralization event occurred at $2.65 \pm 0.06$ Ga, which was followed by another metamorphic event that occurred between 2.52 and 2.56 Ga; a post cratonic event associated with the intrusion of the Great Dyke of Zimbabwe is dated about $2.41 \pm 0.07$ Ga (Campbell and Pitfield, 1994). The minerals associated with gold from the granitic complexes are arsenopyrite, chalcopyrite, galena, molybdenite, pyrite, pyrrhotite, scheelite, sphalerite and stibnite (Mann, 1984). The mineralization style of the Zimbabwean greenstone belts is similar to the greenstones in the Kaapvaal Craton in South Africa and Yilgarn Block in Australia (Groves *et al.*, 1998; Houstoun, 1987; Martin, 1993).
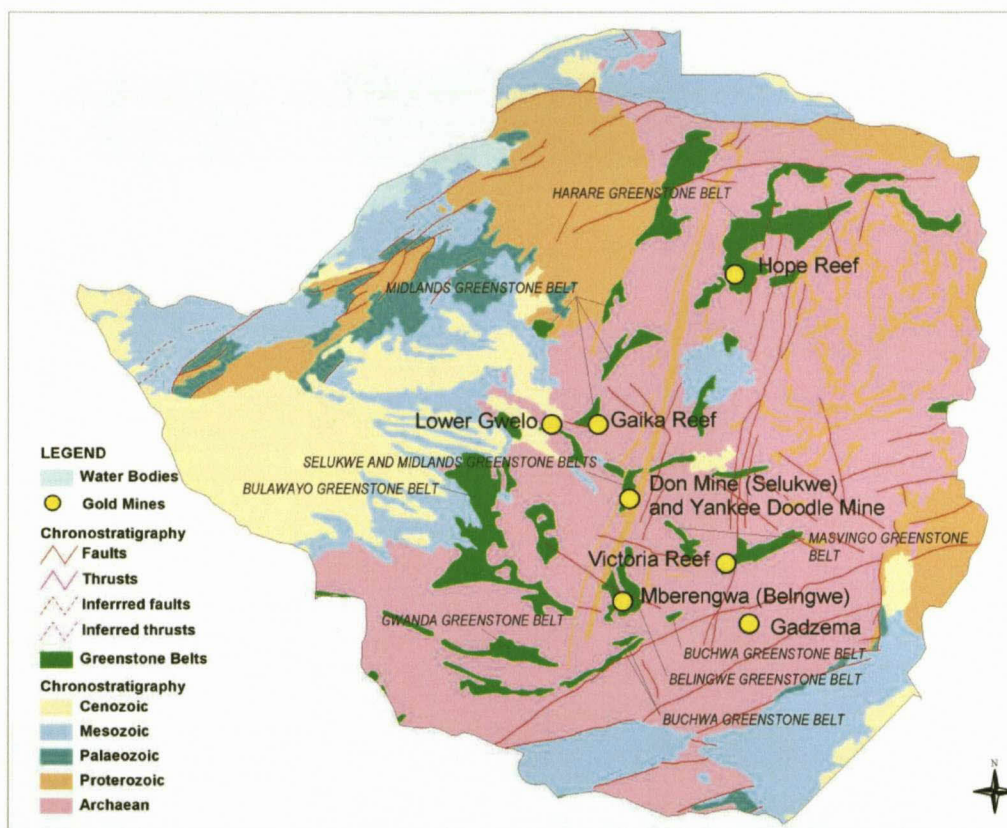


**Figure 2-4 A simplified geological map showing different gold ore deposit localities and the adjacent greenstone belts in Zimbabwe (Buitendag, 2007).**

24

Table 2-2 Macroscopic descriptions of the visible gold samples collected in Zimbabwe. The sample numbers are those assigned by the donors. Where applicable, samples are referred to figures. Continued on page 26.

| Sample no. | Gold deposits (Locality) | Geological setting and the environment of formation | Sample description |
|---|---|---|---|
| G24 | Gaika Reef, Gwelo district | Gold is mineralized at the Kwekwe Ultramafic Complex of the Midland Greenstone Belt. Gold is hosted in talc-carbonatite schist, magnesite rock, tonalitic gneiss (diabase, keratophyre dykes) on greenstone margin (Bartholomew, 1990; Campbell and Pietfield, 1994). The gold is hydrothermal. | Striation pattern was identified in the host rock. The gold has mineralized with pyrite and galena in talc-dolomite schist. The gold is visible and massive, and seems to follow the striation pattern on the contact zone. The gold has a grain size of >2 mm (Figure 2-13). |
| G34 (a, b) | Hope Reef, Millwood gold | Greenstone (hydrothermal) | The host rock is light greenish in colour and consists of quartz. The gold ore has carbonate minerals as it fizzes with HCl. Gold was visible, localized and fine grained (<2 mm) and disseminated throughout the host rock. |
| G117 | Belingwe Mine | Gold is hosted in tonalitic gneiss, amphibolite, sepentine, and/or mylonite schist in gneiss of the Mtshingwe Group in the Mberengwa (Belingwe) Greenstone Belt (Martin, 1993; Campbell and Pietfield, 1994). The gold is hydrothermal. | The ore is greenish due to the presence of the malachite mineral. The gold is visible and consists of grains <1 mm (Figure 2-14). |
| G123 | Don Mine, Selukwe | The host rocks are mafic greenstone, schist, serpentine, and granite in the major Archaen shear zone at the Kwekwe Ultramafic Complex of the Midland Greenstone Belt. The gold is hydrothermal. | The ore consists of quartz. The quartz has vessel-like structures and mineralization has taken place within these structures. Gold is visible and finely disseminated within the host rock. The gold grains are <2 mm. The gold is bronze yellow in colour with a metallic lustre (Figure 2-15). |
| G47 | Don Selukwe Mine | The host rocks are mafic greenstone, schist, serpentine, and granite in the major Archaen shear zone at the Midland Greenstone Belt. The gold is hydrothermal. | The gold ore consists of milky quartz. Mineralization has occurred along the fractured zone within the quartz. Gold is associated with some sulphide minerals (pyrite). Gold is visible and finely disseminated within the fractures of the host rock (Figure 2-15). |
| G124 | Yankee Doodle Mine | The gold is hosted on felsites, mafic greenstone, schist, serpentine and granite on the greenstone margin. The gold deposit is also hosted within the rocks of the Kwekwe Ultramafic Complex of the Midland Greenstone Belt. The gold is hydrothermal. | The gold ore was greenish especially at the mineralization zone where malachite is finely disseminated, along with pyrite or chalcopyrite. Gold was visible, likely to be finely disseminated (Figure 2-16). |

| G92 | Gadzema Mine | The host rocks are amphibolite and ultramafic schist in the major Archaen shear zone of the Buchwa Greenstone Belt. The gold is hydrothermal. | The gold ore consists of copper mineral (malachite), pyrite, and tiny disseminated chromite with other sulphide minerals. Gold was finely (<2 mm) disseminated, visible and localized throughout the host rock. |
|------|--------------|---|---|
| G79 | Lower Gwelo Mine | The gold deposit is associated with the hydrothermal process at the Midland Greenstone Belt. | The gold ore sample has a reddish and occasionally yellowish surface due to the presence of hematite and goethite respectively. The malachite is disseminated throughout the host rock. The gold has mineralised within the quartz zone. Gold was visible and massive likely disseminated within the host rock (Figure 2-17) |
| G43 | Gadzema Mine | The host rocks are amphibolite and ultramafic schist in the major Archaen shear zone of the Buchwa Greenstone Belt. The gold is hydrothermal. | The gold ore was greenish due to the presence of copper minerals (malachite and azurite). The gold is associated with some of the sulphide minerals like pyrite and galena. The gold is visible and finely (<2 mm) disseminated throughout the host rock. |
| G45 | Victoria Reef, Balabala | The gold deposit is hosted at the rocks of the Masvingo Greenstone Belt. | The gold ore sample consists of milky quartz. At the mineralized zone the quartz becomes smoky. The minerals presence in the ore includes hematite, galena and probably other sulphide minerals. The gold is visible, and massive, rather partly disseminated on the mineralized zone (Figure 2-18). |
| G72 | Zambezi (?) | The source and geological setting was not found in literature. It can be presumed to have come from the northern part of Zimbabwe at the alluvial deposit associated with the Zambezi river. | The gold ore is reddish due to the presence of iron rich minerals. The gold was visible and locally massive within the milky quartz. The gold in some places was disseminated. The gold grains range from <2 mm to 4 mm (Figure 2-19). |

## 2.3 Archaeological Artefacts

The archaeological artefacts were sourced from the Zimbabwean craton and were obtained from the Museum of Human Sciences (formerly Queen Victoria Museum) in Zimbabwe. The artefacts include the bangle fragments, the gold beads, the pellets, the foil fragments, the wire fragments and a tack fragment. The provenance details with the geographical coordinate system of the artefacts were received in the form of grid references. The descriptions of gold artefact samples are presented in Table 2-3 and Figure 2-20. The samples were given on the local grid in meters and were converted into proper latitude and longitude using ArcGIS software.

The Mapungubwe gold artefacts samples were described in detail by Desai, (2001). In the summary of Desai's (2001) descriptions, the following was evident: (1) Mapungubwe artefacts were marked as M1231 (A-F). (2) The artefacts types were mainly round gold beads starting from A to F. (3) The artefacts diameter was as follows: A = 3.5 mm; B = 3.2 mm; C = 2.1 mm; D = 1.9 mm; E = 2.1 mm; F = 3.4 mm. (4) The artefacts sizes were as follows: A = 2.2 mm; B = 1.5 mm; C = 1 mm; D = 1 mm; E = 1.3 mm; F = 2 mm. (5) The artefacts masses were as follows: A = 0.191 g; B = 0.099 g; C = 0.041 g; D = 0.037 g; E = 0.045 g; F = 0.201 g.

## 2.4 Sample Selection

A total of eighteen gold ore samples from South Africa were investigated and eleven from Zimbabwe. Not all the samples described here were analyzed because in some cases it was not possible to remove gold grains from the ore. The problem was probably due to the type of ore and the method used to remove the gold grains (see next chapter). The samples were not supposed to be destroyed or crushed, as

27

instructed by the donors. The samples which were excluded for these reasons are: Birimiam Reef, Birthday Mine, Gravellote Mine and De Kaap Goldfield in South Africa, as well as Hope Reef, Yankee Doodle Mine and Zambezi from Zimbabwe. The twenty-three artefacts from Zimbabwe archaeological artefact samples were all analyzed.

Table 2-3 Macroscopic descriptions of the archaeological artefacts collected in southern Africa. The Z number refers to Figure 2-20 and was used during the analysis. Terminology used for objects such as rings: OD = outer diameter, ID = inner diameter.

| Sample no. | Colour | Lustre | Descriptions of the artefacts | Diameter (mm) | Thickness (mm) | Length (mm) | Mass (g) |
|---|---|---|---|---|---|---|---|
| 4824 (Z1) Bangle fragment | Bronze yellow | Earthly to vitreous | A thin wire ring of gold, flattened on one side; consists of double coil | 3.2 | <1 | 2.5 | 0.160 |
| 4924 (Z2, 3) Bead (2) | Bronze yellow | Vitreous to metallic | A rounded bead showing no visible join, with barrel shape and flat ends | 2.4 | n/m | 1.3 | 0.05; 0.06 |
| 4835 (Z4) Gold bead | Yellow | Metallic | Hole, hour glass shaped (not uniform thickness) | 6.95 OD, 2.1 ID | n/m | 5.5 | 2.653 |
| 4836 (Z5) Bead | Bronze yellow | Metallic | Barrel shaped bead; consists of the flattened ends | 3.8 OD, 1.5 ID | n/m | 2.9 | 0.401 |
| 4839 (Z6) Pellet | Bronze yellow | Metallic | Spherical shaped pellet without hole | 2.9 | n/m | 3.2 | 0.315 |
| 4940 (Z7) Foil fragment | Yellowish, with brownish spots | Metallic | Platy, crumbled, short cut or tear on one side, no other holes | n/m | 6.45 and 3.0 | 7.8 | 0.065 |
| 4918 ((Z8 (a); Z9 (b)) Bead and fragment | Bronze yellow with some contamination | Metallic | Cylindrical, with flat ends with an hole (a), uncorked melting fragment, platy with irregular surface (b) | (a) 2.4 OD, 1.0 ID. | 6.7, 4.35, and 5.1 (b) | (a) 1.8 ; (b) 9.6 | (a) 0.100, (b) 4.478 |
| 4919 (Z10) Cylinder bead | Bronze yellow | Metallic | A tubular cylinder bead rolled up with smooth surface, made up of strip of foil or sheet | 3.1 | n/m | 9.8 | 0.216 |
| 4930 (Z11) pellet | Bronze yellow, with brownish spots | Vitreous to metallic | Oval or spherical shaped without uniform surface | 4.0; 3.3 | n/m | n/m | 0.498 |
| 4922 (Z12) Bead | Yellowish with dark brown spots | Earthly to metallic | Spherical, and barrel shaped with flattened ends | 2.7 OD, 1.1 ID | n/m | 2.1 | 0.132 |
| 4928 ((Z14 (a); Z15 (b)) Foil, Foil fragment | (a) Bronze yellow; and (b) | Both metallic | (a) Platy, or sheet-like structure; consists of thin layer bent to make double layer; (b) Irregular fragment; consists of hole on one side and bump on the other side | n/m | (a) 2.6; (b) 2.0 | (a) 4.1; (b) 3.2 | (a) 0.024; (b) 0.072 |

| Sample no. | Colour | Lustre | Descriptions of the artefacts | Diameter (mm) | Thickness (mm) | Length (mm) | Mass (g) |
|---|---|---|---|---|---|---|---|
| 4936 ((Z24 (a); Z22 (b); Z21(c) a) Wire Fragment; (b) Bead: and (c) Tack fragment | Bronze yellow (a), (b), and (c). | Metallic (a), (b), (c). | (a) Coil, long and rounded wire; (b) small spherical; (c) and platy | (a) 2.7; (b) 2.15; | (a) 1.6; (c) 2.0 | (a) 56.9; (b) 2.7; and (c) 2.3 | (a) 1.265; (b) 0.016; and (c) 0.039 |
| 4937 (Z16) Gold bead | Bronze yellow | Earthly to metallic | Cylindrical gold bead; consists of flat surface (flattened) and a hole. | 2.8 OD and an opening is 0.95 | n/m | 1.7 | 0.129 |
| 4938 (Z17) Gold bead | Bronze yellow with brown spots | Metallic | Cylindrical, hole | 4.0 OD and an opening is 1.5 | 0.6 | 1.3 | 0.106 |
| 4939 (Z18) Pellet | Bronze yellow with brown spots | Metallic | Nearly spherical with a pit on the surface | 4.8 | n/m | n/m | 0.430 |
| 4942 ((Z20 (a); Z23 (b); Z19 (c). (a) Foil fragment; (b) Wire fragment; and (c) Pellet | Bronze yellow for (a) and (b); (c) shows some brownish spots on the surface | Metallic for (a) and (b); (c) range from earthly to metallic | (a) Platy: (b) oval shaped; and (c) oval or rounded shaped (a) Thin layer with two tack holes; (b) elongated in an oval shape to form thin gold wire; (c) shows pitting on a surface | (c) 4.7 | (a) 5.5, and 0.2; (b) 0.4 | (a) 9.5; (b) 48.3 | (a) 0.060; (b) 0.090; (c) 0.370 |
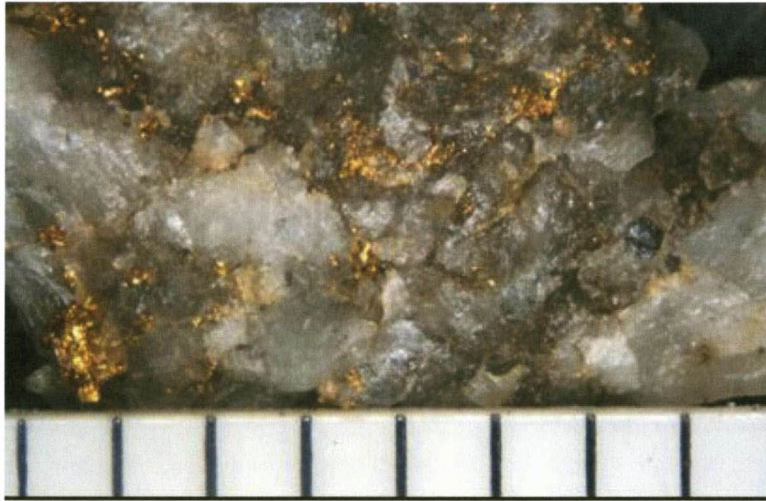
**Figure 2-5 Gold ore from City Deep Mine (G84) located in the Witwatersrand Supergroup (scale divisions = 2.5 mm).**



**Figure 2-6 Gold ore sample from New Consort Mine (MGS10591) located in the Barberton Greenstone Belt (scale divisions = 2.5 mm).**

31
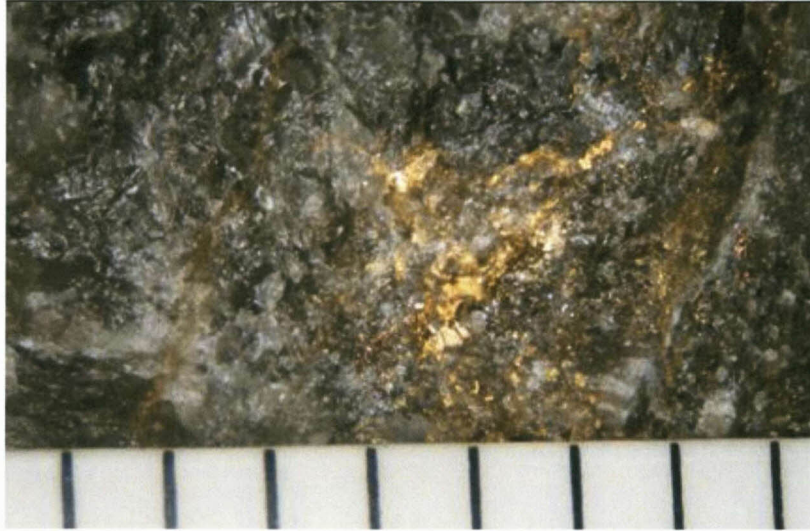
Figure 2-7 Gold ore sample from the Agnes Mine (MGS101) located in the Barberton Greenstone Belt (scale divisions = 2.5 mm).
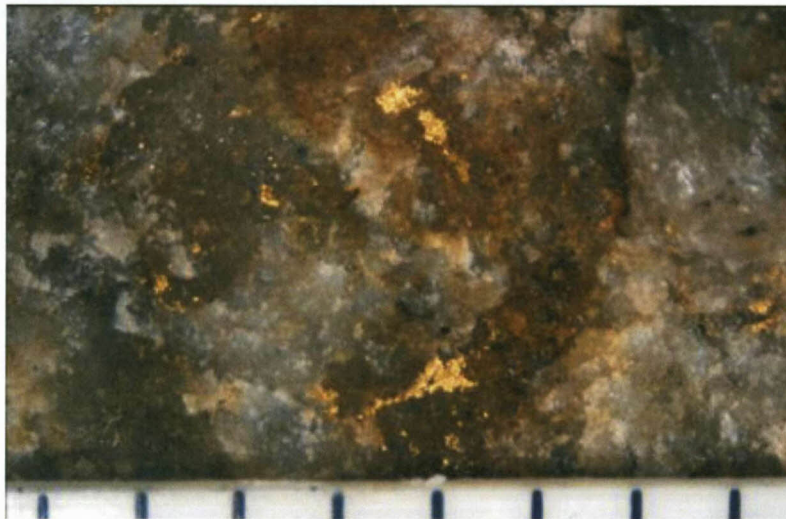


Figure 2-8 Gold ore sample from Birthday Mine (MGS) located in the Giyani Greenstone Belt (scale divisions = 2.5 mm).

32

Figure 2-9 Two gold ore samples from Marabastadt (MGS112 (a, b)) located in the Pietersburg
Greenstone Belt (scale divisions = 2.5 mm).

**Figure 2-10 Gold ore sample from Gravelotte Mine (G80) located in the Murchison Greenstone Belt (scale divisions = 2.5 mm).**
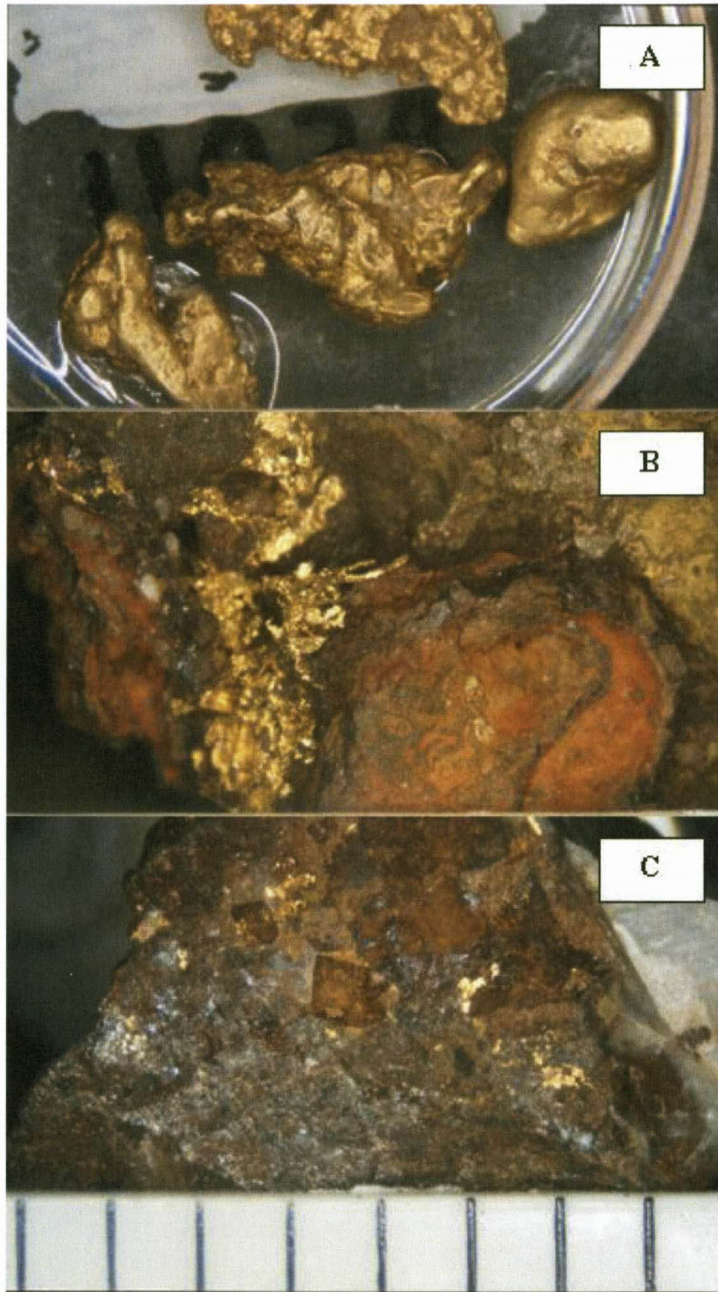
**Figure 2-11 Three gold ore samples from Sabie Pilgrim's Rest Goldfield (G85): A. Lydenburg B. Goedeverwacht at Lydenburg C. New Chum Pilgrim's Rest Goldfield (scale divisions = 2.5 mm).**

**Figure 2-12 Gold ore sample from Knysna Mine (G111b) located in the Cape Supergroup (scale divisions = 2.5 mm).**



**Figure 2-13 Gold ore sample from Gaika Reef (G24) located in the Midland Greenstone Belt (scale divisions = 2.5 mm).**
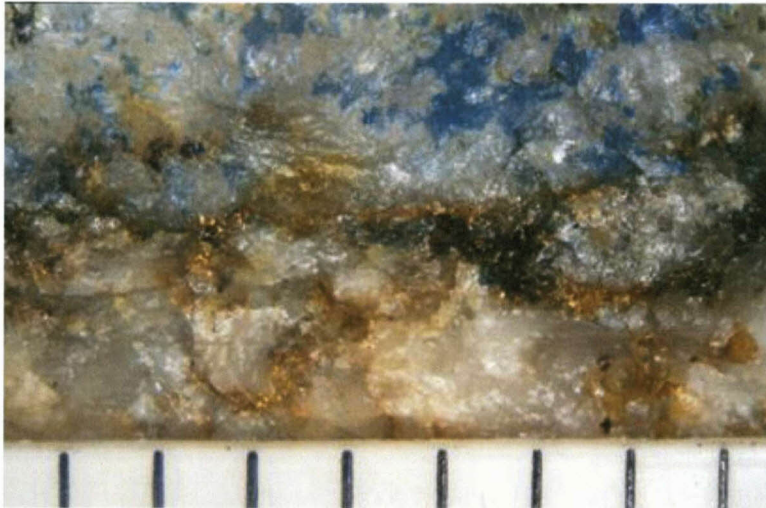
Figure 2-14 Gold ore sample from the Mberengwa (Belingwe) Greenstone Belt (G117) (scale divisions = 2.5 mm).

**Figure 2-15 Gold ore sample from Don Selukwe Mine located in the Midland Greenstone Belt: A is G 123 and B is G 47 (scale divisions = 2.5 mm).**

**Figure 2-16 Gold ore sample from Yankee Doodle Mine (G124) located in the Midland Greenstone Belt (scale divisions = 2.5 mm).**
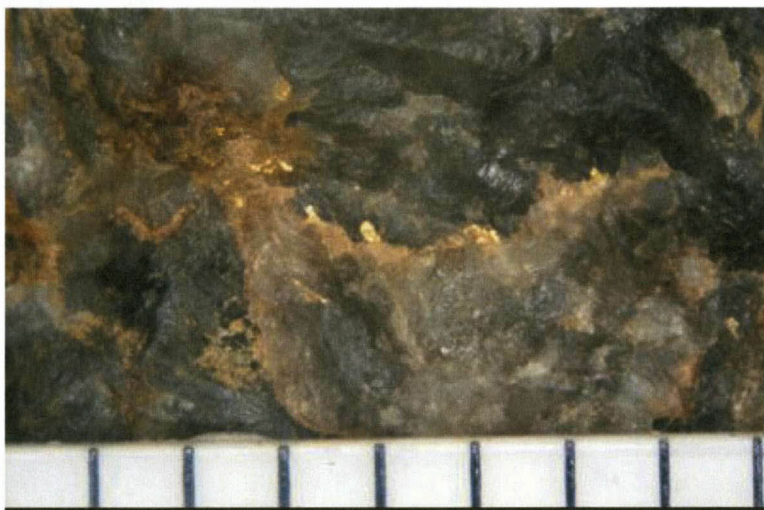


**Figure 2-17 Gold ore sample from Lower Gwelo Mine (G79) located in the Midlands Greenstone Belt (scale divisions = 2.5 mm).**
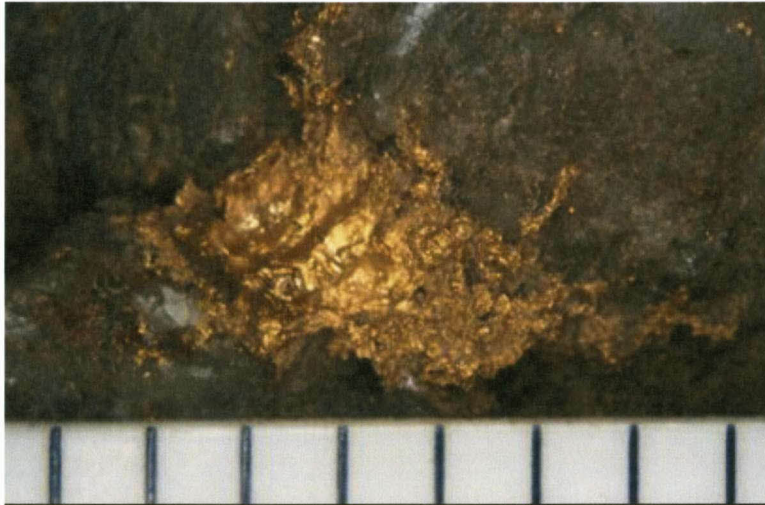
**Figure 2-18 Gold ore sample from Victoria reef (G45) located in the Masvingo Greenstone Belt (scale divisions = 2.5 mm).**
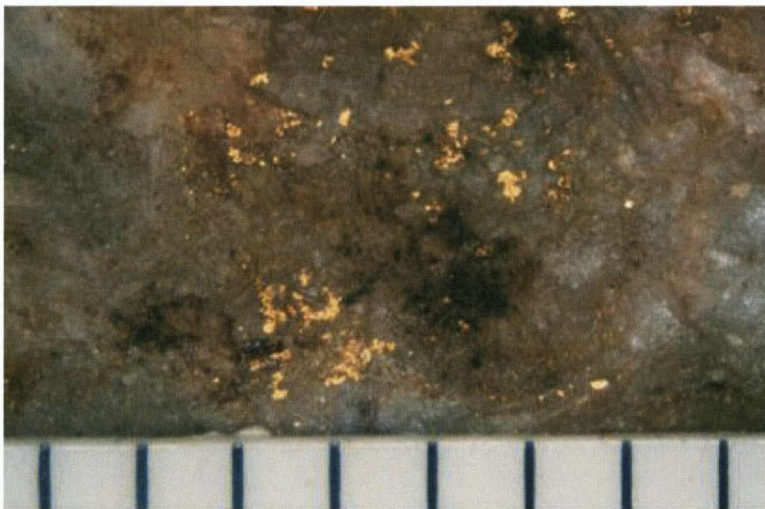


**Figure 2-19 Gold ore sample from Zambezi (G72) (scale divisions = 2.5 mm).**
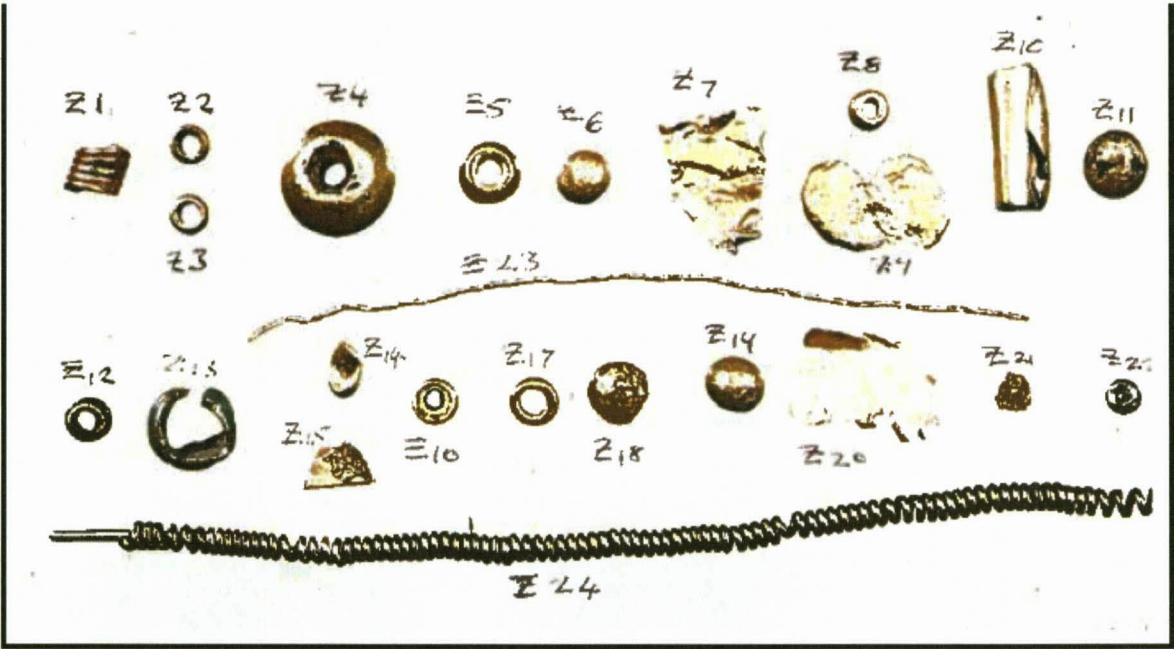
Figure 2-20 The archaeological gold artefacts from Great Zimbabwe.

# 3 SAMPLE PREPARATION AND ANALYTICAL METHODS

The native gold and artefact samples were analyzed for trace and ultra-trace elements by laser ablation inductively coupled mass spectrometry (LA-ICP-MS). The silver concentration in the gold samples was analyzed by a scanning electron microscope (SEM).

The large sizes of the ore samples meant that they could not be mounted into the sample chambers of the instruments and therefore required pre-analytical sample preparation. This was kept to a minimum for both analytical techniques (to avoid causing alteration to the chemistry of the gold) and involved removal of the visible gold grains from the ore sample in the following way: The grains were removed with a pair of tweezers, mounted on a glass slide and secured with glue (cyanoacrylate adhesive), using optical microscope with reflected light and a magnification range of between 8 to 20x. The slides were then placed directly into the sample chamber. No pretreatment was required for the artefact samples as they were small enough to be placed into the sample chamber whole.

## 3.1 Scanning Electron Microscope (SEM)

The SEM consists of an electron gun, in conjunction with an energy dispersive X-ray spectrometer (EDEX-type), which enables semi-quantitative chemical analyses to be carried out. A Cambridge S200 SEM in the Electron Microprobe Unit of the University of Cape Town was used to obtain the data reported on in this study.
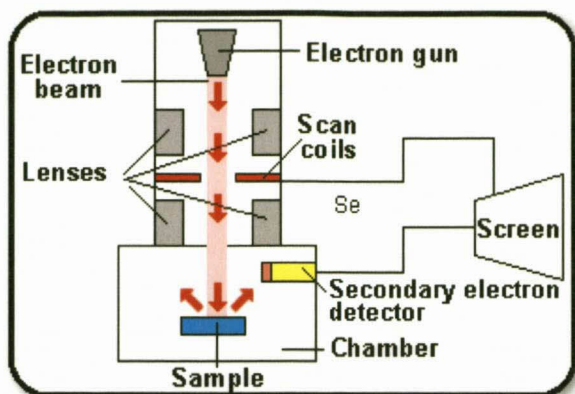
**Figure 3-1 A schematic representation and a picture of the Scanning Electron Microscope at the University of Cape Town (UCT) (http://sbio.uct.ac.za/Webemu/SEM_school/)**

Figure 3-1 shows that a SEM consists of an electron gun, which produces a stream of electrons. A set of coils scans or sweeps the beam in grid fashion, dwelling on points for a period of time determined by the scan speed (in microsecond range). When the beam strikes the surface of the sample material, different interactions take place. Some electrons from the surface material are knocked out of their orbitals and are called secondary electrons. These electrons are detected by the secondary electron detector. The SEM can magnify up to 100 000 times. The images can be on topography, elemental composition or density of the sample.

In EDEX-type analysis, the whole spectrum of X-ray energies emitted by an irradiated sample is recorded simultaneously and the typical time of analysis is 100s with a count rate of several counts per second, giving precision in the order of ±1 % (Reed 1995). The operating conditions used in this study are shown in Table 3-1.

Samples were not coated since gold has high electrical and thermal conductivity and can prevent the accumulation of electric charge on the specimen during analysis. The silver concentration results (in wt %) are presented in the following chapter.

**Table 3-1 The operating conditions of the SEM for the analysis of gold and silver concentrations in gold.**

| SEM Conditions | |
|---|---|
| **A. General** | |
| Background method | Fit |
| Devolution method | Gaussian |
| Devolution ChiSquared | 10.16 |
| **B. Analysis** | |
| Quantitative method | ZAF |
| Acquired time | 60 s |
| Normalization factor | 100 |
| **C. Sample** | |
| Accelerating voltage | 20 keV |
| Beam current | 200 Pico Amps |
| Working distance | 25.00 mm |
| Tilt angle | 0.0 Degrees |
| Takeoff angle | 35.0 Degrees |
| Solid angle | 1.2 |

## 3.2 Laser Ablation Inductively Coupled Mass Spectrometry (LA-ICP-MS)

The ELAN 2000 CETAC LSX200 ICP-MS in the Department of Geoscience at the University of Cape Town was used in this study in conjunction with a CETAC LSX200 Nd:YAG laser for vaporising the solid samples. The LA-ICP-MS method was chosen because of its capability to analyze solid samples *in situ* for major, trace and ultra-trace elements. Furthermore, the detection limits of this technique for the elements of interest are down to the part per million (ppm) range (Ohata *et al.*, 2002; Günther and Hattendorf, 2005).

Another advantage of using a laser is that it permits high-resolution direct sampling

44

without the need for lengthy chemical sample preparation. Lengthy dissolution processing may be incomplete and can also potentially introduce contamination to the sample (Longerich *et al.,* 1993, 1996; Jarvis *et al.,* 1995). The use of a laser for solid sampling is considered non-destructive, because the size of the ablated pit is very small ($\mu$m in diameter) (Jackson *et al.,* 1992; Hall *et al.,* 1998; Vlachou-Mogire *et al.,* 2007).
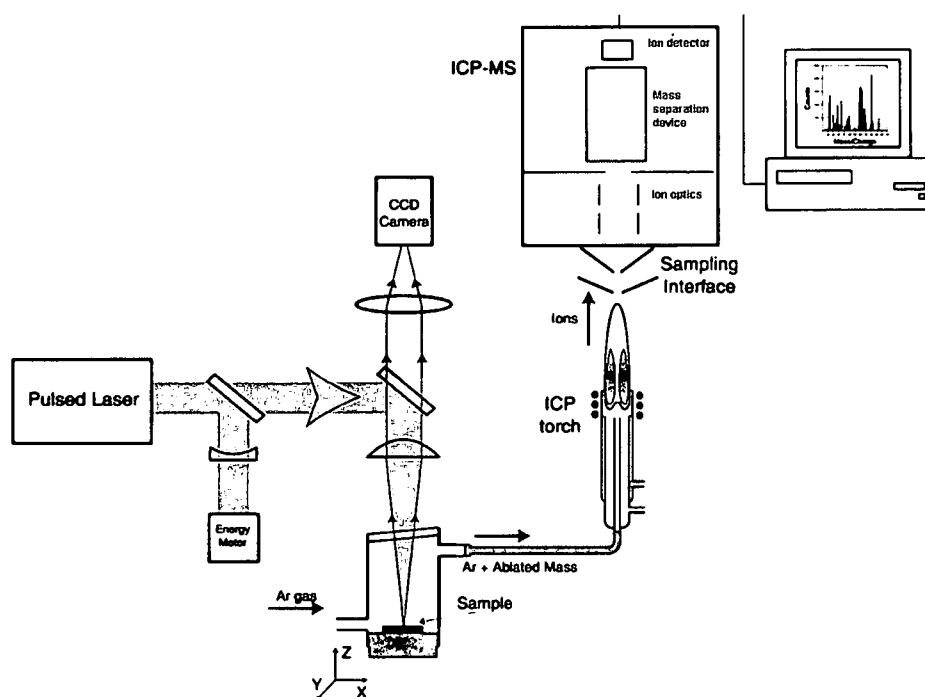


**Figure 3-2 A schematic diagram showing the general components of the ICP-MS analytical technique and laser for solid sampling (after Russo *et al.,* 2002).**

The disadvantages of the LA-ICP-MS include the limit of detection dependent on the laser resolution compared to some other micro beam techniques (Vlachou-Mogire *et al.,* 2007). There is also a need for well-characterized homogenous standards in order to obtain accurate results. Elemental fractionation, which is the sum of all non-stoichiometric effects occurring during the ablation process, transport to and

45

ionization in the ICP source, can limit precision and accuracy.

The general components of a typical LA-ICP-MS are shown in Figure 3-2. The operational procedure is commonly as follows: A dry sample is ablated and then introduced into the plasma. The ablated materials are atomized and ionized, which results in a lack of polyatomic interference species produced by the interaction of water and acid species with the argon plasma (Longerich *et al.*, 1993; Watling *et al.*, 1994, 1999). Exceptions include some of the large particles that are not completely ionized and likely cause elemental fractionation.

As can be seen from Figure 3-1 a LA-ICP-MS machine is divided into four sections, namely; sample introduction area, plasma chamber and interface region, mass separation device and ion detector. The sample chamber consists of a quartz glass relatively transparent to UV light at 266 nm. It is designed to allow an argon gas to enter through a small opening in the floor, swirl in a cyclonic pattern through the interior and exit at the top with the ablated material in the form of a fine (<1 μm) aerosol to the ICP source (Günther *et al.*, 1999; Longerich and Diegor, 2001).

The argon gas transports fine aerosol through the plasma torch to the ICP source (Outridge *et al.*, 1998; Günther *et al.*, 1999). The aerosol is then atomized into a gas phase and then ionized (Thomas, 2001). Only a portion of the plasma gas generated is then directed through to the interface region. In this region, residual gas is separated from the positive ions and pumped away. The positive ions pass through the ion optics, where they are guided into the quadrupole to be detected separately, depending on mass to charge ratio (Perkins and Pearce, 1995; Longerich and Diegor, 2001; Thomas, 2001). The opposite charged rods of the quadrupole allow only one species or ion, according to the selected mass to charge ratio, to make its way through to the

ion detector (Longerich and Diegor, 2001).

An ion detector consists of a semi-conductor to attract ions that make their way from the quadrupole along a curved path through to the electron multiplier detector, which strengthens the signal. An ion will hit the first dynode and produce electrons. The electrons produced at the first dynode are attracted to the second dynode and produce more electrons. The electrons are then measured as an electrical pulse that can be counted on a multi-channel analyzer. The multi-channel analyzer consists of 6 000 channels and each mass typically has 20 channels assigned to it in this current research.

**Table 3-2 A list of elements (isotopes) commonly occurring in gold, which were selected for analysis on the basis of natural abundance, as well as the ones with least interference.**

| ELEMENT | ISOTOPE(S) | REASON FOR A CHOICE |
|---------|------------|---------------------|
| Fe | 56 | Most abundant |
| Co | 59 | Most abundant |
| Ni | 60 | Least interfered |
| Cu | 63 | Most abundant |
| Zn | 66 | Least interfered |
| As | 75 | Least interfered |
| Pd | 105 | Least interfered |
| Ag | 107,109 | Most abundant |
| Pt | 195 | Most abundant |
| Hg | 202 | Least interfered |
| Pb | 204, 206, 207, 208 | Most abundant |
| Bi | 209 | Most abundant |

The isotopes that were selected for analysis are shown in Table 3-2. Criteria for selection were based on the most abundant and commonly occurring elements in gold (as discussed in Chapter one), as well as the "least interfered with" isotopes, i.e. those which were not subject to isobaric overlap. Most of the isotopes omitted for this study were the rare earth elements, which were below the limit of detection. The limit of detection was calculated as three times the mean background values and is listed in Table 3-3.

Table 3-3 The lower limit of detection (LLD (3 times mean background values)) for the isotopes selected for analysis by LA-ICP-MS. Values are in counts per second (cps) and 1-3 are repeat measurements of a blank sample.

| Isotopes | Background at mass value | | | Mean | 1σ | LLD |
|---|---|---|---|---|---|---|
| | 1 | 2 | 3 | | | |
| $^{56}$Fe | 45 | 36 | 50 | 44 | 7 | 132 |
| $^{59}$Co | 0 | 2 | 1 | 1 | 1 | 3 |
| $^{60}$Ni | 4 | 2 | 1 | 2 | 1 | 6 |
| $^{63}$Cu | 5 | 6 | 3 | 4 | 1 | 12 |
| $^{66}$Zn | 1 | 1 | 1 | 1 | 0 | 3 |
| $^{75}$As | 6 | 4 | 3 | 4 | 1 | 12 |
| $^{105}$Pd | 1 | 1 | 1 | 1 | 0 | 3 |
| $^{107}$Ag | 31 | 41 | 36 | 36 | 5 | 108 |
| $^{185}$Re | 1 | 1 | 1 | 1 | 0 | 3 |
| $^{188}$Os | 1 | 1 | 2 | 1 | 1 | 3 |
| $^{195}$Pt | 1 | 1 | 1 | 1 | 0 | 3 |
| $^{202}$Hg | 10 | 8 | 10 | 10 | 1 | 30 |
| $^{204}$Pb | 1 | 1 | 1 | 1 | 0 | 3 |
| $^{206}$Pb | 3 | 4 | 2 | 3 | 1 | 9 |
| $^{207}$Pb | 6 | 7 | 4 | 6 | 1 | 18 |
| $^{208}$Pb | 80 | 70 | 70 | 73 | 6 | 219 |
| $^{209}$Bi | 6 | 7 | 7 | 7 | 1 | 21 |

### 3.2.1 LA-ICP-MS procedure used for this work

The LA-ICP-MS operating conditions employed during this study are listed in Table 3-4. Different operational conditions of dwell time, spot size and the repetition rate

(Table 3-5) were set to obtain better precision. The data is presented in Table 3-6 below.

Total acquisition time (also known as sweep time) is defined as the total time required for the acquisition of intensity information from the complete list of selected masses (Longerich, 2001). A total time of 120s was used in this study, because the laser ablation signals are noisy, therefore the total time taken to collect data for the complete list of masses should be as short as possible.

**Table 3-4 Operating conditions of LA-ICP-MS in this study.**

| (a) Laser | |
|---|---|
| Laser type | Nd: YAG |
| Wavelength | 266 nm |
| Repetition rate | 5 Hz |
| Pulse energy | 10 mJ |
| Spot diameter | 150 µm |
| (b) Mass spectrometer | |
| RF power | 1250 W |
| Acquisition mode | Pulse counting |
| Dwell time | 20 ms |
| No. of replicates | 5 |
| Total acquisition time | 120 s |

Dwell time is defined as the time used acquiring data at a particular mass (Longerich, 2001; Vlachou-Mogire *et al.,* 2007). The same dwell time may be used for every mass. If the dwell time decreases, the fraction of time wasted on settling increases (Longerich *et al.,* 1996). Settling time is the time between acquisitions, while the

mass analyser and the detector are settling, following the discontinuous change in mass and ion signal (Gray, 1985; Longerich *et al.*, 1996).

**Table 3-5 Variation of operational conditions tested on samples A and B from Mapungubwe.**

| Samples | Conditions | Spot size(μm) | Repetition rate | Dwell time(ms) |
|---------|-----------|---------------|-----------------|----------------|
| A | M1 | 150 | 5 | 20 |
|   | M2 | 100 | 10 | 20 |
|   | M3 | 100 | 10 | 20 |
| B | M4 | 100 | 5 | 10.24 |
|   | M5 | 150 | 5 | 10.24 |
|   | M6 | 150 | 5 | 20 |

**Table 3-6 Comparative isotope response (cps) to different LA-ICP-MS technique operational conditions tested in two gold samples (A and B) from Mapungubwe.**

|  | M1 | M2 | M3 | M4 | M5 | M6 |
|---|----|----|----|----|----|----|
| $^{56}$Fe | 368 | 341 | 311 | 168 | 437 | 697 |
| $^{59}$Co | 1 | 1 | 1 | 1 | 3 | 4 |
| $^{60}$Ni | 10 | 5 | 6 | 17 | 61 | 76 |
| $^{64}$Cu | 1746 | 663 | 825 | 257 | 1141 | 1318 |
| $^{75}$As | 1219 | 1427 | 1509 | 522 | 482 | 893 |
| $^{202}$Hg | 18 | 7 | 9 | 3 | 13 | 15 |
| $^{204}$Pb | 23 | 10 | 13 | 6 | 23 | 12 |
| $^{206}$Pb | 296 | 111 | 153 | 63 | 328 | 144 |
| $^{207}$Pb | 326 | 117 | 159 | 68 | 353 | 159 |
| $^{208}$Pb | 748 | 261 | 367 | 158 | 777 | 370 |
| $^{209}$Bi | 667 | 238 | 306 | 82 | 418 | 192 |

In Table 3-5 and Table 3-6 it is clearly demonstrated that a spot size of 150 μm for both samples (M1 and M6) shows higher intensities (cps) for most isotopes, compared to the spot size of 100 μm, as expected. A spot size of 150 μm, therefore, was used in this research.

A pulse repetition rate of 5 was selected in consideration of the size of samples involved. A pulse repetition rate controls the rate of sample removal and consequently peak to background ratios and ablation time available for a given pit size (Vlachou-Mogire *et al.*, 2007). The natural gold samples were much smaller and thinner than

50

the gold artefacts, thus limiting the number of pulse repetition rates which could be used without burning a hole through the sample.

## 3.2.2  Effects of Mass Interference

There was a problem of isobaric mass interference, which was mainly produced by the presence of isotopes of different elements with the same mass, which resulted in a spectral interference at the mass of interest (Watling *et al.,* 1994; Thomas, 2001). Lead and mercury both have isotopes at mass 204, and nickel and iron at mass 58 (Table 3-7).

Table 3-7 Isobaric interferences at mass 58 and 204, with the elements involved and their relative natural abundances.

| MASS | ELEMENTS AFFECTED | NATURAL ABUNDANCES (%) |
|---|---|---|
| 58 | Ni | 63.3 |
| 58 | Fe | 0.28 |
| 204 | Pb | 6.9 |
| 204 | Hg | 1.4 |

The procedure of interference correction on masses listed in Table 3-7 was corrected as follows:

$$X = M - (n / m)(Y)$$

where $M$ is the total counts detected at the mass of interest (analyte mass), $X$ is the counts in the channel contributed by the isotope of interest, $Y$ is the counts of the interfering isotope measured at a different (interference-free) mass, $n$ is the natural abundance of the isotope which is causing the isobaric interference, and $m$ is the natural abundance of its sister isotope with the interference-free mass (Thomas,

51

2001).

## 3.3 Data Reduction and Quality

Data reduction was done by the selection of integration region for the background and analyte values. The first values of the background value were rejected to allow the stabilization of the laser induced plasma and rejection of the surface contamination. The integration region for the background and analyte values selected was averaged to get the mean net analyte signal. The mean net analyte was calculated as the difference between the mean gross (mean analyte plus mean background) and the mean background. Mass interference correction was done for the following isotopes: $^{58}$Ni, which was interfered with by $^{58}$Fe; $^{204}$Pb, which was interfered with by $^{204}$Hg. Mass interference corrections were done using the formula in section 3.2.2.

In order to assess the quality of data, a set of three internal gold reference standards was used to assess possible errors in the SEM data for gold and silver concentration. Pure gold and silver granules were melted together in appropriate proportions, using a jeweller's propane torch, to make up the reference standards for the SEM (D. Miller, pers. comm., 2005). These were in nominal 5 wt % steps, from 100 wt % gold (fine gold) downward (Table 3-8). Sources of potential error are in weighing the small quantities of gold and silver, possible minor losses of silver (because silver is a volatile element during melting), and possible minor contamination from the ceramic crucible used for melting the alloys (D. Miller pers. comm., 2005).

The result of the gold and silver concentrations has confirmed that the SEM data and the weighed values correlate with an R2 value of, hence the SEM data can be regarded as good (Figure 3-2). The highest difference between the SEM data and

weighed values was observed in the 80 % gold standard, probably due to inhomogeneity in the button at silver concentrations ≥ 20 %, which was ignored because the native gold ore samples analyzed all had a silver concentration less than or equal to 15 %.

Table 3-8 Gold and silver concentrations, measured by SEM, in a set of internal gold standards.

| Weighed gold | SEM analysis | 1 | 2 | 3 | Average | STDEV (σ) | Systematic error % |
|---|---|---|---|---|---|---|---|
| 100 % | Au | 96.89 | 97.28 | 97.41 | 97.19 | 0.27 | 1.81 |
| | Ag | 3.11 | 2.72 | 2.59 | 2.81 | 0.27 | 1.81 |
| 95 % | Au | 95.18 | 93.58 | 94.24 | 94.33 | 0.8 | 0.67 |
| | Ag | 4.82 | 6.42 | 5.76 | 5.67 | 0.8 | 0.67 |
| 90 % | Au | 91.16 | 91.06 | 90.91 | 91.04 | 0.13 | 1.04 |
| | Ag | 8.4 | 8.94 | 9.09 | 8.81 | 0.36 | 1.19 |
| 85 % | Au | 84.82 | 83.39 | 83.02 | 83.74 | 0.95 | 1.26 |
| | Ag | 15.18 | 16.61 | 16.98 | 16.26 | 0.95 | 1.26 |
| 80 % | Au | 77.13 | 75.96 | 77.78 | 76.96 | 0.92 | 3.04 |
| | Ag | 22.87 | 24.04 | 22.22 | 23.04 | 0.92 | 3.04 |

The result of gold and silver concentrations has confirmed that the SEM data and the weighed values correlate, hence the SEM data can be regarded as good ($r^2 = 0.9707$) (Figure 3-2). The highest difference between the SEM data and weighed values was observed in the 80 % gold standard, probably due to inhomogeneity in the button at silver concentrations ≥ 20 %, which was ignored because the native gold ore samples analyzed all had silver concentration less than or equal to 15 %.

The SEM and LA-ICP-MS [107]Ag data was compared. There was a strong correlation ($r^2 = 0.9898$) between the silver concentration measured by the SEM and the counts per second of [107]Ag isotopes from the LA-ICP-MS (Figure 3-4). Therefore the silver counts per second data reliably represent the relative concentration of the element.
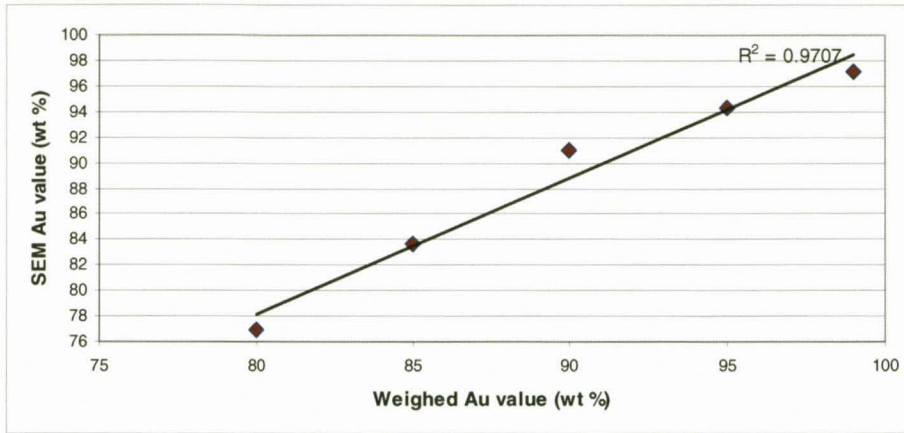
**Figure 3-3 SEM gold versus Weighed gold values (wt %) of an internal gold reference standard.**
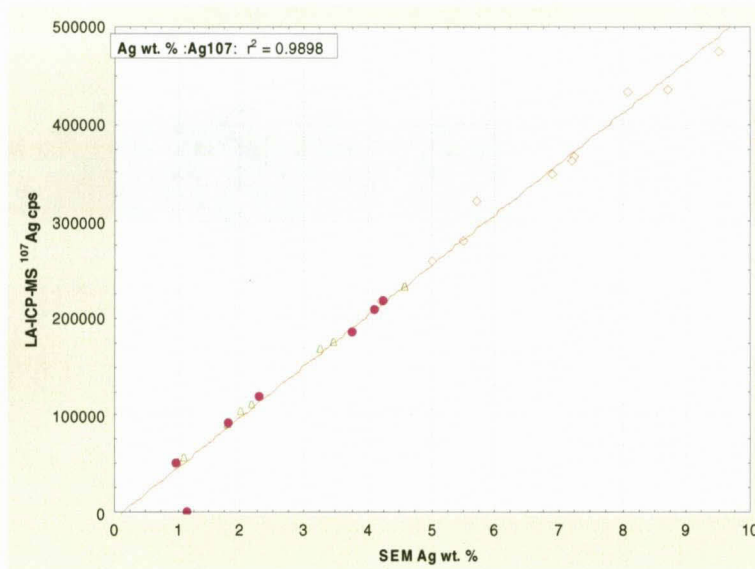


**Figure 3-4 Plot of the silver concentration (wt %) measured from the SEM versus the total counts for $^{107}$Ag from the LA-ICP-MS.**

The technique of comparing the LA-ICP-MS data with the data analyzed by other analytical techniques can be done successfully (Figure 3-4). There is a need to set up in-house standards for various elements for analysis but this was not done. Instead silver was used as an internal standard. In this study the counts per second data of $^{107}$Ag from LA-ICP-MS were successfully compared to Ag wt % from the SEM. As

54

high-quality analytical data was not required, it was decided that the other isotopes can also be compared successfully using the above technique. A ratio of $^{107}$Ag and each isotope was used during the interpretation of the results.

# 4 RESULTS AND INTERPRETATION

The LA-ICP-MS and SEM analytical techniques (see Chapter 3) were used to analyze thirty-three native gold samples from various gold ore deposits, as well as twenty-eight archaeological artefacts, all of which were described in Chapter 2. Results are presented in Table 4-1 to Table 4-3 in the form of averaged counts per second for all isotopes except for the silver concentrations, which were measured by SEM, and are given as weight percentage (wt %).

The data presented in Table 4-1 are those of the gold ore samples from the Witwatersrand Basin, Barberton Greenstone Belt and Zimbabwean plateau. Table 4-2 contains samples from the minor gold deposits of Marabastadt, Sabie-Pilgrim's Rest and Knysna. Table 4-3 includes archaeological artefact samples from Great Zimbabwe and Mapungubwe.

The geochemical signatures of distinct ore provinces are presented on the box and whisker plots, with all data (Figure 4-1) for the Witwatersrand, Barberton and Zimbabwean gold samples (Table 4-1). Data for the minor South African gold deposits, in other words for the Gravellote (Murchison Greenstone Belt), Marabastadt (Pietersburg Greenstone Belt), Sabie-Pilgrim's Rest and Knysna (Cape Supergroup) gold samples, are presented in Table 4-2. The archaeological artefact data from Zimbabwe and Mapungubwe are presented in Figure 4-3. The selected ratio, ternary and correspondence analysis plots are also presented in section 4-4.

The natural gold samples presented in Table 4-1 and 4-2 show that the following isotopes are highly variable because the standard deviation is close to or above the mean and median values and the coefficient of variation is close to or above 100 %: the $^{206,207}$Pb for Witwatersrand gold; $^{75}$As, $^{204,206,207,208}$Pb and $^{209}$Bi for Barberton gold; the $^{59}$Co, $^{202}$Hg, $^{207,208}$Pb and $^{209}$Bi for Zimbabwean gold; the $^{204}$Pb and $^{209}$Bi for Marabastadt gold; $^{59}$Co, $^{60}$Ni, $^{66}$Zn, $^{202}$Hg, $^{204,206,207,208}$Pb for Sabie-Pilgrim's Rest gold and $^{202}$Hg, $^{207,208}$Pb for Knysna gold.

The artefact samples presented in Table 4-3 show that the following isotopes are also variable: the $^{56}$Fe, $^{60}$Ni, $^{63}$Cu, $^{66}$Zn and $^{188}$Os for the Zimbabwean artefacts; the $^{56}$Fe for Mapungubwe artefacts are highly variable.

Table 4-1 and Table 4-2 show that $^{75}$As, $^{105}$Pd, $^{188}$Os, $^{195}$Pt and $^{209}$Bi isotopes are consistently below or closer to the lower limit of detection (LLD) for the major and minor gold provinces. In Table 4-3, $^{60}$Ni, $^{75}$As, $^{105}$Pd, $^{188}$Os and $^{209}$Bi are consistently below or closer to LLD for the Zimbabwean and Mapungubwe artefact samples.

## 4.1 The Major Ore Provinces (Witwatersrand, Barberton and Zimbabwe)

The silver concentrations show that the samples from the Witwatersrand province have silver concentration ranging from the minimum of 4 wt % to the maximum of 9 wt %, with the highest value found in the two samples from City Deep Mine (Table 4-1). The Barberton province has silver concentrations ranging from the minimum of 1 wt % to the maximum of 5 wt %. The samples from the Zimbabwean province have silver concentrations which are similar to those of the Barberton Greenstone Belt, ranging from a minimum of 1 wt % to the maximum of 4 wt % (Table 4-1).

Therefore, silver concentrations cannot be used to distinguish between gold from these two regions. The maximum silver concentration values of the Zimbabwean and the Barberton gold ore correspond with the minimum silver concentration value of the Witwatersrand gold ores.

The results obtained by LA-ICP-MS also show much higher [107]Ag concentration in counts per second (cps) in the Witwatersrand than in the Barberton and Zimbabwean samples (Figure 4-1). This is because silver in cps measured by LA-ICP-MS and the silver in wt % measured by the SEM correlate strongly, as discussed in Chapter 3.

Apart from the silver concentration, there is also an elevated [202]Hg concentration in the Witwatersrand samples compared to the Barberton and Zimbabwean samples. Most samples from the Witwatersrand Basin have above 1000 cps for the [202]Hg isotope, while only one gold sample from the Witwatersrand set, from City Deep Mine, has below 1000 cps (Figure 4-1, Table 4-1). However, some of the Zimbabwean samples have [202]Hg concentration comparable to some samples from the Witwatersrand Basin (Figure 4-1, Table 4-1).

The samples from the Barberton and Zimbabwean greenstone belts have [56]Fe concentration comparable to each other (Figure 4-1). Consequently, [56]Fe concentration alone cannot be used to differentiate between the greenstone belts. The Witwatersrand samples have lower [56]Fe concentration than the greenstone belt samples.

The majority of the Witwatersrand samples have relatively lower [63]Cu concentrations compared to many of the Barberton and Zimbabwean samples (Figure 4-1). The highest [63]Cu concentration was observed in samples from City Deep Mine, but

61

comparable to the samples from the Belingwe and Lower Gwelo mines of the Zimbabwean greenstones (Figure 4-1, Table 4-1).

The Barberton and Zimbabwean samples have more elevated $^{60}$Ni concentration isotope than the Witwatersrand samples. The $^{60}$Ni and $^{59}$Co concentration is slightly higher in the Barberton and Zimbabwean samples than in the Witwatersrand samples, but $^{64}$Zn values are slightly elevated in the Zimbabwean samples. The Witwatersrand samples have $^{59}$Co concentration similar to those samples from the Barberton Greenstone Belt (Figure 4-1). There is a spread of other base metals like lead isotopes and $^{209}$Bi isotopes in the Witwatersrand, Barberton and Zimbabwean samples (Table 4-1). Witwatersrand samples have low lead isotope concentrations compared with those of typical greenstone belts (Table 4-1).
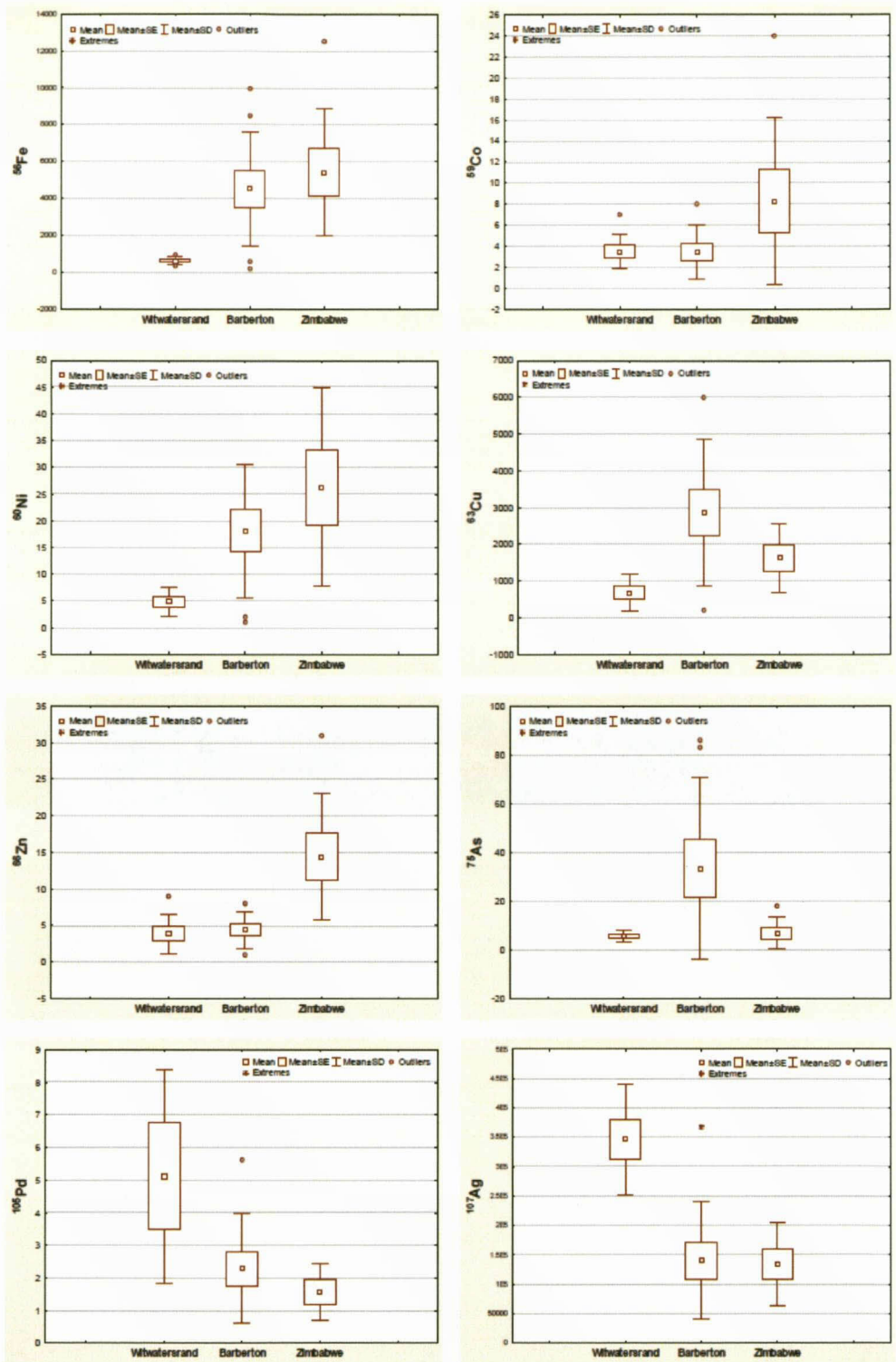
**Figure 4-1 Box and whisker plots presenting mean, mean plus standard error, mean plus 1 standard deviation, outliers and extreme values of all the data for the gold samples from the Witwatersrand Basin, Barberton and Zimbabwean greenstone belts. Continued on pages 63 and 64.**
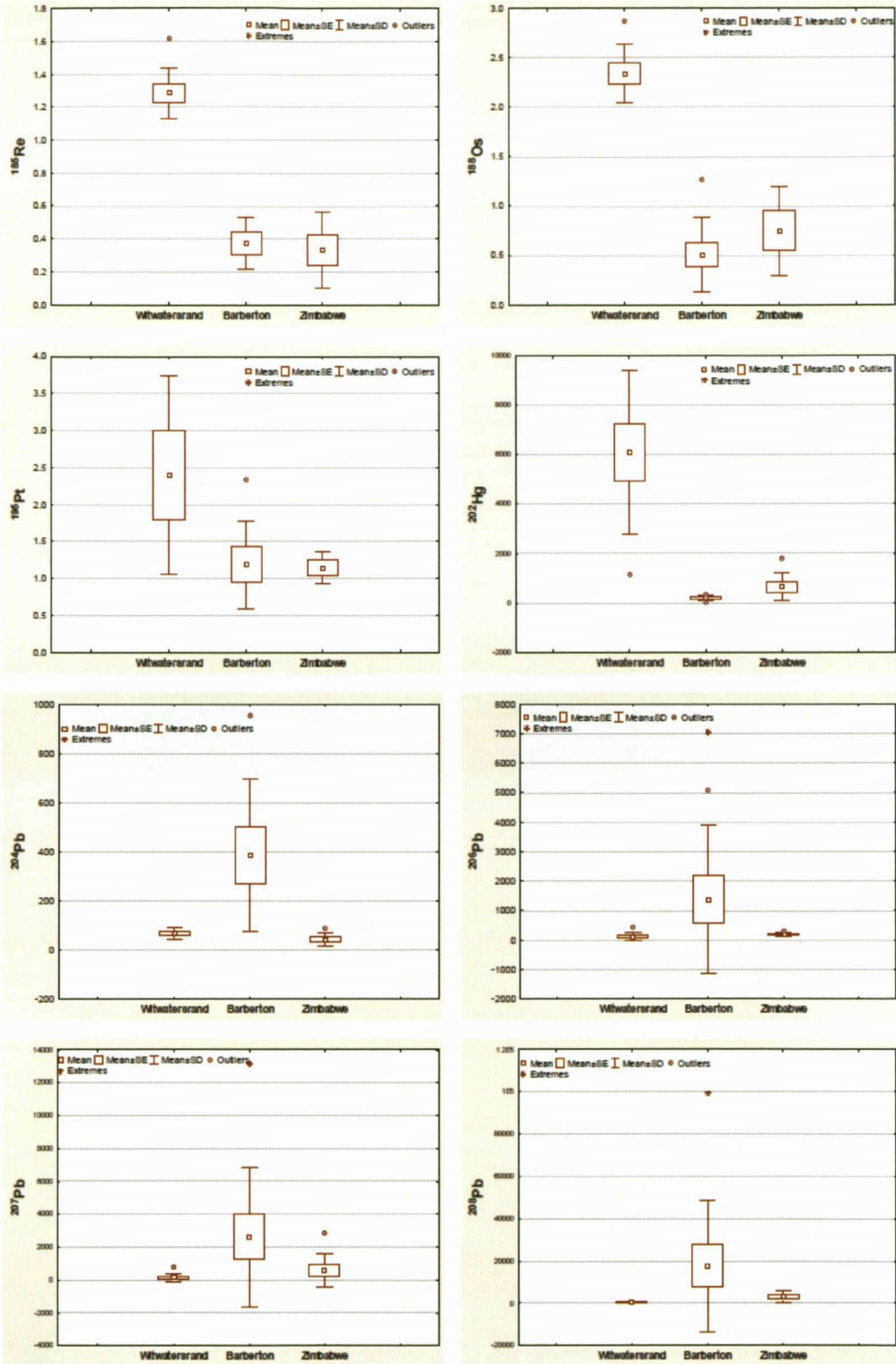
**Figure 4-1. Continued.**

64
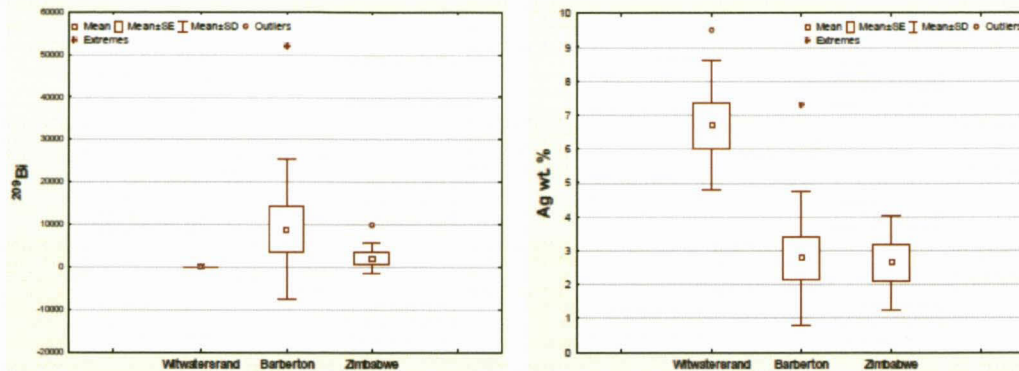
**Table 4-1. Continued.**

## 4.2 Minor Gold Ore Deposits

The data of the minor gold deposits, including Marabastadt, Gravellote and Knysna were compared with the three major ore provinces discussed in the previous section. Samples from Marabastadt have silver concentrations comparable with those of Barberton and the Zimbabwean greenstone belts (Figure 4-2). The $^{202}$Hg concentration is lower relative to the Zimbabwean samples, but comparable to those from Barberton samples, and even lower than samples from the Witwatersrand Basin (Figure 4-2). The $^{63}$Cu concentration is comparable to both the Barberton and the Zimbabwean greenstones and lower than those of the Witwatersrand Basin (Figure 4-2).

Figure 4-2 shows that a sample from Gravellote Mine has $^{107}$Ag concentration comparable to those of the Barberton and Zimbabwean greenstone belts, and lower relative to those from the Witwatersrand Basin. The $^{202}$Hg concentration is higher than samples from the Barberton and Zimbabwean Greenstone Belts, but comparable to those of the Witwatersrand Basin. The $^{60}$Ni concentration was not detected in the

Gravellote Mine sample. The $^{63}$Cu concentration is comparable to samples from the Barberton and Zimbabwean greenstone belts, and higher than most of those from the Witwatersrand Basin.

Figure 4-2 shows that samples from Lydenburg, Goedeverwacht and New Chum-Pilgrim's Rest mines from the Sabie-Pilgrim's Rest Goldfield have $^{107}$Ag concentration higher than those of the Barberton and the Zimbabwean greenstones. The $^{202}$Hg concentration is higher than those from Barberton and Zimbabwean greenstones and comparable with those samples from Witwatersrand Basin.

The two samples from Knysna Mine have silver concentration similar to those of the Witwatersrand Basin (Table 4-2, Figure 4-2). The $^{202}$Hg concentration is low compared with samples from the Witwatersrand Basin, but comparable to those from the Barberton and the Zimbabwean greenstone belts (Figure 4-2). The $^{60}$Ni concentration is lower than most of the Barberton and Zimbabwean greenstones, but comparable with those from the Witwatersrand Basin (Figure 4-2). The $^{63}$Cu concentration is lower than samples of the Barberton and Zimbabwean greenstones and comparable to those of the Witwatersrand Basin (Figure 4-2).
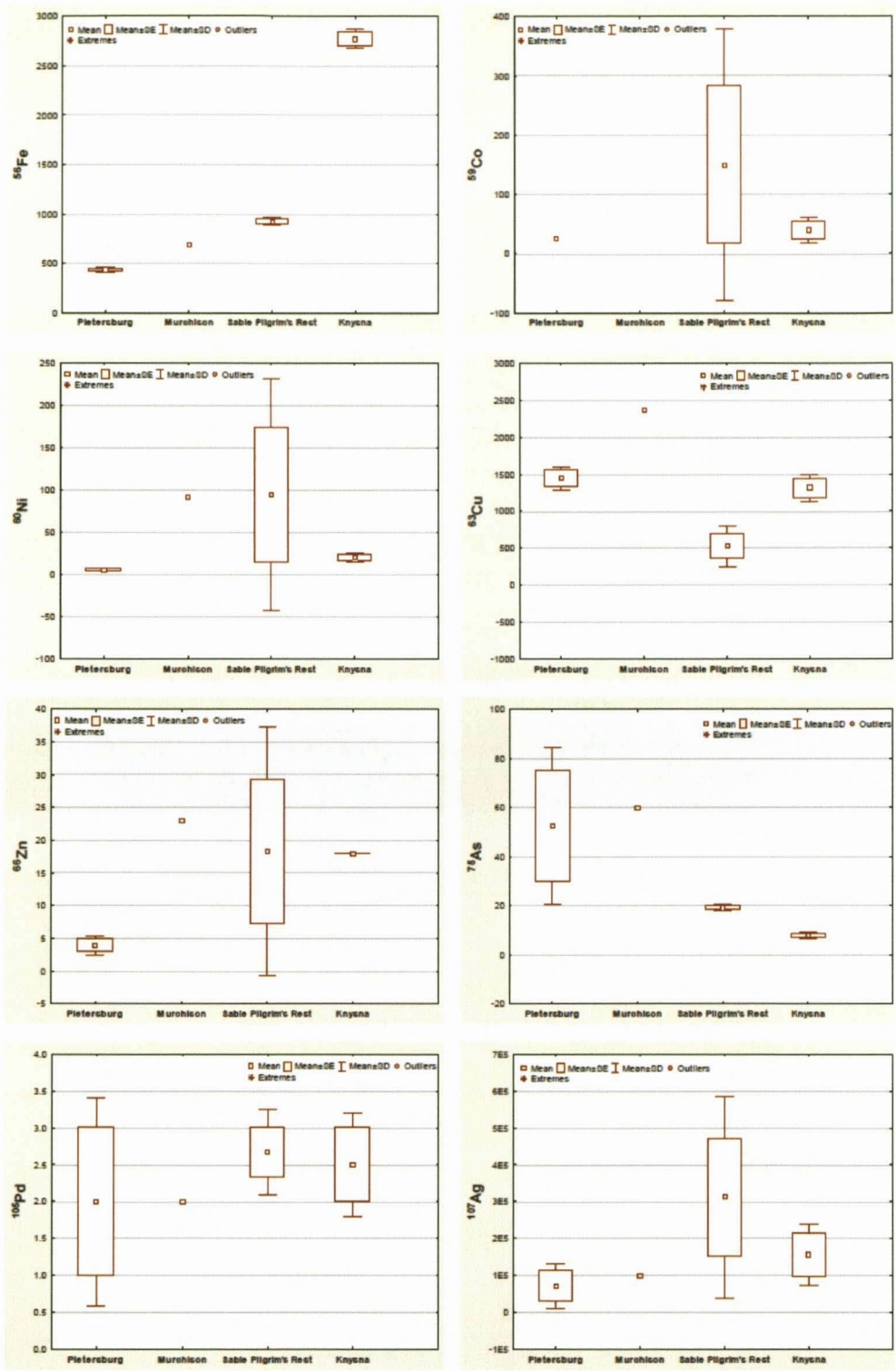
Figure 4-2 Box and whisker plots presenting mean, mean plus standard error, mean plus 1 standard deviation, outliers and extreme values of all the data for the gold samples from Pietersburg and Murchison Greenstone Belts, Sabie-Pilgrim's Rest Goldfield and Knysna mines. Continued on page 67.
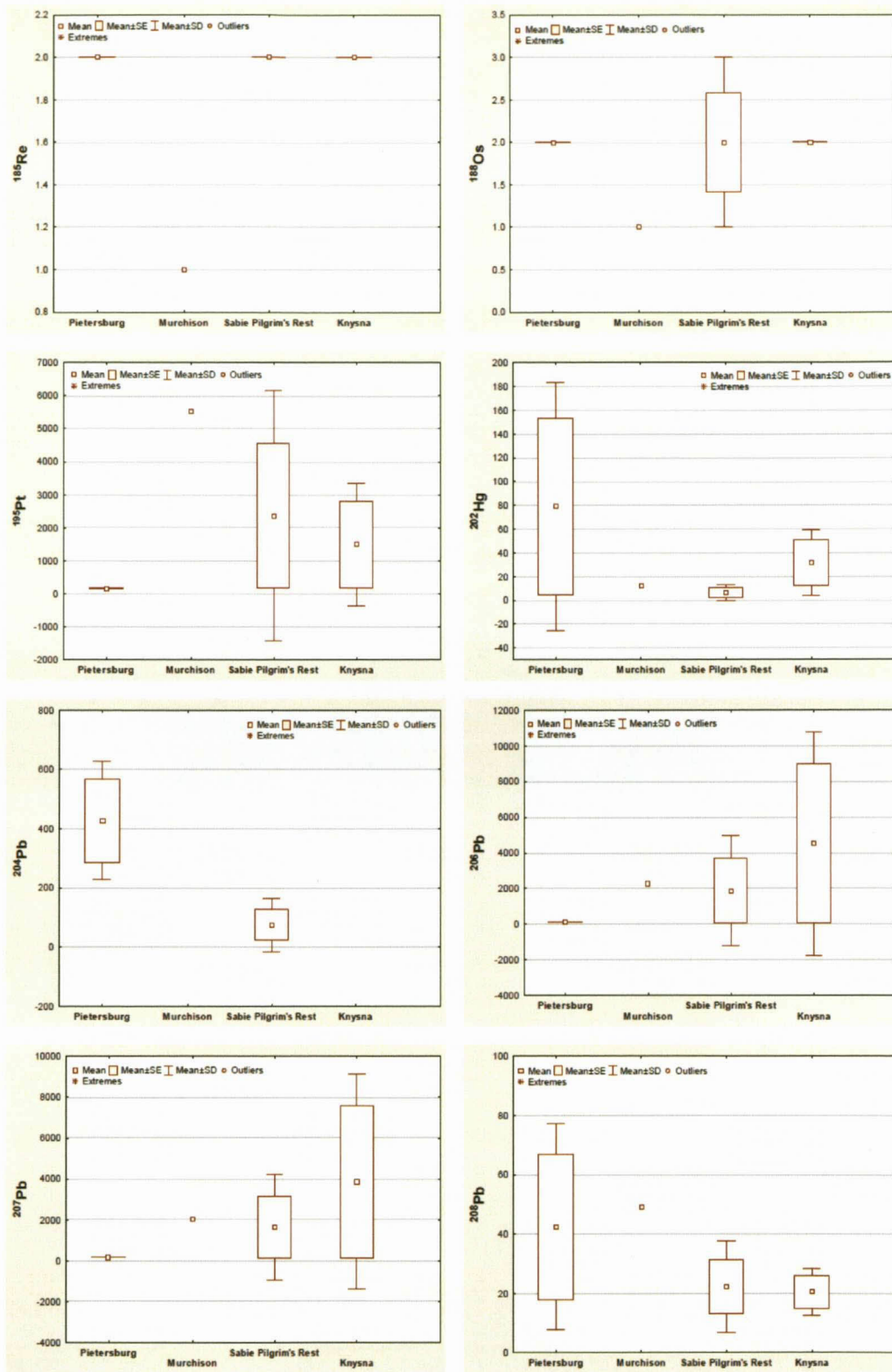
**Figure 4.2. Continued.**

## 4.3 Archaeological Artefacts

The data of the artefacts recovered from the Zimbabwe and Mapungubwe sites were compared to the major ore provinces presented in Section 4.1. The twenty-three artefacts from the Zimbabwean plateau have silver concentration comparable to those of the Witwatersrand (Table 4-3, Figure 4-3). The $^{63}Cu$ concentration is low compared with those samples from the greenstone belts and comparable with most of the Witwatersrand samples (Figure 4-3). Figure 4-3 shows elevated $^{66}Zn$ concentration compared with the three major ore provinces. The $^{188}Os$ and $^{195}Pt$ isotopes have higher concentrations compared with those from the greenstones and some samples have concentrations comparable to some samples from the Witwatersrand Basin (Figure 4-3). The artefacts from the Zimbabwean plateau have $^{188}Os$ concentration more elevated than those of the Witwatersrand ore samples. The Zimbabwean artefacts have lower $^{202}Hg$ concentration compared with those of the three major provinces (Figure 4-3).

Table 4-3 and Figure 4-3 show that the silver concentration of artefacts analyzed from Mapungubwe is lower than that of the Witwatersrand Basin and comparable to that of the greenstones. The $^{63}Cu$ concentration is comparable to those from the Witwatersrand Basin, but slightly low. $^{66}Zn$ and $^{188}Os$ cps were not detected. Like the Zimbabwean artefacts discussed above, Mapungubwe artefacts have $^{195}Pt$ concentration elevated above those of the entire natural samples. The $^{202}Hg$ concentration of Mapungubwe artefacts is also lower than that of the Zimbabwean artefacts and the natural samples.
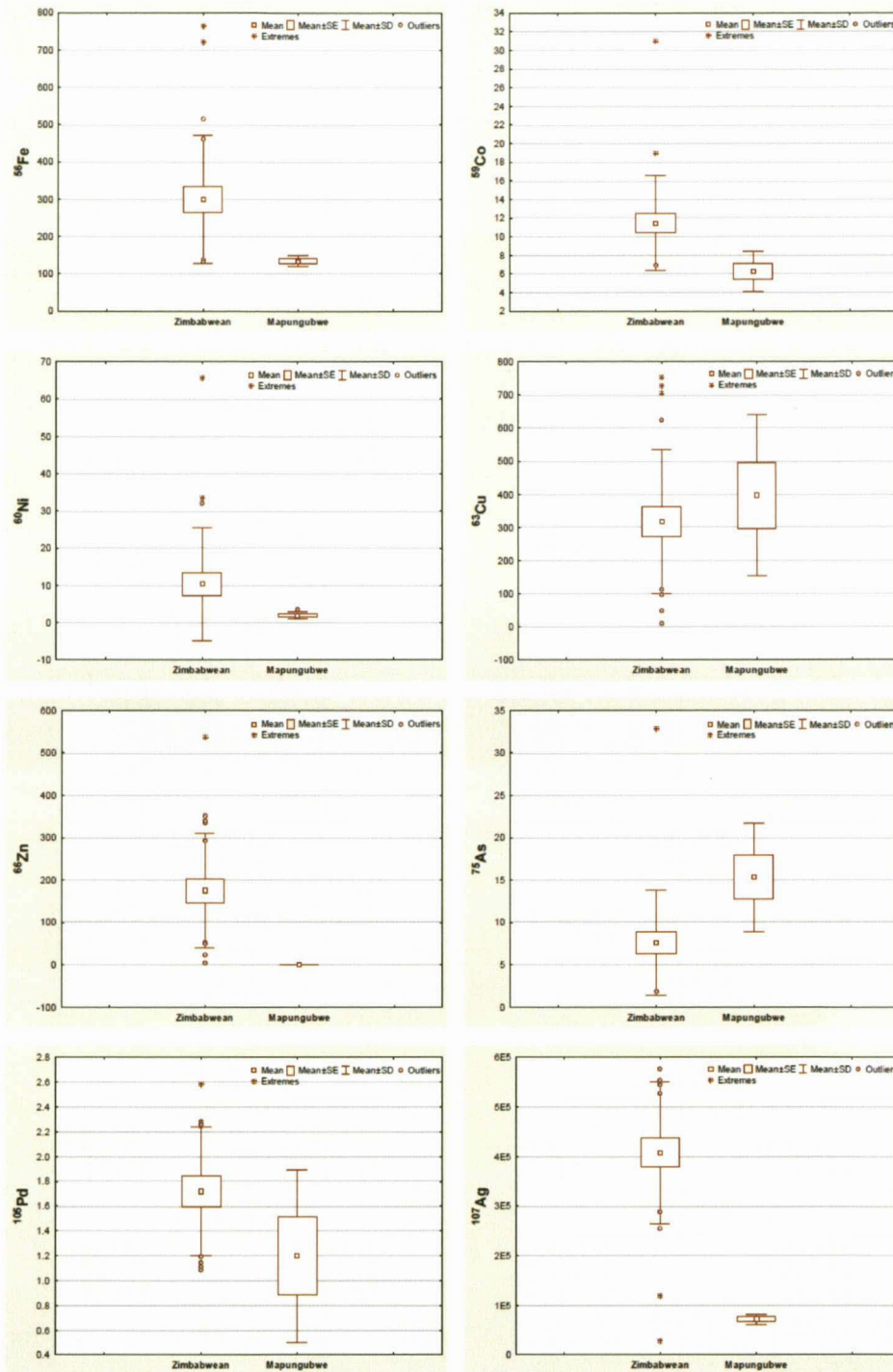
**Figure 4-3 Box and whisker plots presenting mean, mean plus standard error, mean plus 1 standard deviation, outliers and extreme values of all the data for the Zimbabwean and Mapungubwe artefacts. Continued on page 70.**
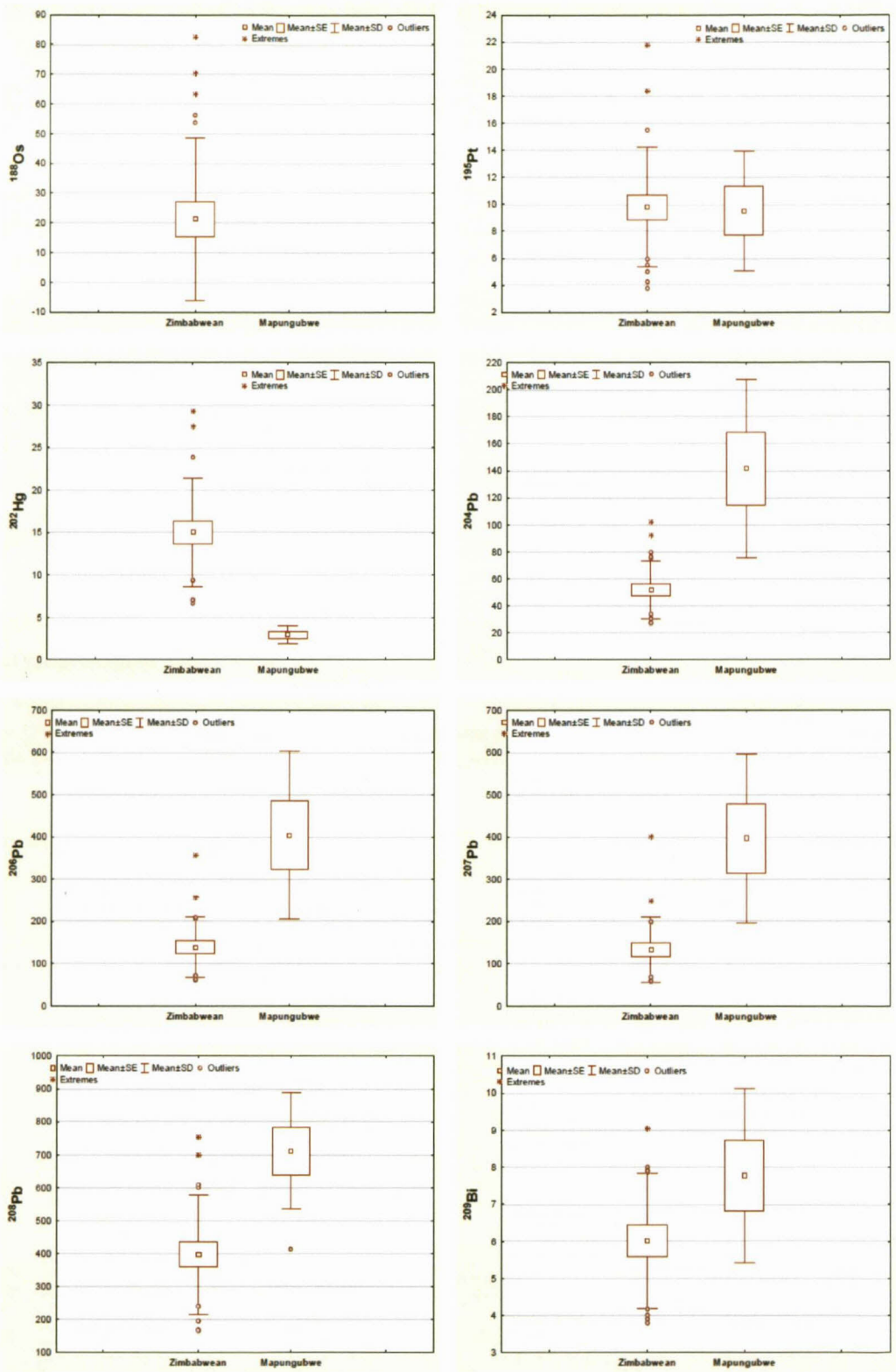
**Figure 4-3. Continued.**

## 4.4 General Observations and Multivariate Statistics

This section is a summary of the data described in section 4.1 to 4.3. It is groundwork for the discussion chapter that follows, where more details will be discussed. Only general statements will be made in this section.

### 4.4.1 Major Gold Ore Province

Table 4-4 summarizes the major distinctions between the greenstone belts and the Witwatersrand Basin samples. The distinctions are based on either high or low concentrations for the $^{56}$Fe, $^{63}$Cu, $^{60}$Ni, $^{66}$Zn $^{107}$Ag and $^{202}$Hg isotopes in cps.

**Table 4-4 Summary of the trace element signatures of gold samples from Witwatersrand Basin and the greenstone belts.**

| Gold ore provinces in southern Africa | Major distinctions | |
|---|---|---|
| | High concentrations (cps) | Low concentrations (cps) |
| Greenstone belts | $^{56}$Fe | $^{107}$Ag |
| | $^{63}$Cu | |
| | $^{60}$Ni | $^{202}$Hg |
| Witwatersrand Basin | $^{107}$Ag | $^{56}$Fe |
| | | $^{63}$Cu |
| | $^{202}$Hg | $^{60}$Ni |

**Figure 4-4 A ternary plot of $^{63}$Cu, $^{66}$Zn and $^{202}$Hg of gold samples from Witwatersrand Basin (w's and red cross), Barberton (b's and light green diamonds) and Zimbabwean (z's and blue boxes) greenstone belts. Normalised data in Table 4-1.**

The combination of $^{63}$Cu, $^{66}$Zn and $^{202}$Hg isotopes in Figure 4-4 point out the three major groups of the major gold samples. There is a group formed by the majority of the samples from Witwatersrand Basin. The group is discernible because of low $^{66}$Zn and $^{63}$Cu and high $^{202}$Hg. The greenstone belt samples are clustered into two groups. The first group is formed by a good number of the samples from Zimbabwe and two from Barberton. The group is distinct because of being low in $^{63}$Cu and $^{202}$Hg, although high in $^{66}$Zn. Apart from the two samples that cluster with the most of the Zimbabwean samples, the rest of the Barberton samples have low $^{66}$Zn.

A combination of $^{56}$Fe with $^{63}$Cu and $^{202}$Hg in Figure 4-5 does not discriminate between the samples from the greenstone belts. This is because half of the samples from Barberton have high $^{56}$Fe, $^{63}$Cu and low $^{66}$Zn. The other half and the majority of the Zimbabwean samples are low in $^{56}$Fe and $^{63}$Cu other than those high in $^{66}$Zn. However, with the exception again of sample w1, this ternary system discriminates well between the Witwatersrand gold and the greenstone belts.
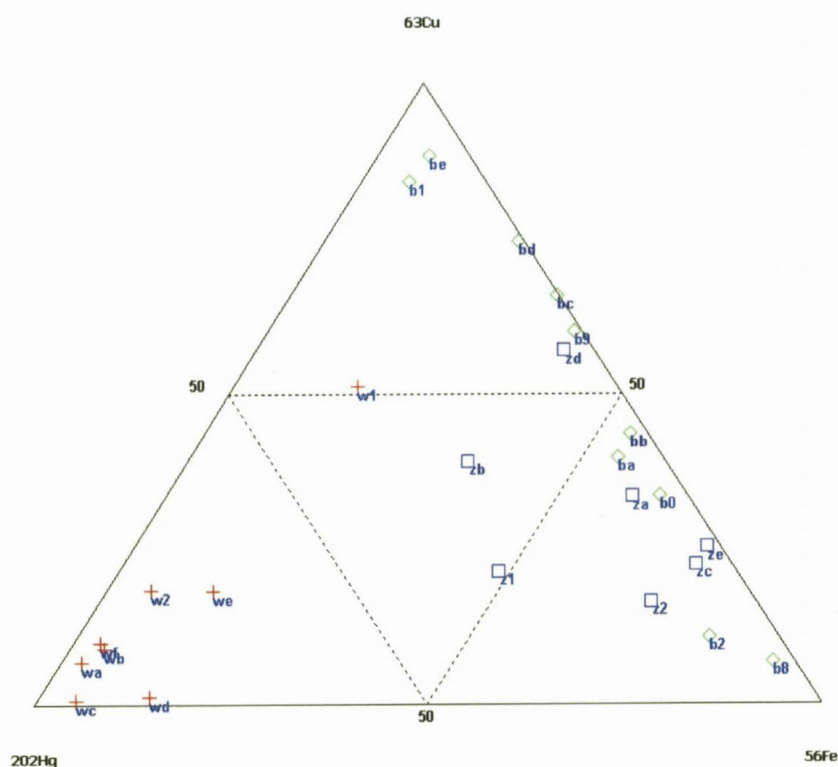


**Figure 4-5 A ternary plot of $^{63}$Cu, $^{56}$Fe and $^{202}$Hg of gold samples from Witwatersrand Basin (w's and red cross), Barberton (b's and light green diamonds) and Zimbabwean (z's and blue boxes) greenstone belts. Normalised data in Table 4-1.**

A combination of $^{60}$Ni with $^{56}$Fe and $^{202}$Hg in Figure 4-6 clusters the Witwatersrand samples into a particular group and forms an extensive group of the greenstone belt

74

samples. This is because of the low or below detection limit $^{60}$Ni in the majority of the samples analyzed.
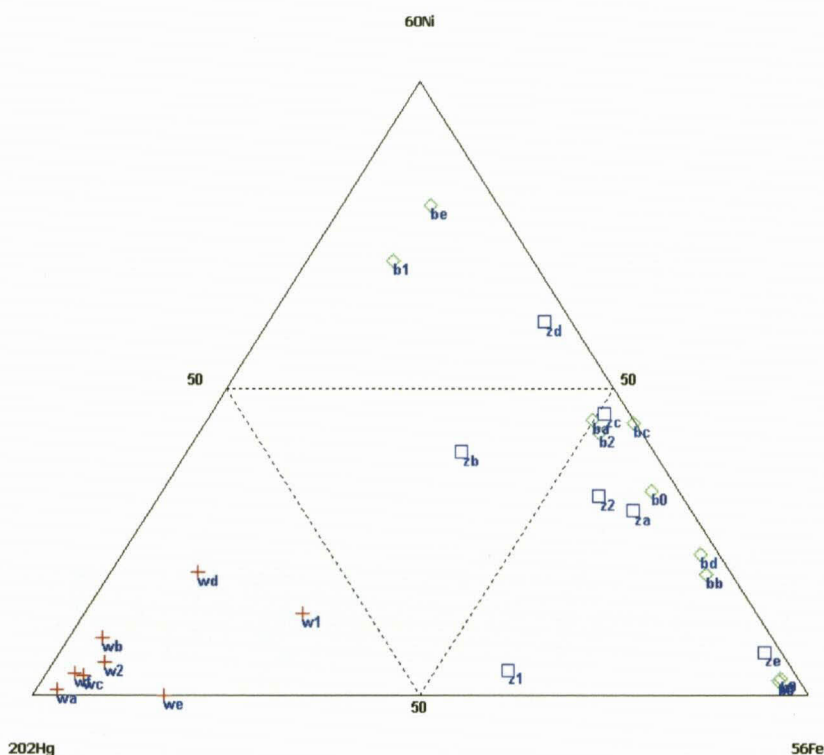


**Figure 4-6 A ternary plot of $^{58}$Ni, $^{66}$Zn and $^{202}$Hg of gold samples from Witwatersrand Basin (w's and red cross), Barberton (b's and light green diamonds) and Zimbabwean (z's and blue boxes) greenstone belts. Normalised data in Table 4-1.**

Figure 4-7 is the multivariate correspondence analysis plot, using a combination of $^{56}$Fe, $^{63}$Cu, $^{60}$Ni, $^{66}$Zn$^{107}$Ag and $^{202}$Hg. It shows once more that samples from the greenstone belts cannot be discriminated. However, the Witwatersrand samples plot differently to the greenstone belt samples. Using Ward's method (Ward, 1963) of clustering presented in Figure 4-8, it shows that one of the Zimbabwean samples can be grouped with the Witwatersrand samples. No conclusive statement can be made as only one sample is involved.

75
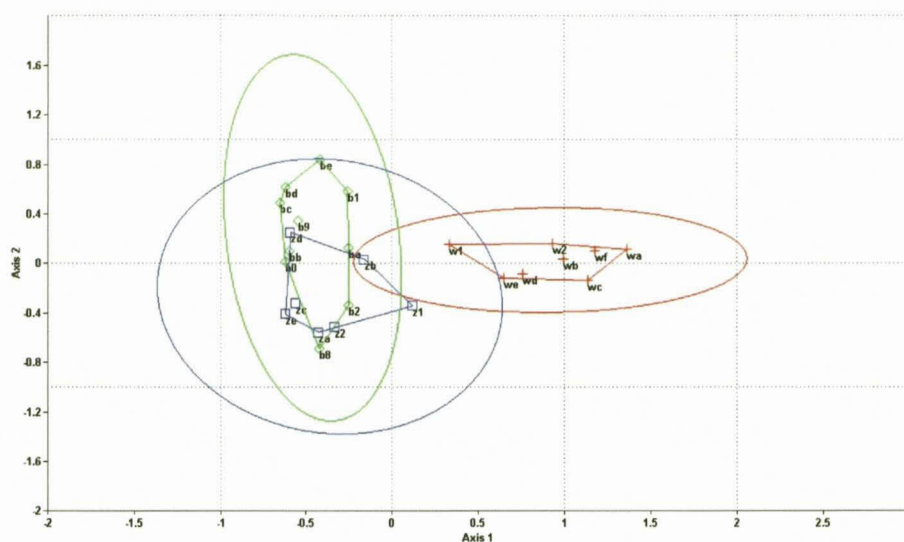
**Figure 4-7** Multivariate correspondence analysis at 95 % confidence interval for the gold samples from Witwatersrand Basin (w's and red cross), Barberton (b's and light green diamonds) and Zimbabwean (z's and blue boxes) greenstone belts. Axis1 = 0.5 eigenvalue and 59 % of total. Axis2 = 0.14 eigenvalue and 17 % of total.
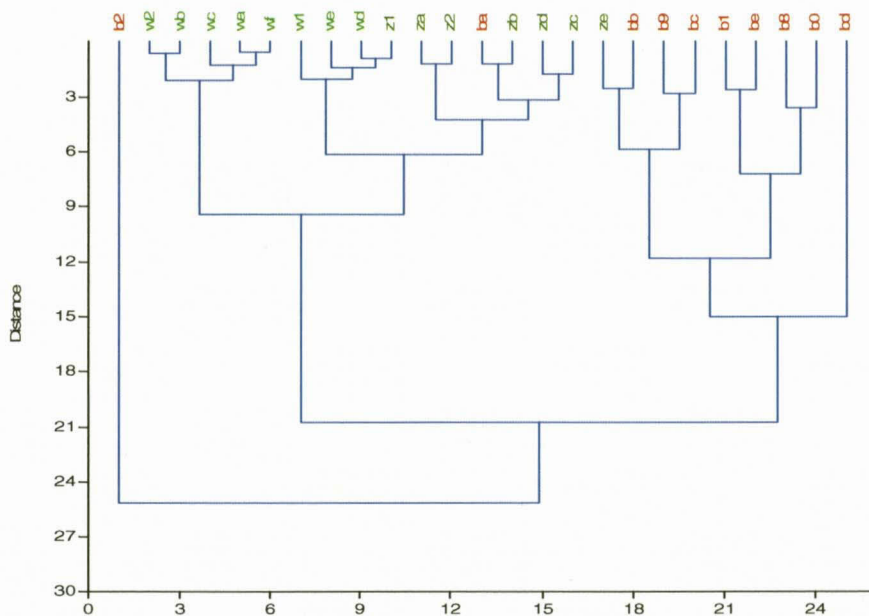


**Figure 4-8** Ward's method (Ward, 1963) for cluster analysis for the gold samples from the Witwatersrand Basin (w's), Barberton (b's) and Zimbabwean (z's) greenstone belts.
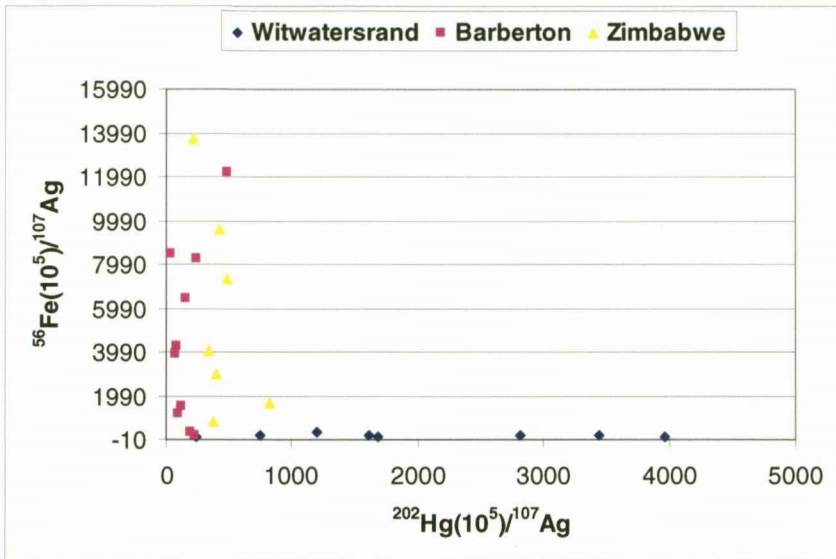
**Figure 4-9 A ratio plot for $^{56}Fe/^{107}Ag$ and $^{202}Hg/^{107}Ag$ for the gold samples from the Witwatersrand Basin, Barberton and Zimbabwean greenstone belts.**

The ratio plot in Figure 4-9 shows that there are low $^{56}Fe/^{107}Ag$ ratios for the gold samples from the Witwatersrand, compared to those of the greenstone belts. The greenstone belts have low $^{202}Hg/^{107}Ag$ ratios compared to the Witwatersrand.
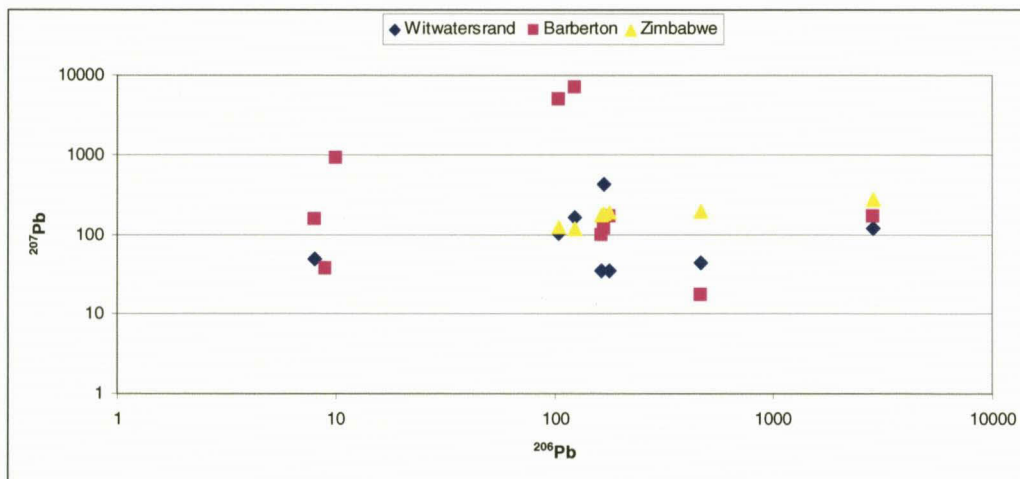


**Figure 4-10 Bivariate plot of $^{206}Pb$ vs $^{207}Pb$ for the Witwatersrand, Barberton and Zimbabwean gold samples.**

77

The lead isotopes were highly variable for the Barberton, Zimbabwean greenstone belts and the Witwatersrand samples (Figure 4-10). It was impossible to distinguish between the Witwatersrand and greenstone samples because of the variability.

## 4.4.2 Minor Gold Ores

The chemistry of the minor gold samples was compared to the one of the major gold samples. The samples were not used potentially to source the archaeological artefacts because of the small number of samples involved. Figure 4-11 shows that the two samples from Marabastadt in the Pietersburg Greenstone Belt have comparable signatures to the other greenstone belt samples. In Figure 4-12, a sample from Gravellote of the Murchison Greenstone Belt indicates a comparable signature to the greenstone belts as well.

From the three samples presented in the Sabie-Pilgrim's Rest Goldfield shown in Figure 4-13, two samples have a similar signature to the greenstone belt samples. The other sample shows a completely different signature but near the greenstone belts field. Figure 4-14 shows the two samples from Knysna in the Cape Supergroup also are comparable to the greenstone belt samples.
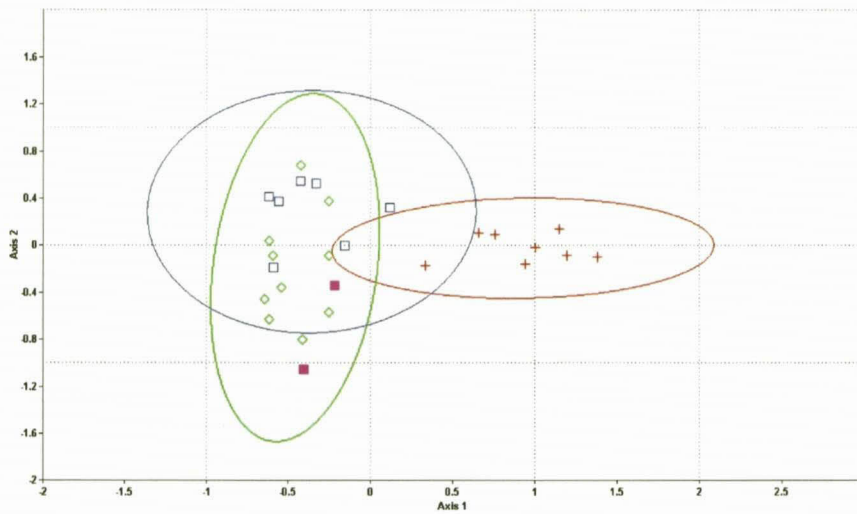
**Figure 4-11 Multivariate correspondence analysis at 95 % confidence interval for the gold samples from Witwatersrand Basin (red cross), Barberton (light green diamonds) and Zimbabwean (blue boxes) greenstone belts and Marabastadt samples (pink solid boxes) from Pietersburg greenstone belt. Axis1 = 0.5 eigenvalue and 58 % of total. Axis2 = 0.14 eigenvalue and 17 % of total.**
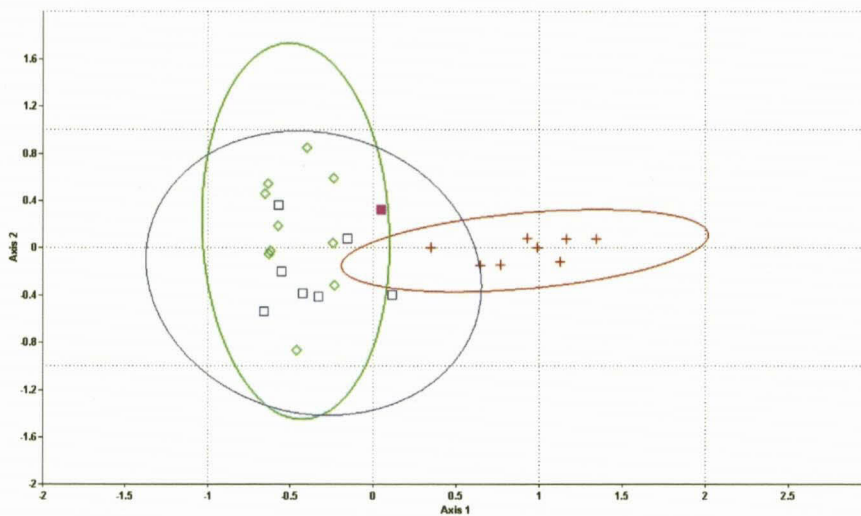


**Figure 4-12 Multivariate correspondence analysis at 95 % confidence interval for the gold samples from Witwatersrand Basin (red cross), Barberton (light green diamonds) and Zimbabwean (blue boxes) greenstone belts and Gravellote (g1) sample (pink solid box) from Murchison greenstone belt. Axis1 = 0.5 eigenvalue and 55 % of total. Axis2 = 0.13 eigenvalue and 16 % of total.**

79
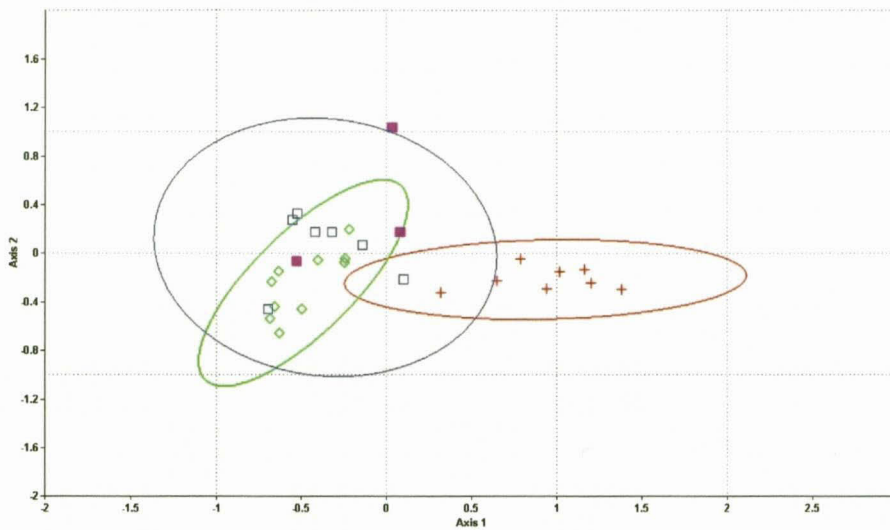
**Figure 4-13** Multivariate correspondence analysis at 95 % confidence interval for the gold samples from Witwatersrand Basin (red cross), Barberton (light green diamonds) and Zimbabwean (blue boxes) greenstone belts and Sabie-Pilgrim's Rest Goldfields (sl, sn and sq) samples (pink solid boxes). Axis1 = 0.4 eigenvalue and 48 % of total. Axis2 = 0.2 eigenvalue and 23 % of total.
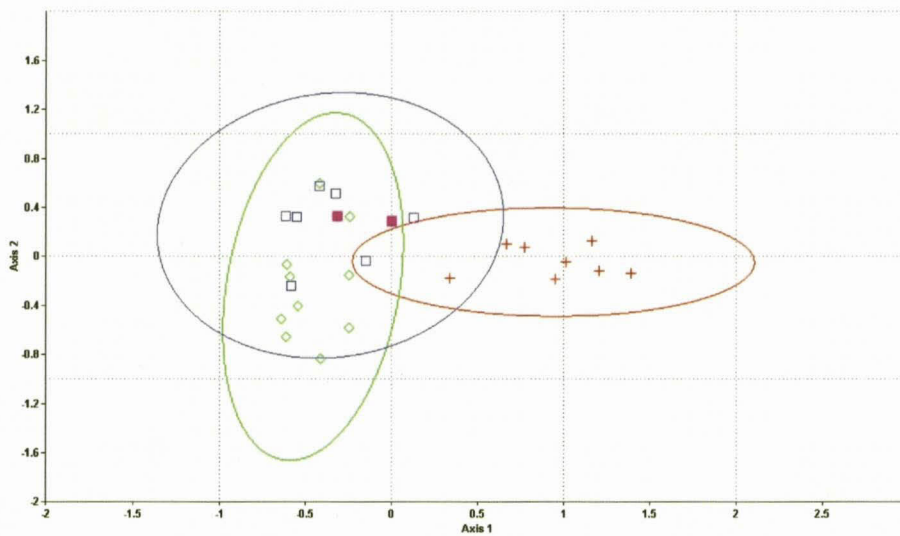


**Figure 4-14** Multivariate correspondence analysis at 95 % confidence interval for the gold samples from Witwatersrand Basin (red cross), Barberton (light green diamonds) and Zimbabwean (blue boxes) greenstone belts and Knysna (k1 and k2) samples (pink solid boxes). Axis1 = 0.14 eigenvalue and 59 % of total. Axis2=0.13 eigenvalue and 17 % of total.

80

### 4.4.3  Archaeological Artefacts

Table 4-5 below summarizes the major dissimilarity of the archaeological artefacts from Zimbabwe and Mapungubwe in South Africa. The distinctions between the artefacts were based on either high or low concentration in cps of the following isotopes: $^{66}$Zn, $^{75}$As, $^{107}$Ag, $^{202}$Hg and the Pb isotopes.

Table 4-5 Summary of the trace elements signatures of gold artefacts samples from Zimbabwe and Mapungubwe.

| Artefacts | | Major distinctions | |
|---|---|---|---|
| | | High concentration (cps) | Low concentration (cps) |
| Zimbabwe | | $^{66}$Zn | $^{75}$As |
| | | | $^{204}$Pb |
| | | $^{107}$Ag | $^{206}$Pb |
| | | | $^{207}$Pb |
| | | $^{202}$Hg | $^{208}$Pb |
| Mapungubwe | | $^{75}$As | $^{66}$Zn |
| | | $^{204}$Pb | |
| | | $^{206}$Pb | $^{107}$Ag |
| | | $^{207}$Pb | |
| | | $^{208}$Pb | $^{202}$Hg |

The combination of the $^{63}$Cu, $^{66}$Zn and $^{202}$Hg cps in Figure 4-15 indicates the three different groups of the artefact samples. The first group is of the Mapungubwe artefacts, which is clustered into a single group discerned by high $^{63}$Cu and low $^{66}$Zn concentrations (Figure 4-15). The second group is formed by the Zimbabwean artefacts samples, which can be divided into two groups. The first group is on the intermediate region of the ternary plot. The group consists of a wide range of low $^{202}$Hg to high $^{202}$Hg concentrations samples. The second group is formed by the two

samples, which are characterized by high $^{66}$Zn, low $^{202}$Hg and low $^{63}$Cu concentrations.
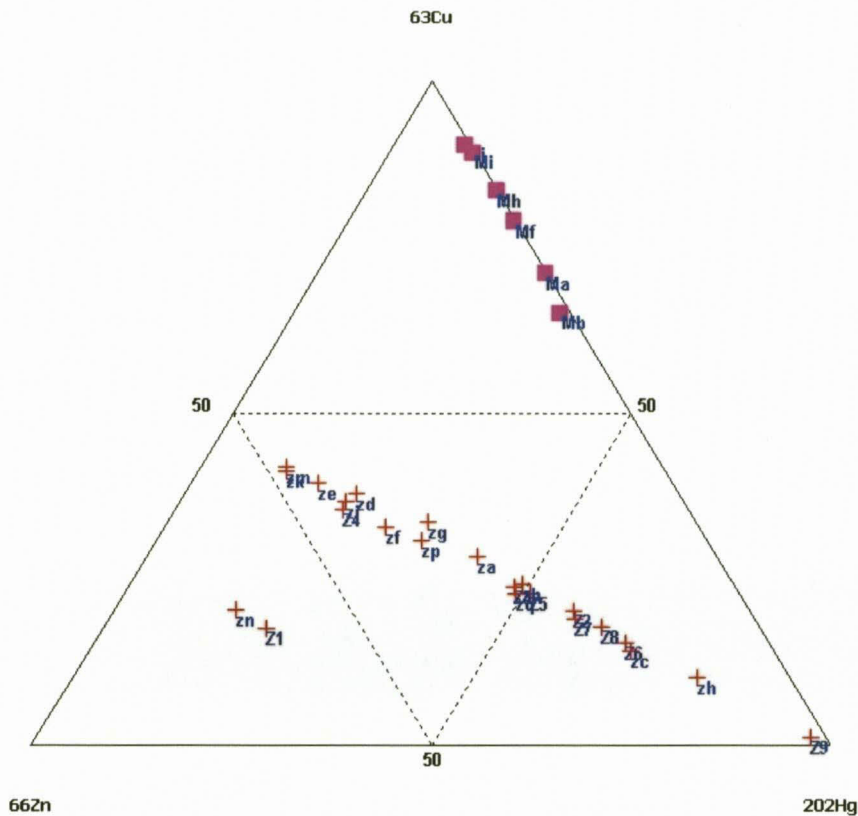


**Figure 4-15 A ternary plot of $^{63}$Cu, $^{66}$Zn and $^{202}$Hg of gold samples from Zimbabwe (z's and red cross) and Mapungubwe (m's and solid purple squares) in South Africa. Normalised data in Table 4-3.**

When the artefact samples are plotted against the major gold deposits of Witwatersrand, Barberton and Zimbabwean samples (see Figure 4-16), the following can be seen: (1) Mapungubwe samples are comparable to the majority of the Barberton samples. (2) The two samples with high $^{66}$Zn but low in $^{202}$Hg and $^{63}$Cu concentrations from Zimbabwean artefacts, are plotting with the majority of the Zimbabwean ore samples. (3) There is a wide group of the Zimbabwean artefacts

samples plotting next to the majority of the Witwatersrand samples. (4) The intermediate Zimbabwean artefacts plot with one sample from Witwatersrand Basin and one from Barberton Greenstone Belt.



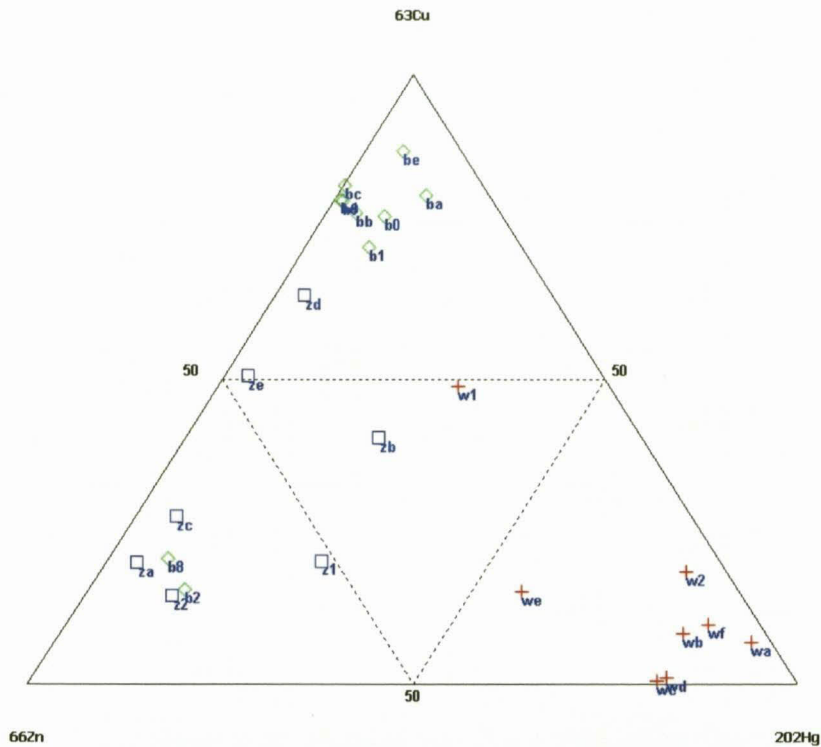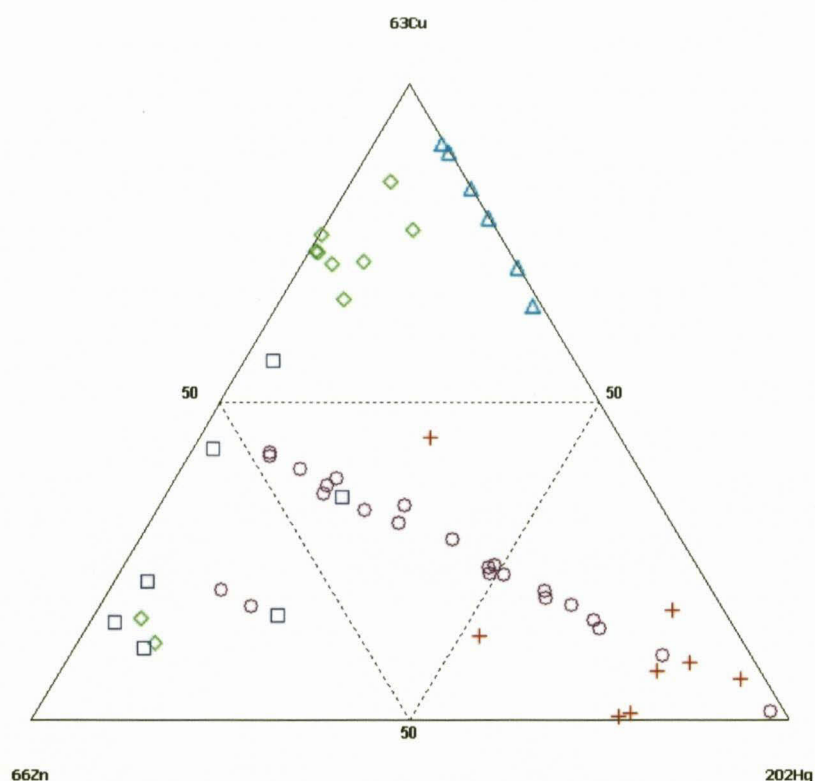**Figure 4-16 A ternary plot of $^{63}$Cu, $^{66}$Zn and $^{202}$Hg of gold samples from Witwatersrand Basin (red cross), Barberton (light green diamonds) and Zimbabwean (blue boxes) greenstone belts with Mapungubwe (light blue triangle) and Zimbabwe (brown circles) artefacts. Normalised data in Table 4-3.**

The multivariate correspondence analysis presented in Figure 4-17 also shows that the Zimbabwean artefacts differ from the Mapungubwe artefacts. The Zimbabwean artefacts are divided into two groups as shown in Figure 4-17, but with enough samples for each group here. Figure 4-17 shows that the small group, marked yellow in the correspondence analysis plot, can be identified as having 50 % of $^{202}$Hg, about

83

70 % of $^{66}$Zn and about 20 % of $^{63}$Cu concentrations (Figure 4-16). The large group can be identified as having less than 50 % of the metals (Figure 4-16).
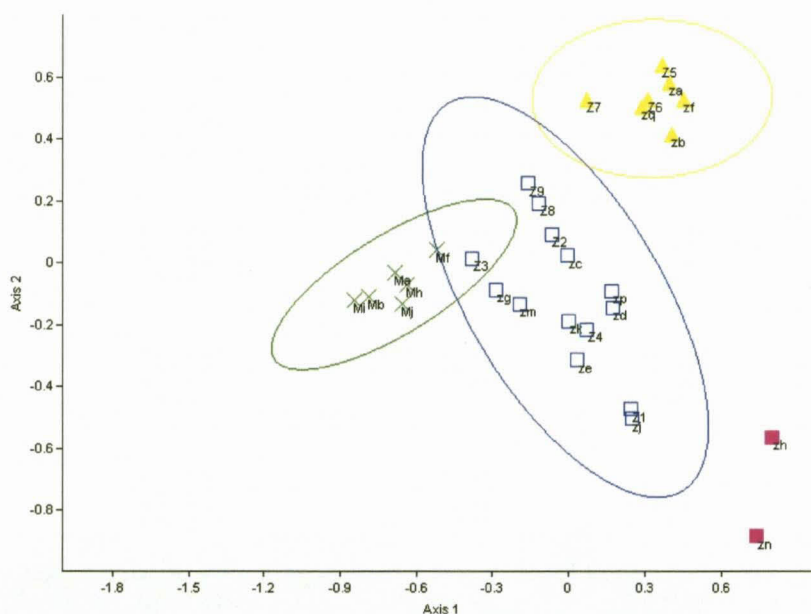


**Figure 4-17 Multivariate correspondence analysis for the gold artefacts from Zimbabwe (z's) and Mapungubwe (m's).**

The Ward's Method (Ward, 1963) of clustering in Figure 4-18 also indicates the three major groups of the artefacts. The Mapungubwe artefacts form a group while the Zimbabwean artefacts are also divided into two groups. Only two samples from Zimbabwe artefacts are closely related to the Mapungubwe artefacts.

The platinum group isotopes were mainly extremely low in concentration, except the $^{188}$Os and $^{195}$Pt for the Zimbabwean and Mapungubwe artefacts (Figure 4-3). The details of this subsection will be discussed in the following chapter of interpretation and discussion of the results.
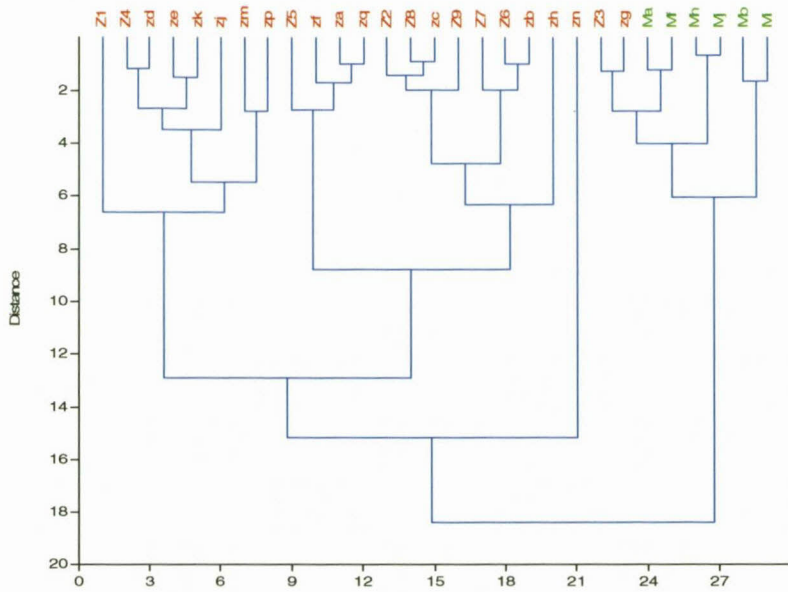
**Figure 4-18 Ward's method for cluster analysis for the gold artefacts from Zimbabwe (z's) and Mapungubwe (m's).**
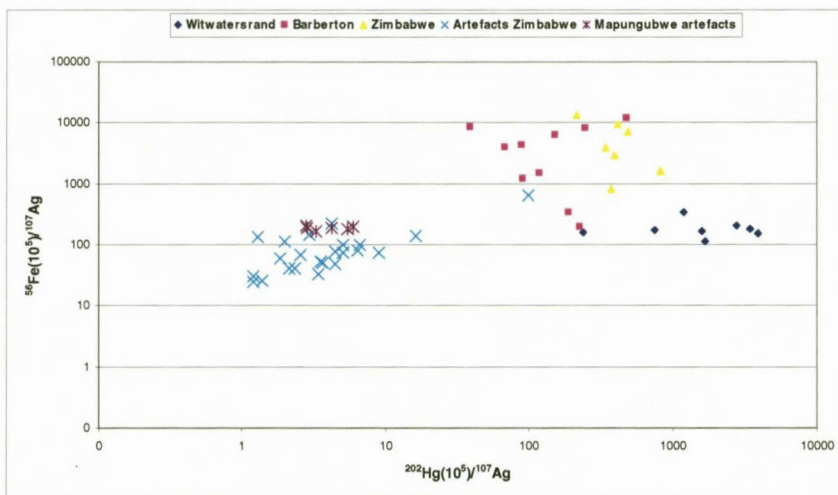


**Figure 4-19 A ratio plot for $^{56}Fe(10^5)/^{107}Ag$ and $^{202}Hg(10^5)/^{107}Ag$ for the gold samples from Witwatersrand Basin, Barberton and Zimbabwean greenstone belts, as well as Zimbabwean and Mapungubwe artefacts.**

The ratio plot in Figure 4-19 shows that the chemistry of the archaeological gold artefacts differs completely from the natural gold analysed. This is based on the low Hg/Ag ratios of the artefacts compared to the natural gold from Witwatersrand, Barberton and Zimbabwe samples.

# 5  DISCUSSION

## 5.1  Chemical Signature of the Major Gold Deposits

One of the prerequisites in trying to trace the geological source of artefacts is to determine whether the different gold deposits exhibit different chemical signatures. Chisholm (1979) suggested that, on the basis of the major elements in gold only, it is difficult to distinguish between deposits of the same geological association.

A clear chemical difference between the Witwatersrand Basin and greenstone belt gold was observed in this study, based on the analysis of major and trace isotopes in gold. The geochemical difference observed may represent different histories of the gold mineralization process. To recap from the previous chapter, isotopes which discriminate between the Witwatersrand and greenstone gold, include $^{56}$Fe, $^{58}$Ni, $^{63}$Cu, $^{66}$Zn, $^{107}$Ag and $^{202}$Hg (Table 4-4; Figures 4-4 to 4-9). The gold sample set is clearly not large enough yet for detailed work and only the most general comparisons and statements can be made.

There are distinct chemical characteristics associated with individual goldfields (e.g. Hayward *et al.,* 2005), but the current data will not be able to resolve them. Large numbers of samples are needed in order to distinguish between the individual gold mines with statistical confidence. For example, eight samples from the Witwatersrand Basin can only give an indication of the geochemical characteristics of gold in the Witwatersrand Basin as a whole. Also, only eight and ten samples were available from the Zimbabwean and Barberton greenstone belts, respectively.

The geochemical difference between the Witwatersrand and greenstone gold is presented in Figures 4-4 and 4-5. These major distinctions are based on high

87

concentrations of $^{56}$Fe, $^{58}$Ni, $^{63}$Cu isotopes in native gold from the greenstone belts compared to the Witwatersrand Basin, and the higher concentrations of $^{107}$Ag and $^{202}$Hg isotopes in native gold from the Witwatersrand Basin than the greenstone belts summarized in Table 4-4. The multivariate correspondence analysis diagram also shows a clear distinction between the Witwatersrand Basin and greenstone belts (Figure 4-7). The distinction could be based on the mode of occurrences of gold.

The gold mineralization associated with the granite-greenstone terranes located in the Kaapvaal and the Zimbabwean cratons occurs in dilational veins, within brittle to ductile shear zones that are controlled by hydrothermal fluids. The most likely reason why the Barberton and Zimbabwean gold have similar geochemical signatures is because of similar geological histories (Figure 4-7).

The gold in the Witwatersrand Basin is generally hosted in the Archaean meta-sedimentary rocks in the Central Rand Group within conglomerate units (Frimmel and Minter, 2002; Hayward *et al.,* 2005). These differences in mode of occurrence could explain their distinct chemical signatures, but further investigation is beyond the scope of this study because of the greater number of samples needed.

Chisholm (1979) noted that most of the base metal gets leached from detrital gold in the descending order of leachability: iron>nickel>copper>silver. It is expected therefore that the detrital gold composition could have low concentrations of some of these base metals. The results of the current study indicate fairly high concentration of $^{56}$Fe, $^{58}$Ni and $^{63}$Cu isotopes in most of the greenstone belt samples compared to those from the Witwatersrand Basin. The results of silver do not support the expected leaching order (Table 4-4, Figure 4-4 to 4-6), if the Witwatersrand gold was derived from the greenstone belts.

The silver concentration allows discrimination between the samples from greenstone belts and the Witwatersrand Basin. The silver concentration obtained from the greenstone belts in this study is within the range of 1.01 to 4.6 wt % (Table 4-1). The silver concentration range obtained from the Witwatersrand Basin in this study is 4.2 to 9.3 wt %, within that previously reported in the literature, of 2 to 20 wt % (von Gehlen, 1983; Erasmus et al., 1987; Frimmel and Gartz, 1997; Hayward et al., 2005).

The relatively high silver concentrations in the Witwatersrand Basin have implications for the various mineralization models proposed in the literature (e.g. von Gehlen, 1983; Phillips, 1987; Phillips and Meyer, 1989; Frimmel and Minter, 2002). The Witwatersrand Basin silver concentrations do not show the expected characteristics of either alluvial or hydrothermal native gold as reported in the literature. For example, a low silver concentration is expected in placer gold, probably due to the leaching of silver during the transportation processes (Chisholm, 1979; Nakagawa et al., 2005).

If alluvial gold from the Witwatersrand Basin originated in the greenstone belts, simplistically it would be expected to have a lower silver concentration than gold from the greenstone belts. This study however shows this not to be the case. The majority of the samples analyzed from the Witwatersrand Basin have higher concentrations of silver than gold from the greenstones.

The elevated concentrations of silver in the Witwatersrand Basin may therefore offer support for the modified placer model (Frimmel and Minter, 2002; Frimmel, 2005; Hayward et al., 2005), implying that after deposition the alluvial gold was remobilized and redistributed by hydrothermal fluids. Hence the silver enrichment in

the Witwatersrand gold may have been due to post-depositional hydrothermal activity.

The source and the chemistry of the mobilizing fluids have been studied, but the reported findings do not support the metamorphic origin of a gold transporting fluid or of the gold itself (Frimmel *et al.,* 1999). What needs to be resolved is whether this metamorphosing fluid was enriched in silver when entering the Witwatersrand Basin, or whether the host rocks were enriched in silver, so that when the gold and other metals were carried in solution, the silver that was originally in the host rocks was also liberated and recrystallized with gold. In order to answer these questions, a comprehensive study is needed of the chemistry of the fluids that were responsible for remobilizing gold, and the chemistry of the host rocks. This is beyond the scope of this study.

The Archaean granite-greenstone terranes that hosted most of the gold deposits are older than the Witwatersrand Basin. Most of the gold deposits hosted in the greenstone belts are structurally controlled and have been subjected to post-depositional tectonic and metamorphic events, which may have impacted on the chemistry of the gold. For instance, in the Zimbabwean Craton, Campbell and Pitfield (1994) have suggested that metamorphic events after the first phase of gold mineralization could have caused silver to leach, resulting in a low concentration in the native gold from the greenstone belts.

The distinguishing factor between the greenstone belts and Witwatersrand gold chemistry could be based on the subsequent tectonic and metamorphic events in both regions. The placer model for the Witwatersrand Basin could be supported if tectonic events occurred in the greenstone belts to modify their residual gold signatures after

90

alluvial gold probably originating in the greenstone belt, was deposited. Subsequent leaching of silver in the greenstone belt deposits could have occurred, resulting in the incompatible silver concentrations with the Witwatersrand Basin.

Although the gold from the Witwatersrand Basin is associated with sulphides (e.g. Hayward *et al.,* 2005), the results in the current study show evidence of $^{63}$Cu depletion from the native gold compared to the Barberton Greenstone Belt (Figure 4-4), which could suggest an ultimate placer origin of the gold. In the hydrothermal processes copper and nickel tend to have an affinity with the sulphides, and are commonly found in minerals like chalcopyrite, arsenopyrite, etc. Copper and nickel are therefore expected to be in higher concentrations in most of the hydrothermal gold than in placer gold (Guerra, 2004). The depletion of copper and nickel noticed in samples from the Witwatersrand province does not necessarily reflect the signature of the primary source of gold, which could suggest the loss of these metals during local oxidizing conditions and could support the suggestion made by Dimroth and Kimberly (1976) and again Dimroth and Litchtblau (1978). But this explanation is incompatible with evidence that the Archaean atmospheric conditions were anoxic (Frimmel, 2005 and references therein).

Mercury is a volatile element, and can be expected to leach from placer gold. As with silver, the results of the current study indicate that the $^{202}$Hg concentration is higher in the Witwatersrand Basin than in the greenstone belt, which is unexpected and does not support a simple placer origin of the Witwatersrand gold (Figure 5-4). The source of mercury in the Witwatersrand Basin has been suggested to be enrichment from the surrounding sediments as a result of mobilizing fluids, which also supports the modified placer gold theory (Oberthür and Saager, 1986).

91

The distinction observed between the Witwatersrand and greenstone belts gold in the present study can be summarized. The Witwatersrand gold has elevated silver concentration and $^{202}$Hg concentration compared to the other base metal isotopes. The greenstone gold has elevated counts of base metal isotopes except for silver and $^{202}$Hg. The statistics indicate a closer association of gold chemistry between the Barberton and the Zimbabwean greenstone belts.

## 5.2   Chemical Signature of the Minor Gold Deposits

As explained above, the native gold samples analyzed in the current study do not show clear distinctions between individual gold deposits, but chemical distinctions are evident between the Witwatersrand and greenstone belts.

In comparison with the results obtained from the major gold provinces, gold samples from the Marabastadt Mine have silver concentrations and $^{202}$Hg concentrations comparable to those of the Barberton and the Zimbabwean greenstones (Figure 4-11). The gold in Marabastadt Mine was deposited within quartz veins. Additionally, the Marabastadt deposit is associated with sulphide replacement by carbonate alteration. This is a typical mineralization, which is common in the hydrothermal or the greenstone belt gold (de Wit *et al.,* 1992; Ward and Wilson, 1998). This is evident in Figure 4-11 where multivariate correspondence analysis was used to show that the gold from Marabastadt is hydrothermal.

Three gold samples that come from the Sabie-Pilgrim's Rest Goldfield have signatures resembling both the Witwatersrand Basin and the greenstone belt (Figure 4-13). The gold nuggets from Lydenburg, which were described as being associated with surface enrichment (Ward and Wilson, 1998), have lower silver and mercury

cps, compared to the New Chum Pilgrim's Rest gold hosted in fine-grained gossans. The Geodeverwacht Mine is associated with oxidized gold-quartz-carbonate sulphide veins and has high silver concentrations, but low $^{202}$Hg concentration due to the oxidizing conditions in the gossan. Both the Geodeverwacht and New Chum Pilgrim's Rest gold deposits have silver concentrations comparable to those of the Witwatersrand Basin.

The gold samples from Knysna are hosted in the Table Mountain sandstones of the Cape Supergroup. The two samples are related to the greenstone belt signatures because of the elevated counts of $^{56}$Fe, $^{58}$Co, $^{60}$Ni, $^{63}$Cu and $^{66}$Zn (Figure 4-14). The multivariate statistics plot also shows the gold from Knysna Mine closely associated with the greenstone belts (Figure 4-14). Gold mineralization here probably occurred as a result of hydrothermal processes. It has been reported that the gold is associated with quartz veins, which contain sulphide minerals like pyrite, galena and marcasite (Hammerbeck, 1976). The $^{202}$Hg concentration is comparable to that of the Barberton and the Zimbabwean greenstones.

Before discussing the archaeological artefacts in the next section, let us recap for the natural gold. There is a geochemical distinction evident in the signatures that separate the Witwatersrand gold group from the greenstone belt group. This distinction was observed in the statistics of the elemental analysis and in comparisons of the elemental signatures of $^{56}$Fe, $^{60}$Ni, $^{63}$Cu, $^{66}$Zn, $^{107}$Ag and $^{202}$Hg in native gold samples. The chemical history of any one deposit may be complex, with various elements leached or enriched by post depositional processes. The post depositional processes may alter the original signatures of any particular deposit or occurrence of gold,

93

making it impossible to establish its ultimate geological origin on the basis of the available results.

## 5.3   Chemical Signature of the Archaeological Artefacts

The analysis of archaeological gold artefacts was compared with the analyses reported by Anglo American Research Laboratories (AARL) and Desai (2001). The AARL research and the current research were done in order to understand the following: (a) whether gold used in these artefacts was sourced from a single gold deposit; (b) whether they were derived from more than one source as a consequence of complex trading routes and exchange systems at that time; (c) whether gold from particular sites was predominantly alluvial or reef mined, and (d) whether systematic alloying with silver or copper was practised.

The AARL fingerprint results were summarized by Desai (2001). There were no data tables available to be compared with the current study, in which only samples from Mapungubwe and Zimbabwe were analyzed. The table presented in Desai (2002) was based only on the presence and absence of the elements highlighted in section 1.2.

The archaeologically older Mapungubwe samples than the Thulamela samples (Miller *et al.*, 2000) from the Limpopo Basin clustered into two groups, with one showing the presence of the rare earth elements, whereas the other group showed the presence of mercury. The common characteristics of the Mapungubwe groups were the absence of strontium and barium, and the presence of the platinum-group elements. The single Bosutswe gold artefact from Botswana showed only the presence of bismuth and barium and had a completely distinct signature (Miller *et al.*, 2001). There were two groups of gold artefacts from the Zimbabwean plateau. One had similar characteristics

to the Mapungubwe samples, characterized by the presence of strontium, mercury, rare earth elements, platinum-group elements and barium.

The other group from the Zimbabwean plateau was characterized by the presence of copper, silver, mercury, and lead. The archaeologically younger Thulamela samples from Kruger National Park showed the presence of all the elements outlined above, with a strong correlation to one of the Mapungubwe signatures, perhaps suggesting a common source (Desai, 2001; Miller and Desai, 2004).

The AARL study scanned the entire periodic table and signatures were compared on the basis of a large number of elements (Grigorova et al., 1998; Miller et al., 2001). In the current study the comparisons are based on only a few isotopes, including $^{56}$Fe, $^{107}$Ag, $^{202}$Hg, $^{66}$Zn, $^{63}$Cu and $^{58}$Ni considered most likely to define distinct signatures. The rare earth elements were found below the lower limit of detection. The archaeological gold artefacts analyzed in this study came only from Mapungubwe and Great Zimbabwe, dating from the early 11$^{th}$ to early 14$^{th}$ centuries AD, and the mid-14$^{th}$ to mid-16$^{th}$ centuries AD respectively (Miller, 2002).

In the current study, there are clear distinctions in the archaeological gold artefact signatures from Mapungubwe and Zimbabwe, based on $^{107}$Ag, $^{75}$As $^{66}$Zn, $^{202}$Hg and the Pb isotopes in cps (Table 4-5). Strontium, barium and the rare earth elements were not detected. These are the rock forming elements and are unlikely to bond with gold as they have no siderophile tendency (Levinson, 1974). The presence (or absence) of strontium, barium and the rare earth elements in gold artefacts therefore can give information about silicates (which may be secondary) associated with the gold, but not about the gold itself, and should not be used for classification. The Zimbabwean artefacts have higher $^{107}$Ag and $^{66}$Zn concentrations compared to the low

95

concentrations of these isotopes in Mapungubwe artefacts. There are also overlaps of the Zimbabwean and Mapungubwe artefacts in terms of platinum and mercury.

The Zimbabwean artefacts are chemically distinguishable from the Mapungubwe artefacts (Figures 4-15; 4-17 and 4-18). In the current study, the Zimbabwean artefacts are clustered into two distinct groups, similar to the groups suggested by Desai (2001). One of the Zimbabwe groups, represented by few samples, was distinguished based on the low concentrations of silver, zinc, osmium and mercury, and is similar to the Mapungubwe group. This implies that the earlier Mapungubwe material may have been sourced from the Zimbabwe plateau. The later Great Zimbabwe material probably included material from a diversity of sources, so it is not surprising that there is a wider diversity of signatures in the Great Zimbabwe material (Grigorova et al., 1998; Miller et al., 2001).

Compared to the natural gold samples analyzed in this study, the Mapungubwe gold artefacts in this study were found to be chemically most similar to the gold from the Barberton and the Zimbabwean greenstone belts. It is possible that the gold at Mapungubwe and Thulamela was sourced from the nearest surrounding greenstone belts, which include the southern Zimbabwean greenstones, the Barberton, Giyani, Murchison and Pietersburg greenstone belts in South Africa. It would be premature to trace the source of gold at Mapungubwe based on the few samples analyzed in this study, but it adds to our understanding of the type of source that could be expected.

The suggestion was made by Desai (2001) that the Mapungubwe gold artefacts might be reef mined and cannot be sourced to the alluvial gold ore deposits in the Transvaal vicinity because of their relatively high silver concentration. To resolve this question, alluvial gold samples need to be analyzed and compared to the Mapungubwe samples.

Some of the Zimbabwean artefacts are chemically similar to the gold from the Witwatersrand Basin (Figure 4-16), based on the $^{202}$Hg, $^{63}$Cu and $^{66}$Zn concentrations. It is extremely unlikely that the Witwatersrand Basin was the source of this gold. There is no archaeological evidence of mining from the Witwatersrand reefs, which is not surprising given that the gold was in finely disseminated form and not visible in quartz veins, as on the Zimbabwe plateau (Miller *et al.,* 2001). There are also numerous archaeological gold mines recorded on the Zimbabwe plateau (Swan, 1994), so it is more likely that gold was traded to the south rather the north. This leaves the chemical similarity of the Zimbabwe archaeological material to the Witwatersrand gold as an unresolved archaeological puzzle.

Statistically, there is no chemical similarity between the archaeological gold and the natural gold samples (Figure 4-17). The clear distinction between these two different sets of gold samples may have occurred as a result of the processes involved during the extraction and processing technology of the archaeological gold, or may be due to archaeological sources not represented in the modern samples.

The southern African archaeological gold fabrication technology has been well documented by Miller and Desai (2004). The artefacts they studied had silver concentrations ranging from 2 % to 12 %, which did not correlate with the artefact type. The metals were cold worked and showed no evidence of soldering or welding. Miller and Desai (2004) ascribed the silver concentrations to the natural source(s), but as observed in the current study the silver concentrations in the Zimbabwean artefacts are comparable to those of the Witwatersrand Basin.

If the Zimbabwe artefacts are truly derived from local material then silver may have been added. On the other hand, there is no recorded silver source in the southern

97

African archaeological record (Miller, 2002). Because of its relative volatility, silver is more likely to be lost than concentrated when melting gold in an open crucible. At present the high levels of silver in some of the Zimbabwean artefacts cannot be explained, and this remains a provocative issue for future investigation by archaeometallurgists.

In Table 4-3, the high platinum-group elements in all the archaeological artefacts also cannot be explained easily, although they could point to an alluvial source in proximity to the Bushveld complex. During melting of gold, the heating process does not affect elements like platinum and osmium with high melting points, whereas volatile elements like mercury and copper may have evaporated.

The low $^{202}$Hg concentration observed in most of the gold artefacts from Zimbabwe and Mapungubwe may be the result of melting under oxidizing conditions in an open crucible (Figure 4-19). Miller and Desai (2004) suggested that the metals were cold worked and the artefacts show no evidence of soldering or welding. The low mercury concentrations found in this study do not support Miller and Desai (2004) model, as the gold artefacts was heated (as least sometimes) during the process of manufacture, and has lost mercury as a result.

The elevated $^{66}$Zn concentration (see Figures 4-15 and 4-16) in the Zimbabwean artefacts is also a provocative puzzle. There is also no record of indigenous zinc production in pre-colonial southern Africa. A nodule of zinc-containing alloy found at Mapungubwe was probably imported from India, via East Africa (Miller, 2002). The $^{66}$Zn in the Zimbabwean artefacts could, however, be due to melting gold in crucibles previously used to melt imported brass.

In summary, there are unresolved problems explaining the elevated platinum-group elements, silver and zinc levels in the archaeological gold samples. Until these have been addressed by analysis of natural alluvial samples for comparison, the question of possible silver alloying in the archaeological material has to be left open.

There are also inherent difficulties in tracing gold from any particular archaeological site to source. These include the possibility of mixing gold from multiple sources, recycling, contamination in melting and trade of items (Grigorova *et al.,* 1998; Miller *et al.,* 2001), as well as the need to have sampled all possible sources for comparison.

For example, in the case of Great Zimbabwe it is likely that mixing occurred, because of the diverse potential sources of gold accessible to this powerful trading centre (Miller, 2002). By comparison at Mapungubwe and Thulamela, which were smaller centres, it is likely that gold originated from fewer or even only one source. This seems to be borne out by the greater diversity of elemental signatures from Great Zimbabwe.

Taken together, these problems make it impossible to source the gold artefacts directly to their actual gold ore deposits on the basis of the information at hand. The current study also does not enable us to state clearly if gold from any particular site was sourced in any particular region, because the chemical signatures of the archaeological gold appear to be quite distinct from those of the natural samples currently available for comparison. This is a provocative outcome of the comparative study, and an obvious target for further research. Large numbers of samples are still needed to be used successfully in making statements based on the geochemical signatures with statistical confidence.

# 6 CONCLUSIONS AND RECOMMENDATIONS

The use of the LA-ICP-MS technique to trace the geological source of archaeological gold has not been successful. There were analytical technique limitations involved; the gold sample size varies, thus making it difficult for the selection of a consistent protocol; some samples were too small and were not analyzed. For a successful comparison of the data measured by the LA-ICP-MS with the data on various elements already reported in the literature, there is a need to set up in-house standards for various elements for analysis.

The gold compositional data comparison has been found useful for discriminating between gold samples from the greenstone belts (hydrothermal origin) and the Witwatersrand Basin (modified placer origin) (Table 4-4; Figures 4-4 to 4-9). The major distinctions are elevated concentrations of $^{56}$Fe, $^{60}$Ni, $^{63}$Cu and $^{66}$Zn isotopes of the greenstone belts, compared to the Witwatersrand Basin, with the converse true for the $^{107}$Ag and $^{202}$Hg in the Witwatersrand Basin when compared to the greenstone belts.

The comparison of geochemical data has highlighted some important questions for future research in both geological and archaeological scientific fields of study. The concentrations of silver and other elements in gold from the Witwatersrand Basin and the greenstone belts have raised the following questions.

Does the relatively high silver concentration in the Witwatersrand Basin reflect the original signature of the source?

Was the silver concentration from the host rocks and was it enriched as a result of hydrothermal fluids responsible for remobilizing gold within the Witwatersrand Basin?

Could the relatively low silver concentration in the greenstone belts be a result of post depositional tectonic and metamorphic events?

The platinum-group isotopes in native gold samples from the major gold provinces were found at low concentrations. The low concentrations in some platinum-group isotopes in the Witwatersrand Basin probably occurred as a result of leaching from the gold and could have been concentrated around the vicinity. In order to understand this, there is a need for further investigation through the study of more samples. The question relating to the gold mineralization within the Witwatersrand Basin and the surrounding greenstone belts cannot be answered by the data presented in this study. There is a need for more samples to be drawn from the Witwatersrand Basin and the greenstones.

The $^{63}$Cu and $^{60}$Ni concentrations in the Witwatersrand Basin are low when compared to the concentrations in the greenstone belts. This could be the result of local oxidizing conditions in the Witwatersrand Basin, which must have taken place long after deposition because the Archaean atmosphere generally is thought of as anoxic (Frimmel, 2005). But the oxidizing rationale could be support for some suggestions of less oxygenated atmospheric conditions in the Archaean (Palmer *et al.*, 1987). The issue of the Archaean atmospheric conditions within the Witwatersrand Basin cannot be addressed by data presented in this thesis.

The minor gold deposits cannot be sourced directly to the major gold deposits but their chemical characteristics can be associated with either the greenstone belt or Witwatersrand gold type. The gold samples from Marabastadt Mine, which was located in the Pietersburg Greenstone Belt, were successfully related to the greenstone belt gold type. The two gold samples from the Sabie-Pilgrim's Rest Goldfield were related to the Witwatersrand Basin type. However, the conclusion that they could be traced to the Witwatersrand Basin as their source would be premature. The chemistry of the gold nugget sample from the Sabie Pilgrim's Rest Goldfield was found to be similar to that of the greenstone belts, thus making it different from the other two gold samples. Obviously, more samples are needed to characterise the range of variation in this material. The chemistry of gold from Knysna was found to be similar to the greenstone gold type. The gold from Knysna is hosted in the Table Mountain sandstones, but cannot simply be placer gold. Hydrothermal processes could have been responsible for the deposition or reworking of gold in Knysna.

The compositional data was not found to be very useful in sourcing archaeological gold artefacts to their ultimate source(s). Alluvial gold samples need to be analysed, for comparison with archaeological material. In this study, there are chemical distinctions observed between the Zimbabwean and the Mapungubwe artefacts. The Zimbabwean gold artefacts have higher $^{107}$Ag, $^{66}$Zn, $^{188}$Os and $^{195}$Pt concentrations than the Mapungubwe gold artefacts. Based on the current isotopic data, the gold chemistry of all the archaeological artefacts was statistically different from the natural gold samples. The difference in artefacts when compared to the natural gold signatures could be as a result of the following: (1) mixing gold from multiple sources; (2) recycling of the materials used; (3) contamination in melting or

manufacturing, which affected the composition (e.g. Hg boiled off); (3) trade of ore or items from more distant sources not represented in the present study.

The main requirement for future research is to broaden and deepen the populations represented in the present study. This means the inclusion of many more samples from modern hard rock sources, as well as alluvial gold, and samples from historical collections representing surface material no longer available to modern prospectors. This should include investigations of the homogeneity of the individual artefacts and the natural gold. It may be done by multiple spot analyses on one archaelogical object (e.g. bead or wire ring) in order to assess variability. It might also include replicating the melting cycle and forging of the artefacts. The application can open new insights into African history.

An adequate number of samples could form the basis for future studies of natural gold geochemical history, the sourcing of unprovenanced natural samples to their original sources, the identification of sources of stolen gold and the sourcing of archaeological material if this has not suffered mixing or alloying.

# 7 REFERENCES

Allan, G.C. and Woodcock, J.T. (2001). A review of the flotation of native gold and electrum. *Minerals and Engineering*, 14, 9, pp 931-962.

Anhaeusser, C.R. (1974). The geology of the Sheba hills area of the Barberton Mountain Land, South Africa, with particular reference to the Eureka syncline. *Economic Geology Research Unit Information Circular*, University of Witwatersrand, 94, pp 1-47.

Anhaeusser, C.R. and Maske, S. (1986). Mineral deposits of southern Africa. *The Geological Society of South Africa*, 1, pp 113-115.

Antweiler, J.C. and Campbell, W.L. (1977). Application of gold compositional analyses to mineral exploration in the United States. *Journal of Geochemical Exploration*, 8, pp 17-29.

Bartholomew, D.S. (1990). Gold deposits of Zimbabwe. *Mineral Resources Series, Zimbabwe Geological Survey*, 94, pp 1-213.

Boyle, R.W. (1979). The geochemistry of gold and its deposits (together with a chapter on geochemical prospecting for the element). *Geological Survey of Canada*, 280, pp 1- 584.

Boyle, R.W. (1984). Gold deposits; their geology, geochemistry and origin. *In:* Foster R.P. (ed). *Gold' 82: The geology, geochemistry and genesis of gold deposits.* Geological Society of Zimbabwe, 1, pp 183-189.

Brandl, G. and de Wit, M.J. (1997). The Kaapvaal Craton. *In:* de Wit, M.J. and

Ashwall, L.D. (eds). *Greenstone belts.* Oxford University Press, Oxford, pp 581-607.

Buitendag, W.L. (2007). Gold locality map. *Mineral Resources Unit,* Council for Geoscience, Pretoria.

Campbell, S.D.G. and Pitfield P.E.J. (1994). Structural controls of gold mineralization in the Zimbabwe craton- Exploration guidelines. *Zimbabwe Geological Survey,* Bulletin 101, pp 1-270.

Chapman, R., Leake, B. and Styles, M. (2002). Microchemical characterization of alluvial gold grains as an exploration tool. *Gold bulletin,* 35, 2, pp. 53-65.

Chisholm, J.M. (1979). Composition of native gold. *In:* Glover, J.E. and Groves D.I. *Gold mineralization.* The Geology Department and the Extension Service, University of Western Australia, Publication 3, pp 65-75.

Cochran, A. (1982). Fluid inclusion populations in quartz-rich gold ores from the Barberton Greenstone Belt, Eastern Transvaal, South Africa. Unpublished M.Sc thesis: *University of Arizona,* pp 1-199.

Cowey, A. (1994). Mining and metallurgy in South Africa - a pictorial history. Mintek, South Africa, pp 1-120.

Desai, N. (2001). Technological, social and economic aspects of gold production and the use of Iron Age people of southern Africa. Unpublished MSc. thesis: University of Cape Town.

De Ronde, C.E.J. and de Wit, M.J. (1994). Tectonic history of the Barberton

Greenstone Belt, South Africa: 490 million years of Archean crustal evolution. *Tectonics*, 13, 4, pp 983-1005.

De Ronde, C.E.J., Kamo, S., Davis, D.W., de Wit, M.J. and Spooner, E.T.C. (1991). Field, geochemical, and U-Pb isotopic constraints from hypabyssal felsic intrusions within the Barberton Greenstone Belt, South Africa: implications for tectonics and the timings of gold mineralization. *Precambrian Research*, 49, pp 261-280.

De Ronde, C.E.J., Spooner, E.T.C., de Wit, M.J. and Bray, C.J. (1992). Shear zone related Au-quartz deposits in the Barberton Greenstone Belt, South Africa: field and petrographic characteristics, fluid properties and light stable isotope geochemistry. *Economic Geology*, 87, pp 366-402.

De Vaal, J.B. (1984). Ou handelsvoetpaaie en wapaaie in oos- en noord- Transvaal. *Contree,* 16, pp 5-17.

De Vaal, J.B. (1985). Handel langs die vroegste roetes. *Contree,* 17, pp 4-14.

De Wit, M.J. (1998). On Archaean granites, greenstones, cratons and tectonics: does evidence demand verdict? *Precambrian Research*, 91, pp 181-226.

De Wit, M.J., Roering, C., Hart, R.J., Armstromg, R.A., de Ronde, C.E.J., Green, R.W., Tredoux, M., Peberdy, E. and Hart, R.A. (1992). Formation of an Archaean continent. *Nature*, 357, pp 553-562.

Dimroth, E. and Kimberly, M.M. (1976). Precambrian atmospheric oxygen: evidence in the sedimentary distributions of carbon, sulfur, uranium and iron. *Canadian Journal of Earth Sciences*, 13, pp 1161-1185.

106

Dimroth, E. and Lichtblau, A.P. (1978). Oxygen in the Archaean ocean; comparison of ferric oxide crusts on Archaean and Cainozoic pillow basalts. *Neues Jahrbuch für Mineralogie Abhndlungen,* 133, pp 1-22.

Dirks, P.H.G.M and van der Merwe, J.A. (1997). Tectonic stacking in an Archaean greenstone sequence and its control on gold mineralization at Dalny Mine, Zimbabwe. *Journal of African Earth Science*s, 24, 4, pp 603-619.

Dirks, P.H.G.M., Kroner, A., Jelsma, H.A., Sithole, T.A and Vinyu, M.L. (1999). Structural relations and Pb-Pb zircon ages for the Makuti gneisses: evidence for the crustal-scale Pan-African shear zone in the Zambezi Belt, northwest Zimbabwe. *Journal of African Earth Sciences*, 28, 2, pp 427- 442.

Du Plessis, S.J.P., Engelbrecht, L.N.J. and Visser, D.J.L. (1984). Geological map of the Republic of South Africa, Transkei, Bophuthatswana, Venda and Ciskei and the Africa kingdoms of Lesotho and Swaziland. *Republic of South Africa.* Gravity edition.

Erasmus, C.S., Sellschop, J.P.F. and Waterson, J.I.W. (1987). New evidence on the composition of mineral grains of native gold. *Nuclear Geophysics*, 1, 1, pp 1-23.

Falconer, D.M., Craw, D., Youngson, J.H. and Faure, K. (2005). Gold and sulphide minerals in the Tertiary quartz pebble conglomerate gold placers, Southland, New Zealand. *Ore Geology Reviews*, 20, pp 1-21.

Foster, R.P. and Wilson, J.F. (1984). Geological setting of Archaean gold deposits in Zimbabwe. *In:* Foster R.P. (ed). *Gold' 82: The geology, geochemistry and*

*genesis of gold deposits.* Geological Society of Zimbabwe, 1, pp 521-568.

Frimmel, H.E. (2005). Archaean atmospheric evolution: evidence from the Witwatersrand gold fields, South Africa. *Earth-Science Reviews*, 70, 1-2, pp 1-46.

Frimmel, H.E. and Gartz, V.H. (1997). Witwatersrand gold particle chemistry matches model of metamorphosed, hydrothermally altered placer deposits. *Mineralium Deposita*, 32, pp 523-530.

Frimmel, H.E. and Minter W.E.L. (2002). Recent developments concerning the geological history and genesis of the Witwatersrand gold deposit, South Africa. *Society of Economic Geologists*, Special Publication 9, pp 17-45.

Frimmel, H.E., Hallbauer, D.K. and Gartz, V.H. (1999). Gold mobilizing fluids in the Witwatersrand Basin: composition and possible sources. *Mineralogy and Petrology*, 66, pp 55-81.

Fyfe, W.S. and Kerrich, R. (1984). Gold: Natural concentration processes. *In:* Foster, R.P. (ed). Gold' 82: *The geology, geochemistry and genesis of gold deposits.* Geological Society of Zimbabwe, 1, pp 99-127.

Gan, S. and van Reenen D.D. (1997). Geology of gold deposits in the Southern Marginal Zone of the Limpopo Belt and the adjacent Sutherland Greenstone Belt, South Africa: Klein Letaba. *South African Journal of Geology*, 100, 1, pp 73-83.

Gasparrin, C. (1993). Gold and other precious metals: from ore to market. *Springer-Verlag,* pp 1-397.

Gihwala, D., Jacobson, L., Peisach, M. & Pineda, C.A. (1986). Proton-induced techniques for the determination of some trace impurities in gold objects. *South African Journal of Science,* 82, pp 258-260.

Gray, A.L. (1985). Solid sample introduction by laser ablation for inductively coupled plasma source-mass spectrometry. *Analyst,* 110, no. 5, pp 551-556.

Grigorova, B., Smith, W., Stülpner, K., Tumilty, J.A and Miller, D. (1998). Fingerprinting of gold artefacts from Mapungubwe, Bosutswe and Thulamela. *Gold Bulletin,* 31, 3, pp 99-102.

Groves, D.I. and Foster R.P. (1991). Archaen lode deposits. In: Foster, R.P. (ed). *Gold metallogeny and exploration.* Blackie and Son Ltd, pp 63-103.

Groves, D.I., Goldfarts R.J., Gebre-Marian M., Hagemann S.G. and Robert F. (1998). Orogenic gold deposits: A proposed classification in the context of their crustal distribution and relationship to other gold deposits types. *Ore Geology Reviews,* 13, pp 7-27.

Guerra, M.F. (2004). The circulation of South America precious metals in Brazil at the end of the 17th century. *Journal of Archaeological Science,* 31, pp 1225-1236.

Guerra, M.F., Calligaro, T., Radtke, M., Reiche, I. and Riesemeier, H. (2005). Fingerprinting ancient gold by measuring Pt with spatially resolved high energy Sy-XRF. *Nuclear Instruments and Methods in Physics Research Section B: Beam Interactions with Materials and Atoms,* 240, 1-2, pp 505-511.

Günther, D. and Hattendorf, B. (2005). Solid sample analysis using laser ablation

inductively coupled plasma mass spectrometry. *Trends in Analytical Chemistry*, 24, 3, pp 255-265.

Günther, D., Jackson, S.E. and Longerich, H.P. (1999). Laser ablation and arc/spark solid sample introduction into inductively coupled plasma mass spectrometers. *Spectrochimia Acta Part B*, 54, pp 381-409.

Hall, M.E., Brimmer, S.P., Li, F.H. and Yablonsky, L. (1998). ICP-MS and ICP-OES studies of gold from a late Sarmatian burial. *Journal of Archaeological Science*, 25, pp 545-552.

Hammerbeck, E.C.I. (1976). Gold outside the Witwatersrand triad. *In:* Coetzee, C.B. (ed). *Mineral resources of the Republic of South Africa.* Department of Mines, Geological Survey, Fifth Edition, Handbook 7, pp 75-92.

Harley, M. and Charlesworth, E.G. (1996). The role of fluid pressure in the formation of bedding–parallel, thrust-hosted gold deposits, Sabie-Pilgrim's Rest goldfield, eastern Transvaal. *Precambrian Research*, 79, pp 125-140.

Hayward, C.L., Reimold, W.U., Gibson, R.L. and Robb, L.J. (2005). Gold mineralization within the Witwatersrand Basin, South Africa: evidence for a modified placer origin, and the role of the Vredefort impact event. *Geological Society, London*, Special Publications, 248, pp 31-58.

Houstoun, S.M. (1987). Competency contrasts and chemical controls as guides to gold mineralization: an example from the Barberton Mountain Land, South Africa. *In:* Ho, S.E. and Groves, D.I. (eds). *Recent advances in understanding Precambrian gold deposits.* The Geology Department and University

Extension: The University of Western Australia, 11, pp 147-160.

http://sbio.uct.ac.za/Webemu/SEM_school/. *The Electron Microscope Unit*, University of Cape Town.

Huffman, T.N. (2007). Handbook to the Iron Age. The archaeology of pre-colonial farming societies in southern Africa. Scottsville: *University of KwaZulu Natal Press*.

Huffman, T.N. (2009). Mapungubwe and Great Zimbabwe: The origin and spread of social complexity in southern Africa. *Journal of Anthropological Archaeology* 28: 37-54.

Jacobson, L., Fish, W.S. and van der Westhuizen, W.A. (2002). XRF analysis of pottery from Mutokolwe, a Khami settlement from the Soutpansberg mountains, South Africa. *In:* Glascock, M. (ed.) *Geochemical evidence for long distance exchange*. Westport, Connecticut: Bergin & Garvey, pp 215-228.

Jackson, S.E., Longerich, H.P., Dunning, G.R. and Fryer, B.J. (1992). The application of laser-ablation microprobe-inductively coupled plasma-mass-spectrometry (LAM-ICP-MS) to in situ trace-element determinations in minerals. *Canadian Mineralogy*, 30, pp 1049-1064.

Jarvis, K.E., Williams, J.G., Parry, S.J. and Bertalan, E. (1995). Quantitative determination of platinum-group elements and gold using NiS fire assay with laser ablation-inductively coupled plasma-mass spectrometry (LA-ICP-MS). *Chemical Geology*, 124, pp 37-46.

Kalbskopf, S. and Nutt T. (2003). Lithological contrasts and constrains on gold mineralization in granitoids in the Zimbabwe craton: Structural controls and implications for exploration. *Economic Geology Research Institute, Information Circular*, 370, pp 1-24.

Killick, A.M. and Scheepers, R. (2005). Controls to hydrothermal gold mineralization in the Witwatersberg Goldfield; situated in the floor to the south of the Bushveld Complex, South Africa. *Journal of African Earth Sciences*, 41, pp 238-250.

Letcher, O. (1936). The Gold Mines of Southern Africa: The History, Technology and Statistics of the Gold Industry. *Proclamination of the Witwatersrand and the Jubilee of the city of Johannesburg*. 12- 43.

Levinson, A.A. (1974). Introduction to Exploration Geochemistry. *Applied Publishing Ltd. Wilmette, Illinois, Department of Goelogy and Calgary, USA,* pp 1-924.

Longerich, J. (2001). Chemometrics. *In:* Sylvester, P.J., (ed), *Laser-ablation-ICPMS in the earth sciences: principles and applications.* Mineralogical Association of Canada, Short Course Series, 29, 21-28.

Longerich, H. and Diegor, W. (2001) - Introduction to mass spectrometry. *In:* Sylvester P.J. (ed). *Laser Ablation-ICP-Mass Spectrometry in the Earth Sciences: Principles and Applications.* Mineralogical Association of Canada, Short Course Series, 29, 1-19.

Longerich, H. P., Jackson, S. E., Fryer, B.J. and Strong, D.F. (1993). The laser ablation microprobe-inductively coupled plasma-mass spectrometer. *Geoscience Canada,* 20, pp 21-27.

Longerich, H.P., Jackson, S.E. and Günther, D. (1996). Laser ablation inductively coupled mass spectrometric transient signal data acquisition and analyte concentration calculation. *Journal of Analytical Atomic Spectrometry*, 11, pp 899-104.

Mann, A.G. (1984). Gold mines in Archaean granitic rocks in Zimbabwe. *In:* Foster, R.P. (ed). *Gold' 82: The geology, geochemistry and genesis of gold deposits.* Geological Society of Zimbabwe, 1, pp 553-568.

Martin, H. (1993). The mechanisms of petrogenesis of the Archaean continental crust: comparison with modern processes. *Lithos,* 30, pp 373-388.

Minter, W.E.L., Goedhart, M., Knight, J. and Frimmel, H.E. (1993). Morphology of Witwatersrand gold grains from the Basal reef: evidence for their detrital origin. *Economic Geology*, 88, pp 237-248.

Miller, D. (1995). 2000 years of indigenous mining and metallurgy in southern Africa - a review. *South African Journal of Geology,* 98, pp 232-238.

Miller, D. (2001). Metal assemblages from the Greefswald areas, South Africa: K2, Mapungubwe Hill and Mapungubwe Southern Terrace. *South African Archaeological Bulletin,* 56, pp 83-103.

Miller, D. (2002). Smelter and Smith: Iron age metal age fabrication technology in southern Africa. *Journal of Archaeological Science*, 29, pp 1083-1131.

Miller, D. and Desai, N. (2004). The fabrication technology of southern African archaeological gold. *Annals of the South African Museum,* 111, pp 79-102.

Miller, D., Desai, N. and Lee-Thorp, J. (2000). Indigenous gold mining in southern Africa: a review. *South African Archaeological Society*, Goodwin Series 8, pp 91-99.

Miller, D., Desai, N., Grigorova, D. and Smith, W. (2001). Trace elements study of gold from southern African archaeological sites. *South African Journal of Science*, 97, pp 297-300.

Mosier, E.L., Cathrall, J.B., Antweler, J.C. and Tripp, R.B. (1989). Geochemistry of placer gold, Koyukuk-Chandalar mining district, Alaska. *Journal of Geochemical Exploration*, 31, pp 97-115.

Nakagawa, M., Santosh, M., Nambiar, C.G. and Matsubara, C. (2005). Morphology and chemistry of placer gold from Attappadi valley, southern India. *Gondwana Research*, 8, 2, pp 213-222.

Obethür, T. and Saager, R. (1986). Silver and mercury in gold particles from the Proterozoic Witwatersrand placer deposits of South Africa: metallogenic and geochemical implications. *Economic Geology*, 81, pp 20-31.

Oddy, A. (1983). On the trail of Iron Age gold. *Transvaal Museum Bulletin*, 19, pp 24-26.

Oddy, A. (1984). Gold in the southern African Iron Age: A technological investigation of the Mapungubwe and other finds. *Gold Bulletin*, 17, 2, pp 70-78.

Ohata, M., Yasuda, H., Namai, Y. and Furuta, N. (2002). Laser ablation inductively coupled plasma mass spectrometry (LA-ICP-MS): comparison of different

internal standardization methods using laser-induced plasma (LIP) emission and LA-ICP-MS signals. *Analytical Sciences*, 18, pp 1105-1110.

Outridge, P.M., Doherty, W. and Gregoire, D.C. (1998). Determination of trace elemental signatures in placer gold by laser ablation inductively coupled plasma mass spectrometry as a potential aid for gold exploration. *Journal of Geochemical Exploration*, 60, pp 229-240.

Palmer, J.A., Phillips, G.N. and McCathy, T.S. (1987). The nature of the Precambrian atmosphere and its relevance to Archaean gold mineralization. *In:* Ho, S.E. and Groves, D.I. (eds). *Recent advances in understanding Precambrian gold deposits.* The Geology Department and University Extension: The University of Western Australia, 11, pp 321-326.

Perkins, W.T. and Pearce, N.J.G. (1995). Mineral microanalysis by laser probe inductively coupled plasma mass spectrometry. *In:* Potts, P.J., Bowles, J.F.W., Reed, S.J.B. and Cave, M.R. (eds). *Microprobe techniques in the earth sciences.* Mineralogical Society Series 6, pp 291-323.

Phillips, G.N. (1987). Metamorphism of the Witwatersrand gold fields: conditions during peak metamorphism. *Journal of Metamorphic Geology*, 5, pp 307-322.

Phillips, G.N. and Meyer, R.E. (1989). The Witwatersrand gold fields: Part II. An origin for Witwatersrand gold during metamorphism and associated alteration. *In:* Keays, R.R., Ramsay, W.R.H. and Groves, D.I. (eds). *The geology of gold deposits: the perspective in 1988.* Economic Geology Monograph 6, pp 598-608.

Phimister, I.R. (1976). Pre-Colonial gold mining in southern Zambezi: a reassessment. *African Social Research,* 21, pp 1-30.

Raymond, J., Williams-Jones, A.E. and Clark, J.R. (2005). Mineralization associated with scale and altered rock and pipe fragments from the Berlin geothermal field, El Salvador; implications for metal transport in natural systems. *Journal of Volcanology and Geothermal Research*, 145, pp 81-96.

Reed, S.J.B. (1995). Electron microprobe microanalysis. *In:* Potts, P.J., Bowles, J.F.W., Reed, S.J.B. and Cave, M.R. (eds). *Microprobe techniques in the earth sciences*. Mineralogical Society Series 6, pp 291-323.

Reisberg, L., Olivier, A., Lorand, J.P. and Ohnenstetter, M. (2004). Highly siderophile element behaviour in high temperature processes. *Chemical Geology*, 208, 1-4, pp 1-4.

Robb, L.J. and Robb, V.M. (1998). Gold in the Witwatersrand Basin. *In:* Wilson, M.G.C. and Anhaeusser, C.R. (eds). *The Mineral Resources of South Africa*. Council for Geoscience Handbook 16. Council for Geoscience, Pretoria, pp 294-349.

Robb, J.L. and Meyer F.M. (1995). The Witwatersrand Basin, South Africa: Geological framework and mineralization processes. *Ore Geology Reviews*, 10, pp 67-94.

Roeder, E. (1984). Fluid-inclusion evidence bearing on environments of deposition. *In:* Foster, R.P. (ed). *Gold' 82: The geology, geochemistry and genesis of gold deposits*. Geological Society of Zimbabwe, 1, pp 129-164.

Russo, R.E., Mao, X., Liu, H., Gonzalez, J., Mao, S.S. (2002). Laser ablation in analytical chemistry-a review. Lawrence Berkeley National Laboratory, Beckerly, USA. *Talanta*, 57, pp 425-451.

Schürmann, L.W., Ward J.H.W., Horstmann U.E, Jordan L.J. and Eaton B. (2000). Carbonate dykes associated with Archaean lode-Au mineralization, Barberton Greenstone Belt, South Africa. *Journal of African Earth Sciences*, 30, 2, pp 249-266.

Seward, T.M. (1984). The transport and deposition of gold in hydrothermal systems. *In:* Foster, R.P. (ed). *Gold' 82: The geology, geochemistry and genesis of gold deposits*. Geological Society of Zimbabwe, 1, pp 183-189.

Sie, S.H., Murao, S. and Suter, G.F. (1996). Trace element distribution in native gold. *Nuclear Instruments and Methods in Physics Research B*, 109/110, pp 633-638.

Siebert, C., Kramers, J.D., Meisel, T.H., Morel, P.H. and Nagler, T.H. F. (2005). PGE, Re-Os, and Mo isotope systematics in the Archaean and early Proterozoic sedimentary systems as proxies for redox conditions of the early earth. *Geochimica et Cosmochimica Acta*, 69, 7, pp 1787-1801.

SACS (South African Committee for Stratigraphy). (1980). Part 1: Lithostratigraphy of the Republic of South Africa, South West Africa/Namibia and the Republics of Bophuthatswana, Transkei and Venda. *Stratigraphy of South Africa 8*. Geological Survey of South Africa, Pretoria, pp 1-690.

Summers, R. (1969). Ancient mining in Rhodesia and adjacent areas. Salisbury:

*National Museums of Rhodesia Memoir*, 3, pp 1-2.

Swan, L. (1994). Early gold mining on the Zimbabwean plateau. Studies in African Archaeology 9. *Uppsala: Societas Archaeologica Uppsaliensis*, pp 1-181.

Thomas, R. (2001). A beginer's guide to ICP-MS. www.spectroscopyonline.com, *Spectroscopy*, 16, 4-27, pp 38-48.

Tyler, R. and Tyler, N. (1996). Stratigraphic and structural controls on gold Mineralization in the Pilgrim's Rest goldfield, eastern Transvaal, South Africa. *Precambrian Research*, 79, pp 141-169.

Viljoen, M.J. (1984). Archaean gold mineralization and komatiites in southern Africa. *In:* Foster, R.P. (ed). *Gold' 82: The geology, geochemistry and genesis of gold deposits.* Geological Society of Zimbabwe, 1, pp 595-628.

Viljoen, M.J. and Viljoen, R.P. (1969). An introduction to geology of the Barberton Granite-Greenstone terrain: Special Publication. *Geological Society of South Africa*, 2, pp 7-48.

Vlachou-Mogire, C., Stern, B. and McDonnell, J.G. (2007). The application of LA-ICP-MS in the examination of the thin plating layers found in late Roman coins. *Nuclear Instruments and Methods in Physics Research B*, 265, pp 558-568.

Voges, F.D. (1986). The New Consort Mine, Barberton Greenstone Belt. *In:* Anhaeusser, C.R. and Maske, S. (eds). *Mineral deposits of southern Africa*, Geological Society of South Africa, 1, pp 155-162.

Von Gehlen, K. (1983). The morphology and silver content of gold from the upper Witwatersrand and Vensterdorp systems in the Klerksdorp goldfield, South Africa, Johannesburg. *Mineralium Deposita*, 18, pp 529-534.

Wagner, J.H.F. and Wiegand, J. (1986). The Sheba gold Mine, Barberton Greenstone Belt. *In:* Anhaeusser, C.R. and Maske, S. (eds). *Mineral deposits of southern Africa*, Geological Society of South Africa, 1, pp 155-162.

Ward, J.H. (1963). Hierarchical grouping to optimize an objective function. *Journal of American Statistical Association*, 58, pp 236-244.

Ward, J.H.W. and Wilson, M.G.C. (1998). Gold outside the Witwatersrand Basin. *In:* Wilson, M.G.C. and Anhaeusser, C.R. (eds.). *The mineral resources of South Africa,* 16, Council for Geoscience, Pretoria, pp 350-386.

Watling, R.J., Herbert, H.K, Delev, D. and Abel, I.B. (1994). Gold fingerprinting by Laser Ablation Coupled plasma mass sprectrometrotry. *Spectrochimica*, 49B (2), pp 205-219.

Watling, R.J., Taylor, J.J., Shell, C.A., Chapman, R.J, Warner, R.B., Cahill, M. and Leake, R.C. (1999). The application of laser ablation inductively coupled plasma mass spectrometry (LA-ICP-MS) for establishing the provenance of gold ores and artefacts. *Archaeopress*, 6, pp 54-61.

Williams, P.J. (1997). A metamorphosed, stratabound-epigenetic origin for a gruneritic Archean gold deposit, Barberton, South Africa. *Ore Geology Reviews,* 12, pp 135-151.

Yoshihara, A. and Hamano, Y. (2004). Paleomagnetic constraints on the Archean geomagnetic field intensity obtained from komatiites of the Barberton and Belingwe greenstone belts, South Africa and Zimbabwe. *Precambrian Research*, 131, (1-2), pp 111-142.

Table 4-3 The data presented in counts per second by LA-ICP-MS for selected isotopes and in wt % for silver by SEM of the Zimbabwean and Mapungubwe artefacts samples. Lower limit of detection also presented.

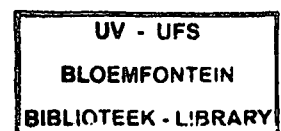| Ore Province | Locality | $^{56}$Fe | $^{59}$Co | $^{60}$Ni | $^{63}$Cu | $^{66}$Zn | $^{75}$As | $^{105}$Pd | $^{107}$Ag | $^{188}$Os | $^{195}$Pt | $^{202}$Hg | $^{204}$Pb | $^{206}$Pb | $^{207}$Pb | $^{208}$Pb | $^{209}$Bi | Ag wt. % |
|---|---|---|---|---|---|---|---|---|---|---|---|---|---|---|---|---|---|---|
| Ore Province | Lower limit of detection | 131 | 3 | 7 | 13 | 3 | 13 | 3 | 107 | 3 | 3 | 3 | 29 | 3 | 10 | 17 | 220 | |
| | Z1 | 236 | 11 | 234 | 370 | 537 | 4 | 2 | 449624 | 2 | 10 | 16 | 102 | 207 | 151 | 701 | 8 | 9 |
| | Z2 | 228 | 11 | 3 | 155 | 70 | 4 | 2 | 447811 | 1 | 11 | 16 | 34 | 98 | 74 | 501 | 8 | 9 |
| | Z3 | 182 | 9 | 2 | 225 | 108 | 2 | 2 | 375032 | ND | 11 | 17 | 200 | 358 | 400 | 700 | 8 | 7 |
| | Z4 | 1204 | 14 | 12 | 496 | 251 | 7 | 2 | 505827 | 1 | 7 | 11 | 45 | 116 | 111 | 331 | 8 | 10 |
| | Z5 | 355 | 9 | 6 | 287 | 137 | 10 | 2 | 469567 | 183 | 22 | 24 | 47 | 122 | 117 | 348 | 8 | 9 |
| | Z6 | 355 | 10 | 3 | 114 | 54 | 4 | 2 | 355607 | 38 | 12 | 18 | 28 | 63 | 60 | 171 | 8 | 7 |
| | Z7 | 233 | 11 | 2 | 164 | 80 | 8 | 3 | 288785 | 54 | 12 | 19 | 76 | 207 | 199 | 602 | 9 | 6 |
| | Z8 | 168 | 9 | 1 | 150 | 69 | 3 | 2 | 119917 | 1 | 11 | 20 | 31 | 72 | 69 | 197 | 7 | 2 |
| | Z9 | 180 | 9 | 2 | 11 | 6 | 3 | 2 | 27713 | 1 | 18 | 28 | 42 | 107 | 103 | 303 | 6 | 1 |
| | Z10 | 187 | 9 | 4 | 348 | 153 | 6 | 1 | 553483 | 63 | 11 | 19 | 42 | 107 | 102 | 304 | 5 | 11 |
| | Z11 | 376 | 15 | 5 | 187 | 84 | 7 | 1 | 547267 | 244 | 9 | 14 | 31 | 72 | 69 | 197 | 5 | 11 |
| | Z12 | 251 | 9 | 4 | 97 | 51 | 5 | 1 | 255374 | 1 | 12 | 17 | 35 | 86 | 83 | 241 | 4 | 5 |
| | Z14 | 515 | 15 | 9 | 440 | 196 | 6 | 1 | 463092 | 8 | 6 | 9 | 44 | 113 | 110 | 322 | 5 | 9 |
| | Z15 | 462 | 9 | 9 | 624 | 294 | 8 | ND | 318311 | 6 | 6 | 9 | 76 | 209 | 200 | 610 | ND | 6 |
| | Z16 | 317 | 10 | 5 | 313 | 155 | 7 | ND | 527842 | 170 | 8 | 10 | 59 | 158 | 155 | 455 | ND | 10 |
| | Z17 | 196 | 11 | 3 | 307 | 129 | 9 | 1 | 469049 | 1 | 9 | 11 | 92 | 257 | 248 | 754 | 4 | 9 |
| | Z18 | 1764 | 8 | 32 | 50 | 24 | 3 | ND | 337736 | 12 | 8 | 14 | 23 | 61 | 58 | 166 | ND | 7 |
| | Z19 | 1138 | 9 | 21 | 313 | 151 | 5 | ND | 554778 | 7 | 4 | 7 | 65 | 176 | 172 | 510 | ND | 11 |
| | Z20 | 173 | 9 | 4 | 706 | 336 | 7 | 1 | 576793 | 4 | 4 | 7 | 51 | 134 | 129 | 385 | 4 | 11 |
| | Z21 | 132 | 10 | 1 | 753 | 353 | 33 | 2 | 516446 | 2 | 5 | 7 | 51 | 134 | 132 | 384 | 6 | 10 |
| | Z22 | 2721 | 19 | 66 | 7261 | 3941 | 11 | ND | 1845116 | 11 | 6 | 7 | 53 | 140 | 137 | 403 | ND | 36 |
| Zimbabwean Artefacts | Z23 | 240 | 31 | 6 | 729 | 352 | 12 | 1 | 324009 | 4 | 16 | 29 | 27 | 62 | 59 | 169 | 4 | 6 |
| | Z24 | 280 | 7 | 5 | 203 | 102 | 12 | 1 | 363895 | 156 | 8 | 16 | 53 | 140 | 136 | 403 | 4 | 7 |
| | Valid number of samples | 23 | 23 | 23 | 23 | 23 | 23 | 18 | 23 | 22 | 23 | 23 | 23 | 23 | 23 | 23 | 18 | 23 |
| | Mean | 517 | 11 | 19 | 622 | 332 | 8 | 2 | 464916 | 44 | 10 | 15 | 57 | 139 | 134 | 398 | 6 | 9 |
| | Median | 251 | 10 | 5 | 307 | 137 | 7 | 2 | 449624 | 7 | 9 | 16 | 47 | 122 | 117 | 384 | 6 | 9 |
| | Minimum | 132 | 7 | 1 | 11 | 6 | 2 | 1 | 27713 | 0 | 4 | 7 | 27 | 61 | 58 | 166 | 4 | 1 |
| | Maximum | 2721 | 31 | 234 | 7261 | 3941 | 33 | 3 | 1845116 | 244 | 22 | 29 | 200 | 358 | 400 | 754 | 9 | 36 |
| | Standard deviation (σ) | 627 | 5 | 49 | 1463 | 797 | 6 | 1 | 331791 | 73 | 4 | 6 | 37 | 72 | 77 | 181 | 2 | 6 |
| | Coefficient of variation (%) | 121 | 44 | 257 | 235 | 240 | 82 | 30 | 71 | 166 | 45 | 42 | 65 | 51 | 57 | 45 | 30 | 71 |
| | Ma | 120 | 5 | 2 | 172 | 1 | 9 | 1 | 62667 | ND | 13 | 3 | 132 | 377 | 352 | 1114 | 5 | 1 |
| | Mb | 532 | 6 | 4 | 206 | 1 | 13 | 1 | 67260 | ND | 15 | 4 | 236 | 687 | 684 | 2043 | 5 | 1 |
| | Mf | 121 | 8 | 2 | 164 | 1 | 10 | 2 | 59763 | ND | 12 | 2 | 72 | 197 | 191 | 574 | 7 | 1 |
| | Mh | 148 | 7 | 1 | 598 | 1 | 15 | 1 | 80147 | ND | 7 | 4 | 101 | 284 | 273 | 835 | 10 | 2 |
| | Mj | 133 | 9 | 2 | 706 | 1 | 20 | ND | 81320 | ND | 3 | 3 | 98 | 275 | 275 | 808 | 10 | 2 |
| | Mi | 154 | 3 | 1 | 533 | 1 | 25 | 1 | 82220 | ND | 7 | 2 | 209 | 607 | 607 | 1802 | 9 | 2 |
| | Valid number of samples | 6 | 6 | 6 | 6 | 6 | 6 | 5 | 6 | 0 | 6 | 6 | 6 | 6 | 6 | 6 | 6 | 6 |
| | Mean | 201 | 6 | 2 | 397 | 1 | 15 | 1 | 72229 | | 10 | 3 | 142 | 405 | 397 | 1196 | 8 | 1 |
| | Median | 140 | 6 | 2 | 370 | 1 | 14 | 1 | 73703 | | 10 | 3 | 117 | 331 | 314 | 974 | 8 | 1 |
| | Minimum | 120 | 3 | 1 | 164 | 1 | 9 | 1 | 59763 | | 3 | 2 | 72 | 197 | 191 | 574 | 5 | 1 |
| | Maximum | 532 | 9 | 4 | 706 | 1 | 25 | 2 | 82220 | | 15 | 4 | 236 | 687 | 684 | 2043 | 10 | 2 |
| Mapungubwe Artefacts | Standard deviation (σ) | 162 | 2 | 1 | 243 | 0 | 6 | 1 | 10165 | | 4 | 1 | 66 | 198 | 200 | 593 | 2 | 0 |
| | Coefficient of variation (%) | 81 | 34 | 47 | 61 | 22 | 42 | 58 | 14 | | 46 | 35 | 47 | 49 | 50 | 50 | 30 | 14 |

Table 4-2 The data presented in counts per second by LA-ICP-MS for selected isotopes and in wt % for silver by SEM of the gold mines from Pietersburg, Murchison Greenstone Belts, Sabie-Pilgrim's Rest and Knysna gold samples. Lower limit of detection also presented.

| Ore Province | Locality | $^{56}$Fe | $^{59}$Co | $^{60}$Ni | $^{63}$Cu | $^{66}$Zn | $^{75}$As | $^{105}$Pd | $^{107}$Ag | $^{188}$Os | $^{195}$Pt | $^{202}$Hg | $^{204}$Pb | $^{206}$Pb | $^{207}$Pb | $^{208}$Pb | $^{209}$Bi | Ag wt. % |
|---|---|---|---|---|---|---|---|---|---|---|---|---|---|---|---|---|---|---|
| Ore Province | Lower limit of detection | 131 | 3 | 7 | 13 | 3 | 13 | 3 | 107 | 3 | 3 | 3 | 29 | 3 | 10 | 17 | 220 | |
| Pietersburg Greenstone Belt | Marabastadt | 419 | 25 | 5 | 1554 | 5 | 75 | 3 | 114992 | 2 | 2 | 169 | 153 | 286 | 112 | 165 | 67 | 2 |
| | Marabastadt | 450 | ND | 7 | 1328 | 3 | 30 | 1 | 29703 | 2 | 2 | 148 | 5 | 569 | 114 | 173 | 18 | 1 |
| | Valid number of samples | 2 | 1 | 2 | 2 | 2 | 2 | 2 | 2 | 2 | 2 | 2 | 2 | 2 | 2 | 2 | 2 | 2 |
| | Mean | 434 | 25 | 6 | 1441 | 4 | 53 | 2 | 72347 | 2 | 2 | 159 | 79 | 427 | 113 | 169 | 43 | 1 |
| | Median | 434 | 25 | 6 | 1441 | 4 | 53 | 2 | 72347 | 2 | 2 | 159 | 79 | 427 | 113 | 169 | 43 | 1 |
| | Minimum | 419 | 25 | 5 | 1328 | 3 | 30 | 1 | 29703 | 2 | 2 | 148 | 5 | 286 | 112 | 165 | 18 | 1 |
| | Maximum | 450 | 25 | 7 | 1554 | 5 | 75 | 3 | 114992 | 2 | 2 | 169 | 153 | 569 | 114 | 173 | 67 | 2 |
| | Standard deviation (σ) | 22 | | 2 | 160 | 1 | 31 | 1 | 60308 | 0 | 0 | 15 | 105 | 200 | 1 | 6 | 35 | 1 |
| | Coefficient of variation (%) | 5 | | 27 | 11 | 27 | 60 | 51 | 83 | 19 | 11 | 9 | 133 | 47 | 1 | 3 | 81 | 81 |
| Murchison Greenstone Belt | Gravellotte Mine | 689 | ND | 92 | 2366 | 23 | 60 | 2 | 98920 | 1 | 1 | 5523 | 12 | ND | 2274 | 2058 | 49 | 2 |
| | Valid number of samples | 1 | 0 | 1 | 1 | 1 | 1 | 1 | 1 | 1 | 1 | 1 | 1 | 0 | 1 | 1 | 1 | 1 |
| | Mean | 689 | | 92 | 2366 | 23 | 60 | 2 | 98920 | 1 | 1 | 5523 | 12 | | 2274 | 2058 | 49 | 2 |
| | Median | 689 | | 92 | 2366 | 23 | 60 | 2 | 98920 | 1 | 1 | 5523 | 12 | | 2274 | 2058 | 49 | 2 |
| | Minimum | 689 | | 92 | 2366 | 23 | 60 | 2 | 98920 | 1 | 1 | 5523 | 12 | | 2274 | 2058 | 49 | 2 |
| | Maximum | 689 | | 92 | 2366 | 23 | 60 | 2 | 98920 | 1 | 1 | 5523 | 12 | | 2274 | 2058 | 49 | 2 |
| | Standard deviation (σ) | | | | | | | | | | | | | | | | | |
| | Coefficient of variation (%) | 0 | | 0 | 0 | 0 | 0 | 0 | 0 | 0 | 0 | 0 | 0 | | 0 | 0 | 0 | 0 |
| Sabie Pilgrim's Rest | Lydenburg | 883 | 415 | 7 | 296 | 5 | 18 | 2 | 10003 | 2 | 3 | 32 | 2 | 35 | 28 | 95 | 40 | 0 |
| | Geodeverwacht | 970 | 29 | 24 | 837 | 10 | 20 | 3 | 546959 | 2 | 2 | 316 | 3 | 180 | 156 | 211 | 16 | 11 |
| | New Pilgrim/s Rest | 936 | 6 | 253 | 446 | 40 | 20 | 3 | 375914 | 2 | 1 | 6752 | 14 | 14 | 5471 | 4606 | 11 | 7 |
| | Valid number of samples | 3 | 3 | 3 | 3 | 3 | 3 | 3 | 3 | 3 | 3 | 3 | 3 | 3 | 3 | 3 | 3 | 3 |
| | Mean | 930 | 150 | 95 | 526 | 18 | 19 | 3 | 310959 | 2 | 2 | 2367 | 6 | 76 | 1885 | 1637 | 22 | 6 |
| | Median | 936 | 29 | 24 | 446 | 10 | 20 | 3 | 375914 | 2 | 2 | 316 | 3 | 35 | 156 | 211 | 16 | 7 |
| | Minimum | 883 | 6 | 7 | 296 | 5 | 18 | 2 | 10003 | 2 | 1 | 32 | 2 | 14 | 28 | 95 | 11 | 0 |
| | Maximum | 970 | 415 | 253 | 837 | 40 | 20 | 3 | 546959 | 2 | 3 | 6752 | 14 | 180 | 5471 | 4606 | 40 | 11 |
| | Standard deviation (σ) | 44 | 230 | 137 | 279 | 19 | 1 | 1 | 274308 | 0 | 1 | 3800 | 7 | 90 | 3106 | 2572 | 15 | 5 |
| | Coefficient of variation (%) | 5 | 153 | 145 | 53 | 103 | 7 | 27 | 88 | 7 | 43 | 161 | 111 | 118 | 165 | 157 | 68 | 88 |
| Cape Supergroup | Knysna Mine | 2704 | 55 | 16 | 1441 | 18 | 7 | 2 | 214384 | 2 | 2 | 189 | 12 | ND | 96 | 150 | 15 | 4 |
| | Knysna Mine | 2846 | 25 | 24 | 1188 | 18 | 9 | 3 | 97596 | 2 | 2 | 2813 | 51 | ND | 8951 | 7591 | 26 | 2 |
| | Valid number of samples | 2 | 2 | 2 | 2 | 2 | 2 | 2 | 2 | 2 | 2 | 2 | 2 | 0 | 2 | 2 | 2 | 2 |
| | Mean | 2775 | 40 | 20 | 1315 | 18 | 8 | 2 | 155990 | 2 | 2 | 1501 | 32 | | 4524 | 3871 | 20 | 3 |
| | Median | 2775 | 40 | 20 | 1315 | 18 | 8 | 2 | 155990 | 2 | 2 | 1501 | 32 | | 4524 | 3871 | 20 | 3 |
| | Minimum | 2704 | 25 | 16 | 1188 | 18 | 7 | 2 | 97596 | 2 | 2 | 189 | 12 | | 96 | 150 | 15 | 2 |
| | Maximum | 2846 | 55 | 24 | 1441 | 18 | 9 | 3 | 214384 | 2 | 2 | 2813 | 51 | | 8951 | 7591 | 26 | 4 |
| | Standard deviation (σ) | 100 | 21 | 5 | 179 | 0 | 2 | 1 | 82581 | 0 | 0 | 1855 | 27 | | 6261 | 5262 | 8 | 2 |
| | Coefficient of variation (%) | 4 | 53 | 27 | 14 | 0 | 22 | 23 | 53 | 13 | 3 | 124 | 86 | | 138 | 136 | 38 | 55 |

Table 4-1 The data presented in counts per second by LA-ICP-MS for selected isotopes and in wt % for silver by SEM of the Witwatersrand, Barberton and Zimbabwe gold samples. Lower limit of detection also presented.

| | Locality | $^{56}$Fe | $^{59}$Co | $^{60}$Ni | $^{63}$Cu | $^{66}$Zn | $^{75}$As | $^{105}$Pd | $^{107}$Ag | $^{188}$Os | $^{195}$Pt | $^{202}$Hg | $^{204}$Pb | $^{206}$Pb | $^{207}$Pb | $^{208}$Pb | $^{209}$Bi | Ag wt. % |
|---|---|---|---|---|---|---|---|---|---|---|---|---|---|---|---|---|---|---|
| Ore Province | Lower limit of detection | 131 | 3 | 7 | 13 | 3 | 13 | 3 | 107 | 3 | 3 | 3 | 29 | 3 | 10 | 17 | 220 | |
| | City Deep (a) | 809 | 5 | 5 | 1383 | 4 | 8 | 6 | 475357 | 4 | 4 | 1158 | 74 | 38 | 39 | 129 | 21 | 10 |
| | City Deep (b) | 765 | 5 | 7 | 1321 | 3 | 7 | 8 | 435628 | 4 | 2 | 7063 | 74 | 37 | 39 | 1039 | 20 | 9 |
| | Inner Basin Reef | 379 | 3 | 3 | 514 | 2 | ND | ND | 218823 | 4 | ND | 8683 | ND | 434 | 811 | 901 | 53 | 4 |
| | Carbon Leader | 547 | 8 | 11 | 589 | 5 | 8 | ND | 433904 | 3 | 4 | 7314 | ND | 46 | 37 | 860 | 27 | 8 |
| | Leader Reef | 760 | 3 | 6 | 59 | 10 | 8 | ND | 348435 | 3 | 5 | 9816 | 63 | 124 | 78 | 230 | 10 | 7 |
| | C' Reef | 591 | 4 | 10 | 31 | 3 | 13 | ND | 320344 | 3 | ND | 2422 | ND | 105 | 52 | 161 | 20 | 6 |
| | B' Reef | 988 | 5 | 4 | 704 | 8 | 13 | 9 | 280506 | 3 | ND | 3389 | 97 | 168 | 188 | 395 | 71 | 6 |
| Witwatersrand Basin | South Deep | 522 | 3 | 6 | 803 | 4 | 11 | 1 | 259230 | 3 | 2 | 8937 | 36 | 52 | 48 | 964 | 39 | 5 |
| | *Valid number of samples* | *8* | *8* | *8* | *8* | *8* | *7* | *4* | *8* | *8* | *5* | *8* | *5* | *8* | *8* | *8* | *8* | *8* |
| | *Mean* | *670* | *5* | *7* | *676* | *5* | *10* | *6* | *346528* | *3* | *3* | *6097* | *69* | *126* | *161* | *585* | *32* | *7* |
| | *Median* | *675* | *5* | *6* | *647* | *4* | *8* | *7* | *334389* | *3* | *4* | *7188* | *74* | *79* | *50* | *628* | *24* | *6* |
| | *Minimum* | *379* | *3* | *3* | *31* | *2* | *7* | *1* | *218823* | *3* | *2* | *1158* | *36* | *37* | *37* | *129* | *10* | *4* |
| | *Maximum* | *988* | *8* | *11* | *1383* | *10* | *13* | *9* | *475357* | *4* | *5* | *9816* | *97* | *434* | *811* | *1039* | *71* | *10* |
| | *Standard deviation (σ)* | *195* | *2* | *3* | *502* | *3* | *2* | *3* | *93463* | *0* | *1* | *3300* | *22* | *133* | *267* | *392* | *20* | *2* |
| | *Coefficient of variation (%)* | *29* | *38* | *40* | *74* | *57* | *24* | *54* | *27* | *9* | *40* | *54* | *32* | *106* | *166* | *67* | *63* | *28* |
| | Agnes Mine (a) | 218 | 3 | 11 | 1345 | 3 | 6 | 3 | 89002 | 2 | 2 | 213 | 235 | 173 | 134 | 8708 | 24 | 2 |
| | Agnes Mine (b) | 2694 | 3 | 20 | 205 | 6 | 6 | 2 | 174928 | 2 | 2 | 217 | ND | 103 | 93 | 99441 | 14 | 4 |
| | Sheba Mine (a) | 4482 | 3 | 35 | 1813 | 2 | 5 | 2 | 367846 | 1 | ND | 347 | ND | 20 | 21 | 237 | 10 | 4 |
| | Sheba Mine (b) | 8538 | 9 | 21 | 3814 | 6 | 76 | 2 | 102501 | ND | 2 | 264 | ND | 170 | 196 | 522 | 24 | 2 |
| | Sheba Mine ( c) | 4748 | 4 | 33 | 5098 | 7 | 90 | 3 | 55642 | 1 | 2 | 32 | 9 | 7054 | 5881 | 14964 | 19519 | 1 |
| | Sheba Mine (d) | 3608 | 5 | 11 | 5999 | 9 | 8 | 7 | 55408 | 2 | 3 | 95 | 330 | 158 | 13169 | 39634 | 52108 | 1 |
| | Sheba Mine (e) | 617 | 2 | 35 | 4308 | 3 | 5 | 2 | 167024 | 2 | ND | 326 | 533 | 40 | 30 | 135 | 40 | 3 |
| | New Consort Mine (a) | 10000 | 9 | 4 | 430 | 9 | 87 | 3 | 232706 | 2 | 2 | 219 | 491 | 124 | 1315 | 3055 | 2755 | 5 |
| Barberton Greenstone Belt | New Consort Mine (b) | 4401 | 3 | 3 | 3763 | 6 | 26 | 5 | 110235 | 2 | ND | 85 | 153 | 5074 | 4702 | 10478 | 12372 | 2 |
| | New Consort Mine ( c) | 6273 | 3 | 29 | 1867 | 3 | 64 | 5 | 50955 | 1 | ND | 257 | 956 | 922 | 798 | 1534 | 1988 | 1 |
| | *Valid number of samples* | *10* | *10* | *10* | *10* | *10* | *10* | *10* | *10* | *9* | *6* | *10* | *7* | *10* | *10* | *10* | *10* | *10* |
| | *Mean* | *4558* | *4* | *20* | *2865* | *5* | *38* | *3* | *140624* | *2* | *2* | *205* | *387* | *1384* | *2634* | *17871* | *8885* | *2* |
| | *Median* | *4441* | *3* | *21* | *2815* | *6* | *17* | *3* | *106368* | *2* | *2* | *218* | *330* | *164* | *497* | *5882* | *1014* | *2* |
| | *Minimum* | *218* | *2* | *4* | *205* | *2* | *5* | *2* | *50955* | *1* | *2* | *32* | *9* | *20* | *21* | *135* | *10* | *1* |
| | *Maximum* | *10000* | *9* | *35* | *5999* | *9* | *90* | *7* | *367846* | *2* | *3* | *347* | *956* | *7054* | *13169* | *99441* | *52108* | *5* |
| | *Standard deviation (σ)* | *3113* | *3* | *12* | *2000* | *3* | *37* | *2* | *99749* | *0* | *1* | *104* | *311* | *2524* | *4258* | *31069* | *16571* | *1* |
| | *Coefficient of variation (%)* | *68* | *58* | *61* | *70* | *48* | *99* | *52* | *71* | *23* | *28* | *51* | *80* | *182* | *162* | *174* | *187* | *54* |
| | Don Mine (a) | 1805 | 3 | 3 | 438 | 7 | 6 | ND | 208778 | ND | ND | 794 | 11 | 195 | 183 | 566 | 500 | 4 |
| | Don Mine (b) | 5582 | 13 | 28 | 732 | 21 | 22 | ND | 186200 | ND | ND | 751 | 22 | 185 | 175 | 1131 | 1744 | 4 |
| | Gadzema | 4853 | 4 | 22 | 1517 | 32 | 7 | 3 | 118980 | 3 | 2 | 415 | 40 | 178 | 170 | 1521 | 132 | 2 |
| | Belingwe | 3651 | 25 | 35 | 2204 | 11 | 7 | 2 | 218320 | 2 | ND | 1811 | 49 | 202 | 477 | 919 | 1661 | 4 |
| | Lower Gwelo | 6254 | 3 | 48 | 1074 | 15 | 6 | 4 | 100 | 2 | 2 | 281 | ND | 286 | 2870 | 6961 | 9940 | 1 |
| | Reef of Gaika | 3686 | 6 | 53 | 2953 | 9 | 10 | 2 | 49707 | 2 | 2 | 254 | 46 | 128 | 110 | 5711 | 9 | 1 |
| Zimbabwean Greenstone Belts | Victoria reef | 2586 | 11 | 10 | 2435 | 13 | 18 | 2 | 91415 | 2 | 2 | 208 | 89 | 120 | 129 | 4940 | 48 | 2 |
| | *Valid number of samples* | *7* | *7* | *7* | *7* | *7* | *7* | *5* | *7* | *5* | *4* | *7* | *6* | *7* | *7* | *7* | *7* | *7* |
| | *Mean* | *4059* | *9* | *29* | *1622* | *15* | *11* | *2* | *124785* | *2* | *2* | *644* | *43* | *185* | *587* | *3107* | *2004* | *3* |
| | *Median* | *3686* | *6* | *28* | *1517* | *13* | *7* | *2* | *118980* | *2* | *2* | *415* | *43* | *185* | *175* | *1521* | *500* | *2* |
| | *Minimum* | *1805* | *3* | *3* | *438* | *7* | *6* | *2* | *100* | *1* | *2* | *208* | *11* | *120* | *110* | *566* | *9* | *1* |
| | *Maximum* | *6254* | *25* | *53* | *2953* | *32* | *22* | *4* | *218320* | *3* | *2* | *1811* | *89* | *286* | *2870* | *6961* | *9940* | *4* |
| | *Standard deviation (σ)* | *1598* | *8* | *19* | *938* | *9* | *6* | *1* | *83572* | *0* | *0* | *566* | *27* | *55* | *1014* | *2666* | *3576* | *1* |
| | *Coefficient of variation (%)* | *39* | *86* | *65* | *58* | *56* | *57* | *35* | *67* | *24* | *10* | *88* | *63* | *30* | *173* | *86* | *178* | *53* |